ANTIBIOTIC RELEASING BONE-VOID FILLER FOR THE TREATMENT OF OSTEOMYELITIS: AN APPROACH TO TREAT INFECTION AND AID BONE REGENERATION

A Dissertation
Submitted to the Graduate Faculty
of the
North Dakota State University
of Agriculture and Applied Science

By

Mohammad Raquibul Hasan

In Partial Fulfillment of the Requirements
for the Degree of
DOCTOR OF PHILOSOPHY

Major Department:
Pharmaceutical Sciences

September 2019

Fargo, North Dakota

North Dakota State University
Graduate School

Title

ANTIBIOTIC RELEASING BONE-VOID FILLER FOR THE TREATMENT OF OSTEOMYELITIS: AN APPROACH TO TREAT INFECTION AND AID BONE REGENERATION

By

Raquib Hasan

The Supervisory Committee certifies that this ***disquisition*** complies with North Dakota State University's regulations and meets the accepted standards for the degree of

DOCTOR OF PHILOSOPHY

SUPERVISORY COMMITTEE:

Dr. Amanda Brooks
Chair

Dr. Kristine Steffen

Dr. Mohiuddin Quadir

Dr. Sanku Mallik

Approved:

April 20, 2020
Date

Dr. Jagdish Singh
Department Chair

ABSTRACT

Osteomyelitis or bone infections remain very difficult to treat despite advances in treatment regimens and surgical technics. The bone microenvironment and compromised vasculature in addition to infected prosthesis and implants that were put in the bone during prior surgery impedes the antibiotic partition into the bone from systemic therapy in many cases. Treatment often includes surgical debridement of the infected bone and surrounding tissue, removal of implants, systemic antibiotic therapy accompanied with antibiotic containing bone void filler, in most cases polymethylmethacylate (PMMA) based bone cement. Unfortunately, PMMA has many associated problems, including non-biodegradability, inconsistent antibiotic release, and a surface susceptible to bacterial biofilm growth, ultimately necessitating removal and causing recurrent infections. Thus, recent studies have focused on designing novel bone void filling materials to deliver antibiotics and to support bone regeneration.

There are two parts to designing a successful bone void filling device/material:(1) local release antibiotic for infection treatment and (2) development of a bone graft substitute to support bone regrowth. In this study, antibiotic releasing bone void filler (ABVF) putty formulations have been designed and tested. Different formulations were examined in this dissertation to describe the three components of the putty formulation - polymer, drug, and substrate. In the first formulation, different custom-made polymers were used to control drug release; Pro Osteon, a hydroxyapatite (HA) and calcium carbonate based bone graft substitute was used to provide support for bone growth. Finally, vancomycin was used as the antibiotic as it is clinically used to treat *Staphylococcus aureus,* the primary cause of osteomyelitis. In second formulation, commercially available and clinically used polymers, poly(lactic-co-glycolic acid) (PLGA), polycaprolactone (PCL) and, polyethylene glycol (PEG), were used to make the ABVF

putty along with Pro Osteon and vancomycin. In the subsequent formulations, delivering combination antibiotics - vancomycin and rifampicin - to treat biofilm infections and, using bioglass (BG) as the substrate for faster bone regrowth were explored; PLGA, PCL and PEG constituted the polymer matrix.

The ABVF putty formulations were customizable in terms of three primary components: polymers, bone graft substitutes, antibiotics. Ultimately, these were successful in curing infection and providing bone growth support.

ACKNOWLEDGEMENTS

I would like to praise the Almighty for blessing me with the opportunities that brought me to this moment. I thank my advisor, Dr. Amanda Brooks, for providing all the support, encouragement, training and freedom to pursue the projects that are mentioned in the thesis and outside of it. My committee members provided timely suggestions and reviewed my progress that kept me aligned with the project progress. The Department of Pharmaceutical Sciences at North Dakota State University provided extraordinary support for carrying out my research. The department research seminars were a source of great feedback and kept me up-to-date with the latest research and advances, and were also a place to develop collaborations. I came across great scientific minds, such as my colleagues in the lab, in the department and collaborators across NDSU; and learned from them immensely. I want to thank Diana, Jean, Janet, and Tiffany of the Pharmaceutical Sciences Department office for making my life very easy by taking care of the paperwork and ordering process. I would like to acknowledge NDSU Electron Microscopy Center, Advanced Imaging & Microscopy Laboratory, Veterinary Technology Department, CPR Core Synthesis Facility, Research 1 & 2 Facilities, Electrical Engineering Department and Mechanical Engineering Department for providing facilities to carry out the experiments. I want to specially acknowledge Discovery Based Learning course, through which I made several very successful collaborations. This class was a tremendous ground for getting the initial training to get involved in and function in multidisciplinary project environments. I thank the co-authors of the chapters and the people who are acknowledged in the chapters for their contribution to the work. I also thank the funding agencies who supported the projects, provided stipends, and travel grants that helped me to seamlessly carry out my graduate works.

I thank NDSU graduate school dean, Dr. Claudia Tomany, for being a great source of encouragement. Her leadership created an amazing environment at NDSU enabling graduate student success. I believe graduate school is not only about academic pursuit and academic training, it also prepares grad students by giving an overall training about life, self and societal improvements, and gives the vision to go above and beyond. I want to thank NDSU and NDSU College of Health Professions for giving me the opportunity to give back to the community, which was very fulfilling for me personally and was helpful in my professional growth.

The city of Fargo touched me to my core. I have made great friends who helped and supported me mentally, emotionally and unconditionally to cope with the pressure of graduate school while I lived far away from my family. I found a wonderful community in Fargo that has made an everlasting impression on me.

I would like to thank all the graduate students who inspired me. As a graduate student, I always felt that I am a part of the broader graduate student community all over. When I met others at NDSU and during conferences, there was a great sense of camaraderie. I believe the sense of unity to be a part of great human endeavor to advance knowledge that will get us to a greater future if we stay vigilant, ethical, compassionate, and courageous. I thank all of them for the support.

Apart from humans, I want to acknowledge the animals, in my case rats, who are very useful and important for many of the biomedical advances that improved the quality of human life in astronomical proportions over the last few decades!

The list of people that I want to acknowledge is very long. I thank everyone, who, in any form or scope, helped me to achieve what I have achieved until today and who will help me to thrive in the future. Thank you!

DEDICATION

To my parents, Abu Sayeed and Tahrina Khatun; my brother, Saquibul Hasan; my extended family in Fargo, David and Sandra Roe; my friends and family!

TABLE OF CONTENTS

LIST OF TABLES

LIST OF FIGURES

LIST OF ABBREVIATIONS

μ-CT.....Micro Computed Tomography

AAOS.....American Academy of Orthopedic Surgeons

ABVF.....Antibiotic releasing bone void filler

ABVF-BG.....Bioglass based antibiotic releasing bone void filler

ABVF-C.....Combination Antibiotic Releasing Bone Void Filler

ADC.....Analog to Digital Converter

ALBC.....Antibiotic loaded based bone cement

BG.....Bioglass

BVF.....Bone void filler

CFU.....Colony Forming Unit

CP.....Calcium phosphate

CS.....Calcium sulphate

DI.....Deionized

DIC.....diisopropylcarbodiimide

DMEM.....Dulbecco's Modified Eagle Media

DMF.....Dimethyl formamide

DMSO.....Dimethyl sulfoxide

DPTS.....4-(Dimethylamino)pyridinium 4-toluenesulfonate

DSC.....Differential Scanning Calorimeter

ECM.....Extracellular Matrix

EDC.....Ethyl-3-(3-dimethylaminopropyl)carbodiimide HCl

EDS.....Energy-dispersive X-ray Spectrometry

EtOAc.....Ethyl acetate

FBS.....Fetal Bovine Serum

GPC.....Gel permeation chromatography

GRAS.....Generally Regarded as Safe

H&E.....Hemotoxin and Eosin stain

HA.....Hydroxyapatitie

HPLC.....High-performance Liquid Chromatography

IACUC.....Institutional Animal Care and Use Committee

IGF-II.....Insulin-like Growth Factor II

IV.....Intravenous

Kg.....Kilogram

LB.....Luria Bertani

LED.....Light Emitting Diode

MeOH.....Methanol

MGP.....Matrix Gla Protein

MIC.....Minimum inhibitory concentration

mm.....Millimeter

MRSA.....Methicillin-resistant Staphylococcus aureus

MTT.....3-(4,5-dimethylthiazol-2-yl)-2,5-diphenyltetrazolium bromide

NDSU.....North Dakota State University

NMP.....N-Methyl-2-pyrrolidone

NMR.....Nuclear magnetic resonance

PBS.....Phosphate Buffered Saline

PCL.....Polycaprolactone

PEG.....Polyethylene glycol

Pi.....Inorganic Phosphate

PJI.....Periprosthetic Joint Infection

PLGA.....Poly(lactic-co-glycolic acid)

PMMA.....Polymethylmethacrylate

PU.....Polyurethane

PVA.....Polyvinyl Alcohol

QSAR.....Quantitative Structure–Activity Relationship

ROI.....Region of Interest

SBF.....Simulated Body Fluid

SEM.....Scanning Electron Microscopy

TBDMS.....t-butyl dimethyl silane

TCP.....Tricalcium phosphate

TFA.....trifluoroacetic acid

T_g.....Glass Transition Temperatures

TGA.....Thermal Gravimetric Analysis

THF.....tetrahydrofuran

THR.....Total Hip Replacements

TJR.....Total Joint Replacements

TKR.....Total Knee Replacements

TSA.....Trypticase Soy Agar

V-fb.....Vancomycin Free-base

V-HCl.....Vancomycin Hydrochloride

WHO.....World Health Organization

XRD.....X-ray Diffraction

ZOI.....Zone of Inhibition

LIST OF APPENDIX TABLES

LIST OF APPENDIX FIGURES

1. INTRODUCTION

1.1. Osteomyelitis

Osteomyelitis or deep bone infections with pyogenic organisms including bacteria, fungi, and mycobacteria, leading to acute or chronic inflammatory processes involving the bone and its structures. This is a relatively old disease evident in the fossil record. Various terms were used to describe infected bone over the years until Nelaton first coined the term "osteomyelitis" in 1844. In the post antibiotic era, the mortality rate due to osteomyelitis related sepsis has decreased significantly [1]. Despite the success, these infections still pose challenges in treatment. In recent years, there has been an increase in the incidence of osteomyelitis with rates increased from 11.4 cases per 100,000 during the period from 1969 to 1979 to 24.4 per 100,000 person during the period from 2000 to 2009 [2]. In adult patients, it is estimated that 47–50% of all osteomyelitis are post-traumatic [3].

Osteomyelitis after orthopedic surgery involving the presence of implants is even harder to treat due to bacterial seeding of the implant and development of a biofilm community. The infection rate after total joint replacements (TJR) remains at 0.5 – 5% [4]. In the context of this finite infection rate and the over 1 million people who undergo a TJR each year, projected to reach 4 million per year in the U.S. by 2030 [5] [6] [7], the number of people suffering from infectious complications is continuing to rise. Furthermore, patients with an infection TJR must undergo a revision surgery, which drives the risk of subsequent TJR infection even higher to 5.2 – 21% [8], [9,10]. Currently, about 492,000 fractures of tibia, fibula, and ankle happen annually [11]. Although most of these are routine, the situation can be dire in the case of open fractures, where infection rates range from 17.5−21.2% compared to 3.6−8.1% for closed fractures [12]. Furthermore, chronic, recurring osteomyelitis is almost insurmountably more difficult to treat

when compared to acute osteomyelitis. In chronic osteomyelitis, the causative organism evades both the clinical treatment and the host immune system by residing in phagocytic cells. Prevention of infection is a necessary strategy.

1.2. Antibiotic Resistance

Antibiotic resistance is rising globally [13]. An alarming situation is present in the US with more than 2 million being admitted to hospitals each year due to antibiotic resistant infections, culminating in 23,000 deaths with an overall financial burden of about $35 billion per year [14]. Unless drastic measures are taken rapidly, the annual worldwide death rate may increase to 10 million per year by 2050 [15]. Rising incidence of methicillin-resistant *Staphylococcus aureus* (MRSA) [16], a resistant variant of *S. aureus*, adds to the grim situation and must be accounted for in the treatment plans for revision TJR. The current gold standard of bone void filler (BVF) used in revision TJR, antibiotic loaded polymethylmethacrylate (PMMA) based bone cement (ALBC), yields inadequate drug release kinetics. This is accompanied by an elevated dose of prolonged (6-8 weeks) systemic and oral antibiotic therapy which can lead to the rise of resistant bacteria. It was reported that gentamicin loaded ALBC led to a rise in gentamicin resistant bacteria [17]. Developing local and controlled antibiotic release strategies to eradicate infection, particularly for hard to penetrate tissues with low blood supply such as bone, by achieving an optimal local antibiotic drug level without exposing the whole body may mitigate the emergence of resistance, allowing time for new antibiotic discovery [18].

1.3. Current Treatments

Current strategies to treat osteomyelitic infections involve surgical debridement of the infected and necrotic bone and surrounding soft tissue followed by 4 to 6 weeks of intravenous antibiotic therapy with a transition to oral antibiotic therapy for up to 8 weeks [19] [20].

Unfortunately, due to poor bone vascularization, which is even more limited in osteomyelitis, high systemic antibiotic doses are essential to achieve adequate local concentrations above the minimum inhibitory concentration (MIC) at the infection site, which may culminate in systemic toxicity. Alternatively, to achieve high and effective local antibiotic concentrations over a longer period of time (4 to 6 weeks) and to fill the void space left after surgical debridement or orthopedic trauma, biomaterial based local antibiotic delivery has shown promise as a more effective treatment option [21]. Currently, ALBC and antibiotic loaded PMMA beads are widely used, non-biodegradable options for osteomyelitis management. Undesirably, PMMA based options suffer from poor antibiotic release kinetics, leaching antibiotic at sub-inhibitory levels over an extended period and leading the cement to be a nidus of infection. Alarmingly, reports suggest that the colonization of the hip joint with antibiotic-resistant bacteria may reach up to 88% upon hip revision surgery when antibiotic containing bone cement was used in a prior surgical intervention [22]. Additionally, due to its non-biodegradable nature PMMA also requires an additional surgery to be removed. These disadvantages have led to a search for biodegradable bone void filling (BVF) materials that provide both osteoconduction and osseointegration as well as act as an antibiotic carrier. These materials can be primarily divided into calcium-based materials such as hydroxyapatite, calcium phosphate or calcium sulphate materials and bioactive glass or, bioglass etc. [17].

1.4. Bone Void Fillers

1.4.1. Calcium Sulphate Based Material

Calcium sulphate (CS) hemihydrate has been used as a resorbable bone substitute. Typically, it has been used as a paste, which when mixed with antibiotic, settles in-situ filling up the void space [23]. Alternatively, calcium sulfate can be used to form antibiotic loaded beads

ex-vivo, which can subsequently be implanted inside an orthopedic void space [24]. In a study, where vancomycin loaded calcium sulphate hemihydrate/hydroxyapatite/collagen was used in a rabbit femoral infection model, the surgical site not only showed no signs of residual infection after 12 weeks but also showed concurrent trabecular bone formation [23]. Although this is a promising new tool in the fight against osteomyelitis, the pharmacokinetics of release were not assessed. Furthermore, gentamicin and vancomycin loaded calcium sulphate beads were clinically evaluated in a metatarsal amputation due to infection [24]. In the study, the infection was eradicated, and the patient remained infection free after 11 months. Although this study seems like a stunning example of the efficacy of calcium sulfate beads, it must be noted that the patient also received 4 to 8 weeks of oral antibiotics. In another small clinical study, 4 patients with either revision knee or hip replacement surgery associated with infection were treated with vancomycin or daptomycin loaded CS beads along with antibiotic loaded bone cement (in this case - hip surgery), resulting in complete infection resolution in three patients after 19 months of follow up [25]. Again, all patients in the study received 2 to 4 weeks of intravenous and oral antibiotic therapy in addition to the local implant, which limits the power of the study. Furthermore, these clinical evaluations showed CS absorption after 4 weeks in these cases, which is too fast to provide adequate support for bone regrowth. In some of these evaluations, antibiotic was loaded in CS beads by soaking the beads in the antibiotic solution. Unfortunately, this passive diffusion often leads to inadequate pharmacokinetics, as was observed when a calcium sulphate and hydroxyapatite composite bead was used as the antibiotic carrier for a gentamicin and vancomycin antibiotic solution, which released almost all the drug within only 10 days. Notably, the composite showed faster release when compared to pure CS [26]. Regardless of the antibiotic loading strategy, using CS as a bone substitute incurs several

significant drawbacks, including cytotoxicity and an increased acidic microenvironment due to degradation of the CS. Importantly, degradation can also lead to both acute and unresolved chronic inflammation as well as catalyze an exothermic reaction in which the solid CS is converted to a paste [26] [23] [27].

1.4.2. Calcium Phosphate Based Material

Compared to CS calcium phosphate (CP) based materials show longer resorption time. Depending on the composition, CP-based materials have different resorption times. Tricalcium phosphate (TCP) is resorbed in 6 to 18 months, whereas hydroxyapatite (HA) and monocalcium phosphate have degradation times of 6 months to 10 years [27]. Similar to CS, CP can also be used as paste, which gradually solidifies into a solid cement in vivo; however, unlike CS, the process is isothermal, protecting the tissues surrounding the implant. Nevertheless, limited porosity after CP cement solidification leads to limited bone ingrowth [28] and inadequate pharmacokinetics. In a study using gentamicin and vancomycin soaked tricalcium phosphate ceramic, Cerasorb® (low porosity, 35%) and Cerasorb® M (high porosity, 65%), it was observed that both of the antibiotics reached therapeutic local concentration within 4 to 5 days, but quickly fell below the minimum inhibitory concentration (MIC) [29]. In an alternative preclinical study of an antibiotic releasing CP-based bone void filler, a porous CP based substrate was embedded in a polymer matrix loaded with tobramycin and showed tobramycin release at therapeutic concentrations up to 8 weeks *in vitro* [30] with the pilot animal study showing promising bone formation after 12 weeks in a rabbit. Notably no infection-model animal study was done using the material. CP based materials show promise as both antibiotic carriers and bone void fillers; however, further improvements in the formulations are necessary to achieve high local antibiotic concentration over longer period. In the current study, we have

formulated antibiotic releasing bone void filling (ABVF) putty using CP and calcium carbonate based bone graft substitute, which provided high antibiotic concentration for up to 6 weeks for both single and combination release.

1.4.3. Bioactive Glass or Bioglass

As opposed to traditional calcium based bone graft substitutes, recent years have seen bioactive glass or, bioglass (BG) garner much attention as a bone graft substitute for its osteoconductive and osteoinductive activity as well as its tailorability [31] and antibacterial properties [32]. In a study of 116 chronic osteomyelitis patients treated with antibacterial bioglass, S53P4, 90% of the patients were infection free after a median follow-up of 31 months [32]. However, in addition to bioglass BVF, patients also received systemic antibiotic therapy. In another study, vancomycin loaded onto borate bioglass pellets were used in a rabbit tibial infection model. After 11 weeks, 81.25% of the animals showed no signs of infection along with good bone growth and osseointegration despite the fact that the pellets only released drug above the MIC for 18 days *in vitro* [33]. Ultimately, bioglass has been increasingly shown as a promising bone substitute and antibiotic carrier to treat osteomyelitis. In this current study, we have developed bioglass based antibiotic releasing bone void filler (ABVF-BG) putty, which was able to achieve therapeutic antibiotic release for 6 weeks as well as to provide bone growth support.

1.5. Organization of the Thesis

The goal of this thesis was to develop easy to use, easy to formulate putty-like ABVF to provide both extended and bioactive antibiotic release, and enhanced bone regrowth. The customizable ABVF could be formulated with either a single antibiotic or a combination of antibiotics to treat challenging biofilm infections. The bone graft substitute in the ABVF was

also customized to achieve similarly effective antibiotic release and infection cure while providing faster bone healing.

The overall hypothesis of the thesis is that a biodegradable ABVF putty that not only provides effective local antibiotic concentration but also shows osteoconductivity, can tackle the challenges of osteomyelitis by killing bone resident bacteria and by supporting bone healing. This is depicted in the following graphical abstract (Figure 1.1).

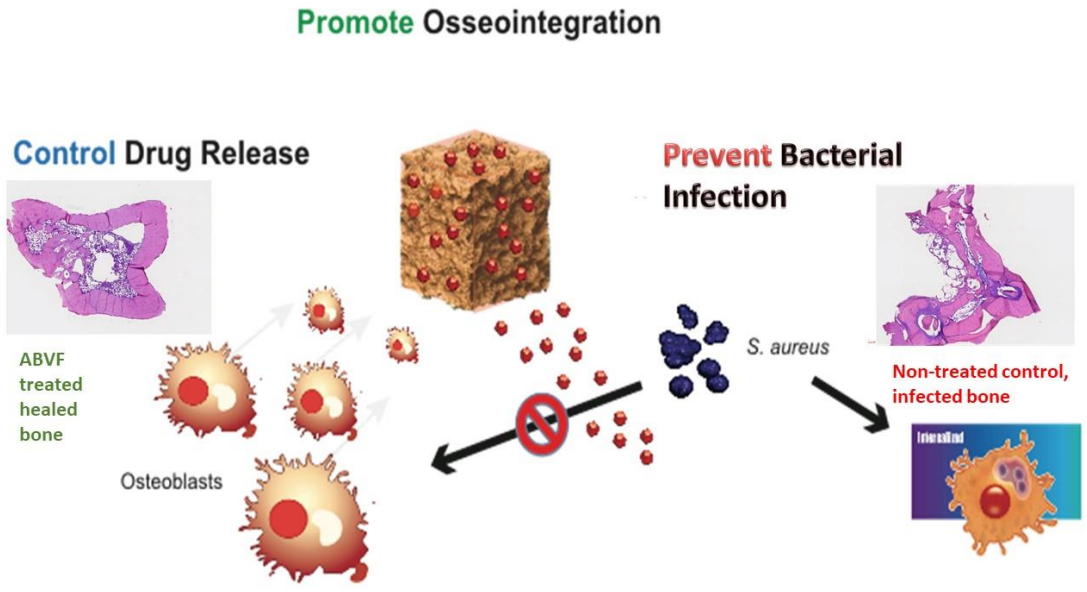

Figure 1.1. Graphical abstract.
AVBF releases antibiotic killing bacteria and preventing bacteria from infecting bone. The biodegradable and osseointegrating nature of the AVBF helps in bone regrowth.

In this thesis, the design and customization of ABVF was investigated by examining the biodegradable polymer matrix, the efficient and effective release of antibiotic and the osseointegration of the material. In chapters 2 and 3, the polymer matrix was explores and customized to provide putty like handling properties. In chapter 4, the antibiotic load was tailored to provide extended bacterial killing. Finally, in chapter 5, the third component of the system, the underlying bone graft substrate, was considered and modified to enhance bone

healing. This is a paper-based thesis and all the chapters are intended for peer-reviewed journal publications.

In chapter 2, an osteoconductive antibiotic eluting putty with a custom polymer matrix, we explored the impact of the polymer composition of the ABVF putty on in vitro drug release by using different custom-made polymers and a Pro Osteon bone graft substitute.

In chapter 3, an antibiotic releasing bone void filling (ABVF) putty for the treatment of osteomyelitis, we continued to develop the ABVF putty using a blended commercial polymer matrix and Pro Osteon substrate to release vancomycin both in vitro and in vivo.

In chapter 4, extended release combination antibiotic therapy from a bone void filling putty for treatment of osteomyelitis, we extended the utility of the developed ABVF-C putty to treat implant related biofilm infection by releasing a combination antibiotics and assessed the activity both in vitro and in vivo.

Finally, in chapter 5, bioglass based antibiotic releasing bone void filler (ABVF-BG) putty for the treatment of osteomyelitis, we have considered the underlying substrate of the putty by using a custom bioglass substrate in the formulation of the ABVF-BG putty to aid in faster bone growth. We have evaluated the ABVF-BG putty for desired antibacterial activity. We also examined the putty in a rat infection drill-hole model for both infection cure as well as bone regeneration.

2. AN OSTEOCONDUCTIVE ANTIBIOTIC ELUTING PUTTY WITH A CUSTOM POLYMER MATRIX[1]

2.1. Abstract

With the rising tide of antibiotic resistant bacteria, extending the longevity of the current antibiotic arsenal is becoming a necessity. Developing local, controlled release antibiotic strategies, particularly for difficult to penetrate tissues such as bone, may prove to be a better alternative. Previous efforts to develop an osteoconductive local antibiotic release device for bone were created as solid molded composites; however, intimate contact with host bone was found to be critical to support host bone regrowth; thus, an osteoconductive antibiotic releasing bone void filling putty was developed. Furthermore, a controlled releasing polymer matrix was refined using pendant-functionalized diols to provide tailorable pharmacokinetics. In vitro pharmacokinetic and bioactivity profiles were compared for a putty formulation with an analogous composition as its molded counterpart as well as four new pendant-functionalized polymers. A best-fit analysis of polymer composition in either small cylindrical disks or larger spheres revealed that the new pendant-functionalized polymers appear to release vancomycin via both diffusion and erosion regardless of the geometry of the putty. *In silico* simulations, a valuable technique for diffusion mediated controlled release models, will be used to confirm and optimize this property.

---

[1] M. R. Hasan, J. Curley et al., "An Osteoconductive Antibiotic Bone Eluting Putty with a Custom Polymer Matrix," Polymers, vol. 8, no. 7, p. 247, Jun. 2016, doi: 10.3390/polym8070247. The material in this chapter was co-authored by Raquib Hasan, John Curley, Jacob Larson, Benjamin D. Brooks, Qianhui Liu, Tanmay Jain, Abraham Joy, Amanda E. Brooks. Raquib Hasan, John Curley, Abraham Joy, and Amanda E. Brooks conceived and designed the experiments. Raquib and John had primary responsibility to conduct all the experiments listed in the section, analyze the data and write the manuscript. Qianhui Liu and Tanmay Jain synthesized and characterized the polymers. Jacob Larson performed the mechanical testing. Imaging was done by Jayma Moore and Scott Payne of NDSU electron microscopy center. Raquib Hasan, John Curley, Qianhui Liu, Tanmay Jain, Jacob Larson, Abraham Joy, Benjamin D. Brooks, and Amanda E. Brooks analyzed the data. Raquib Hasan, John Curley, and Amanda E. Brooks wrote the manuscript.

Keywords: osteomyelitis; controlled drug release; bone void filler; putty; pharmacokinetics; pendant-functionalized diol.

2.2. Introduction

Listed by the World Health Organization (WHO) as one of the top three threats to global public health [34], more than 2 million Americans suffer from an antibiotic-resistant infection [35], imposing an enormous economic burden (≈ $20 billion in direct healthcare costs [36]) on the world's healthcare systems. Multidrug resistant bacteria are becoming almost universal, provoked by the pervasive and often extended use of antibiotics [37]; moreover, many of these once powerful antimicrobial drugs are now rendered impotent by inappropriate prescribing patterns [9,10,38] and poor patient compliance [37,39–41]. Almost 70% of nosocomial infections are linked to antibiotic resistant pathogens [42–45]. Beyond clinical practice, microbial characteristics as well as societal and technical changes have led to the frightening revelation that development of antibiotic resistance is almost virtually certain given enough time [46–48]. Thus, the rise in antibiotic-resistant bacterial strains is quickly outpacing drug discovery and several strategies beyond simply filling the new drug pipeline must be pursued. In the absence of such development, we are facing the return to a pre-antibiotic era, with drugs that are costly and only partially effective.

Periprosthetic Joint Infection (PJI): Despite the clinical success of Total Joint Replacements (TJR) in relieving pain and improving quality of life, up to 10% of implants will fail early (<10 years), requiring a revision procedure to remove the original device and infected bone and replace components [34]. Infection is responsible for 15% of total hip revision surgeries and up to 25% of total knee revisions [49]. A steady increase in TJR procedures (Figure 1) in conjunction with finite infection rates (as low as 1%–2% to as high as 4%–12%

[37]), increased lifelong risk of implant bacterial seeding, the rising tide of antibiotic resistant bacteria, and better microbial detection methods have culminated in an increase in the absolute number of patients suffering from acute or chronic osteomyelitis [35,36,50] (Figure 1). Unfortunately, implant removal and hardware replacement drives the risk of infection to a staggering 20%–30% [9,10]. These grim statistics culminate in a significant loss of life (over 1000 deaths per year), many a direct result of the growing frequency of antibiotic resistant bone infections. Moreover, the economic burden for surgically addressing periprosthetic infections (PIs) with revision TJRs is calculated to be 5.3–7.2 times higher than that of primary TJR operations [39] (each revision surgery is estimated to cost $42,000–$56,000 (US) [40]). This amounts to $750 million in insurance and patient costs to treat spine, knee and hip infections and nearly $250 million in hospital losses yearly [10]. Independent biomaterial- or pharmaceutical-based approaches to implant-centered infection are inadequate to combat osteomyelitis. Instead, using an osseointegrating wound and bone defect filler material as a local delivery vehicle, endowing it with a rate-controlling polymer membrane, may mitigate implant-associated infection and consequent bone destruction. Utilizing principles of intelligent design, an effective, locally deployable, polymer-control antibiotic delivery vehicle can be developed.

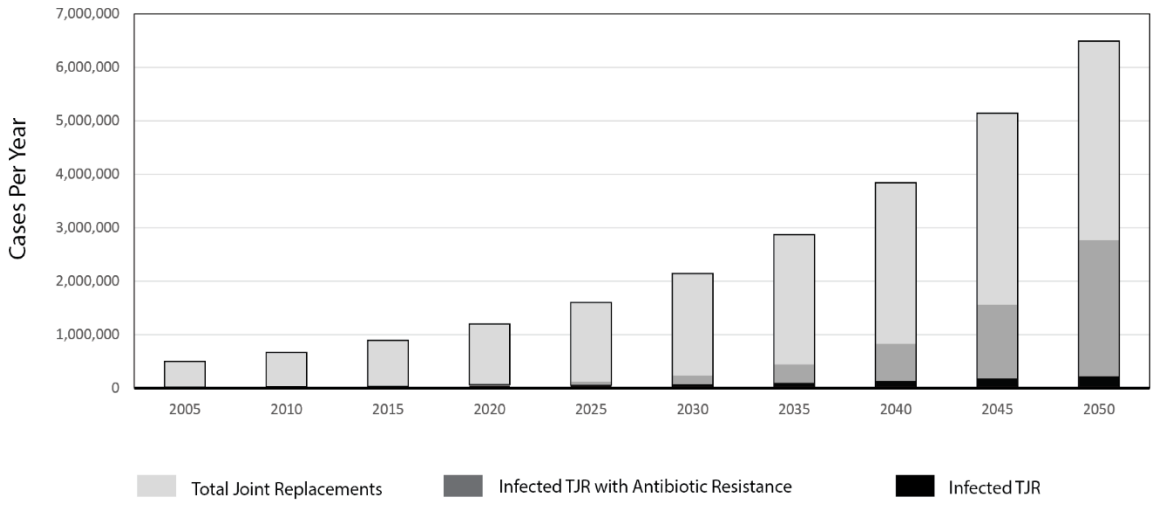

Figure 2.1. Projected total joint replacements (TJR) with infection rates.
Growth rate for TJR was 6% annual growth and the growth rate for antibiotic resistance was 7% conforming with published numbers [5], [51], [49].

Local controlled-release antibiotic delivery to bone: Although osteomyelitis—a serious bone infection accompanied by inflammation, cytokine up-regulation, and bone resorption—is increasingly linked to antibiotic resistant bacteria, current clinical tools to address it are tedious, costly, and often ineffective, compromising the patient's overall bone health, healing, and recovery. Systemic antibiotic prophylaxis is considered the current clinical standard of care; however, studies are lacking to support this approach [42]. While considered generally effective, problems with systemic antibiotic delivery include systemic side effects and low antibiotic concentrations at the local site of infection, unintentionally favoring antibiotic resistance [41,43]. Bone's limited vascular supply and the presence of sequestra or void space [45] compounds the problem, inhibiting both delivery of systemic antibiotics and compromising host defenses [10,37]. Sequestra present a favorable, inert environment for harboring bacteria and allowing their unmitigated persistence in the protected avascular wound space [45]. Bacterial persistence in the protected avascular space can lead to progressive acute and chronic osteomyelitis. Alternatively, localized delivery of antibiotics directly to the site of infection is commonly

embodied by (1) surgical debridement with an antibiotic solution [10]; (2) application of antibiotic solutions to bone grafts by soaking; and (3) implantation of antibiotic-loaded bone cements. Given that over 500,000 orthopedic procedures annually use bone graft materials to restore lost bone mass and support the tissue bed for implantation [37,38,52], utilizing bone graft void filler (BVF) as an implanted drug delivery vehicle represents a viable strategy to treat PJI.

Controlled drug delivery directly to bone presents an unsolved pharmacokinetic challenge. A strictly biomaterials-based approach has proven inadequate to address infection [48]; improved approaches to implant-centered infection must integrate and exploit local, rate-controlled antimicrobial delivery with appropriate bone defect filler materials. Without a controlled delivery strategy on-board, current antibiotic loaded orthopedic graft materials (antibiotic loaded bone cement (ALBC), OsteoSetT (Wright Medical, Memphis, TN, USA) release their antibiotic payloads too quickly (i.e., 1–4 days), often leaching insufficient antibiotic and serving as a nidus of infection. Additionally, most of these do not support host bone ingrowth [44,53,54]. Previously, we endowed BVF with an antibiotic-releasing polymer barrier capable of releasing its payload in vitro and in vivo for up to eight weeks [55–57] as a moldable solid composition. Unfortunately, as with many other antibiotic releasing BVF devices, our device did not allow host bone ingrowth. Additional efforts proved that host bone ingrowth can be enhanced by intimal contact with the BVF [58]. Thus, designing a space-filling BVF putty with a custom polymer composition to control local antibiotic delivery provides a significant advantage [59,60].

2.3. Materials and Methods

2.3.1. Custom Polymer Synthesis

The synthesis of monomers and polymers is based on previously described procedures [61,62]. Synthesis of 3a (Figure 2.2): Mono-*tert*-butyl protected succinic acid (5.57 g, 32 mmol), Ethyl-3-(3-dimethylaminopropyl)carbodiimide HCl (EDC, 6.60 g, 34.4 mmol) and anhydrous dimethyl formamide (DMF, 30 mL) were added into a 250 mL flask and the mixture was stirred for 10 min in an ice bath. To this activated carboxylic acid, compound 1 (8.81 g, 24.6 mmol) dissolved in anhydrous DMF (5 mL) was added and the reaction was stirred overnight. After reacting, DMF was removed under vacuum and the product was extracted with ethyl acetate (EtOAc, 150 mL). The organic layer was washed with water (50 mL, 1×), saturated $NaHCO_3$ solution (50 mL, 1×) and brine (50 mL, 1×) and dried over anhydrous Na_2SO_4. The product was purified by column chromatography (15% EtOAc and 85% Hexane).

Yield: 70%: 1H NMR (300 MHz, Chloroform-d) ppm 0.04–0.06 (m, 12H) 0.88–0.90 (m, 18H) 1.45 (s, 9H) 2.56 (t, J = 6.74 Hz, 2H) 2.67 (t, J = 6.58 Hz, 2H) 3.48 (t, J = 5.70 Hz, 2H) 3.56 (t, J = 5.86 Hz, 2H) 3.74 (t, J = 5.70 Hz, 4H).

Deprotection of *t*-butyl dimethyl silane (TBDMS) was performed by reaction with iodine (20% weight of product) in methanol (MeOH) (15 mL) overnight. $Na_2S_2O_3$ was added dropwise to quench the reaction until the solution turned from brown to colorless. The solvent was removed under vacuum and the product was extracted with CH_2Cl_2 (50 mL, 3×) and dried over anhydrous Na_2SO_4. The product was purified via column chromatography (MeOH-CH_2Cl_2 gradient solvent system, from pure CH_2Cl_2 to 5% MeOH and 95% CH_2Cl_2).

Diol 3a: Yield: 61%, ^{1}H NMR (300 MHz, Chloroform-d) ppm 0.04–0.06 (m, 12H) 0.88–0.90 (m, 18H) 1.45 (s, 9H) 2.56 (t, *J* = 6.74 Hz, 2H) 2.67 (t, *J* = 6.58 Hz, 2H) 3.48 (t, *J* = 5.70 Hz, 2H) 3.56 (t, *J* = 5.86 Hz, 2H) 3.74 (t, *J* = 5.70 Hz, 4H).

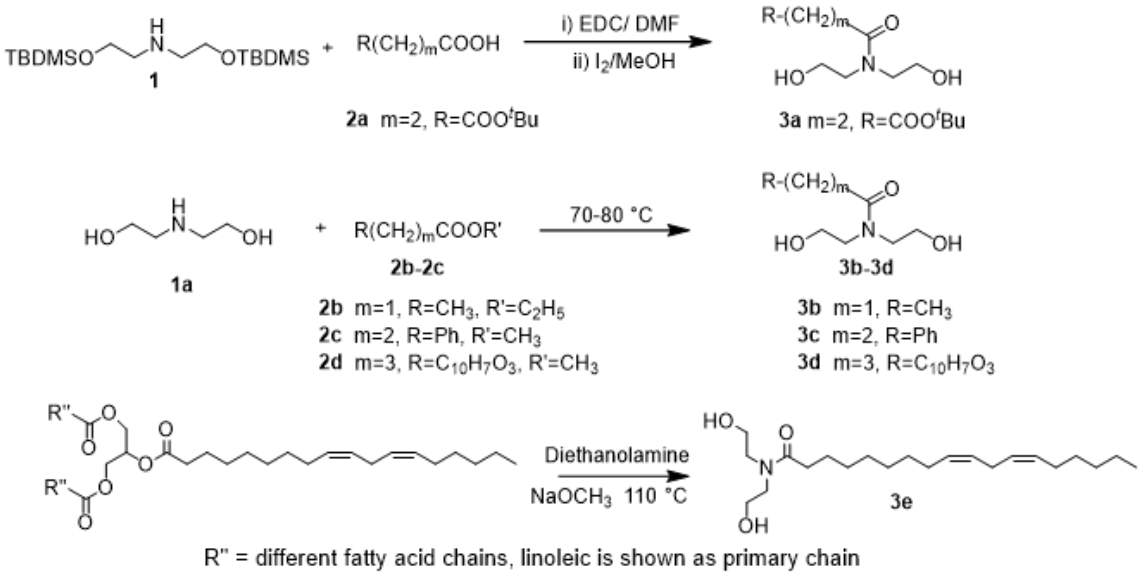

Figure 2.2. Synthesis of diols with different pendant groups.

To synthesize diols from ester derivatives of functionalized carboxylic acids (Figure 2.2), diethanolamine **1a** (2 equivalents) and the ester derivative of functionalized carboxylic acid (1 equivalent) were mixed and refluxed in a flask at 75 °C overnight. The product was subsequently purified by column chromatography (MeOH–CH_2Cl_2) and completely dried in high vacuum line.

Diol **3b**: Yield = 76%, ^{1}H NMR (300 MHz, $CDCl_3$): ppm 1.16 (dd, 3H, *J1* = 7.61 Hz, *J2* = 7.32 Hz), 2.39–2.50 (m, 2H), 3.50–3.59 (m, 4H), 3.78–3.90 (m, 4H).

Diol **3c**: Yield = 63%, ^{1}H NMR (300 MHz, $CDCl_3$) ppm 2.65–2.74 (dd, *J*1 = 7.61 Hz, *J*2 = 8.20 Hz, 2H), 2.95–3.00 (dd, *J*1 = 7.99 Hz, *J*2 = 8.20 Hz, 2H), 3.42 (t, *J* = 4.98 Hz, 2H), 3.54–3.57 (dd, *J*1 = 4.39 Hz, *J*2 = 4.98 Hz, 2H), 3.70 (t, *J* = 4.98 Hz, 2H), 3.85 (t, *J* = 4.68 Hz, 2H), 7.21–7.32 (m, 5H).

Diol 3d: ^{1}H NMR (300 MHz, Chloroform-d) ppm 2.2 (M, 2H) 2.4 (d, *J* = 1.2 Hz, 3H) 2.65 (t, *J* = 7.0 Hz, 2H) 3.53‑3.62 (m, 4H) 3.81 (t, *J* = 5.3 Hz, 2H) 3.91 (t, *J* = 5.2 Hz, 2H) 4.12 (t, *J* = 6.0 Hz, 2H), 6.14 (d, *J* = 1.2 Hz, 1H) 6.82‑6.89 (m,2H) 7.50 (d, *J* = 8.8 Hz, 1H).

To synthesize the soybean oil monomer, diethanolamine (31.5 g, 0.3 mol) was added into a 500 mL round bottom flask. Subsequently, $NaOCH_3$ (0.8 g, 14.8 mmol) was added and stirred at 110 °C until completely dissolved. Soybean oil (43.6 g) was added dropwise via funnel over 30 min. After addition, the reaction was stirred for another one hour at 110 °C under vacuum. EtOAc was added to dilute the reaction mixture, which was then washed with 15% NaCl solution (3×). The product was purified via column chromatography (5% MeOH and 95% CH_2Cl_2).

Diol 3e: ^{1}H NMR (500 MHz, Chloroform-d) ppm 5.30–5.41 (m, 2.88H) 3.76–3.85 (m, 5.5H) 3.49–3.85 (m, 4H) 2.76–2.81 (m, 1.29H) 2.37–2.40 (t, *J* = 7.70 Hz, 2.09H) 2.00–2.07 (m, 3.38H) 1.63 (br. s., 2.11H) 1.26–1.1.39 (m, 18H) 0.87–0.99 (m, 3H).

Polyesterification of functionalized diols and diacids (Figure 2.3) was accomplished by adding the functionalized diol (1 equivalent), diacid (1 equivalent) and 4-(Dimethylamino)pyridinium 4-toluenesulfonate (DPTS, 0.4 equivalent) into a flask, and the system was evacuated and backfilled with N_2 (3×). Anhydrous CH_2Cl_2 (2 mL for 1 mmol of diacid) was syringed into the reaction flask. The mixture was homogenized by warming to 40 °C for 1–2 min. Subsequently, the mixture was cooled on ice and diisopropylcarbodiimide (DIC) (3 equivalents) was added dropwise by syringe. The mixture was stirred for 48 h at room temperature. The polymer was purified by precipitation from cold *iso*-propanol/methanol or dialysis against MeOH and dried under vacuum. Total equivalents of diols were equivalent to that of diacid if more than one functionalized diol was used in the reaction.

p(A-C4): ^{1}H NMR (300 MHz, Chloroform-d) ppm 1.15 (t, *J* = 7.46 Hz, 3H) 2.39 (d, *J* = 7.46 Hz, 2H) 2.62 (br, 4H) 3.60–3.70 (m, 4H) 4.22–4.26 (m, 4H). M_n = 60 KDa, PDI = 1.1, T_d: 238 °C, T_g: 5.3 °C.

p(A-C10): ^{1}H NMR (500 MHz, Chloroform-d) ppm 1.14 (t, *J* = 7.34 Hz, 3 H) 1.29 (br. s., 8 H) 1.56–1.64 (m. 4 H) 2.22–2.35 (m, 4 H) 2.39 (q, *J* = 7.34 Hz, 2 H) 2.66–2.77 (m, 1 H) 3.58–3.64 (m, 4 H) 4.18–4.26 (m, 4 H) M_n: 78 KDa, PDI: 1.19, T_d: 283 °C, T_g: −32 °C.

p(SC-C6): ^{1}H NMR (300 MHz, Chloroform-d) ppm 0.87 (d, *J* = 6.8 Hz, 3H) 1.27 (d, *J* = 18.4 Hz, 16H) 1.59 (s, 15H) 2.04 (q, *J* = 6.2 Hz, 3H) 2.16 (t, *J* = 6.0 Hz, 2H) 2.39–2.30 (m, 12H) 2.59 (t, *J* = 7.0 Hz, 2H) 2.76 (t, *J* = 6.0 Hz, 1H) 3.61 (dt, *J* = 11.0, 5.5 Hz, 8H) 4.11–4.08 (m, 2H) 4.19 (d, *J* = 5.0 Hz, 7H) 5.34 (d, *J* = 5.5 Hz, 3H), 6.11 (s, 1H) 6.87–6.80 (m, 2H) 7.49 (d, *J* = 8.6 Hz, 1H) M_n: 11.9KDa, PDI: 2.13, T_d: 320 °C, T_g: −20 °C.

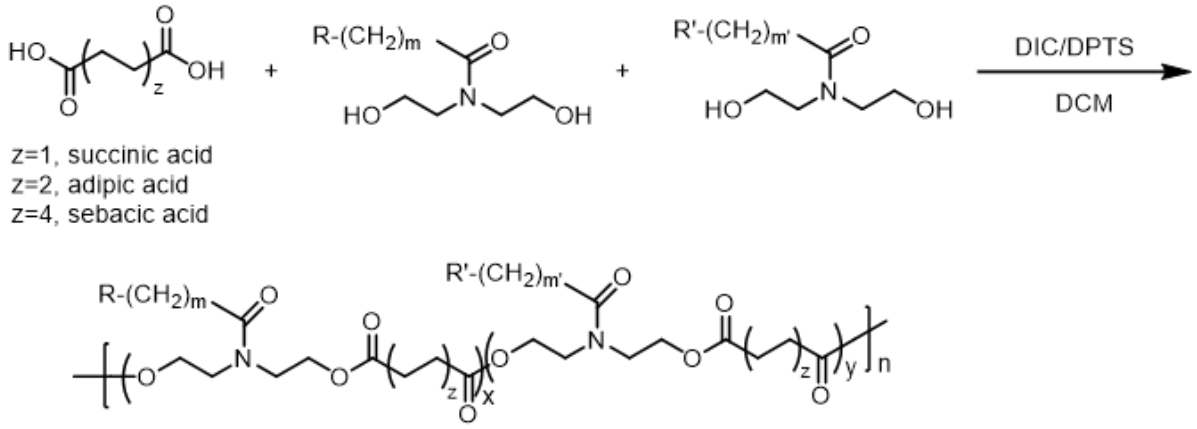

p(A-C4): R=R'=CH_3, m=m'=1, z=1
p(A-C10): R=R'=CH_3, m=m'=1, z=4
p(SC-C6): R-$(CH_2)_m$=soybean oil chain, R'=$C_{10}H_7O_3$, m'=3, z=2, x=y=0.5
^{t}Bu protected p(FD-C10): R=Ph, m=2, R'=COO^{t}Bu, m'=2, z=4, x=0.8, y=0.2

Figure 2.3. Synthesis of pendant functionalized polyesters.

Finally, the tBu-protected p(FD-C10) was deprotected by dissolving the polymer (1 g) in regular CH_2Cl_2 (6 mL), trifluoroacetic acid (TFA) (3 mL) and triisopropylsilane (50 μL) and

stirred for 2 h. After the stirring incubation, TFA and CH_2Cl_2 were removed under vacuum and the polymer was precipitated into diethyl ether twice to obtain pure polymer.

p(FD-C10): ^{1}H NMR (500 MHz, Chloroform-d) ppm 1.25–1.36 (m, 8H) 1.53–1.65 (m, 4H) 2.22–2.35 (m, 4H) 2.64–2.76 (m, 2.4H) 2.94–3.01 (m, 2.4H) 3.52 (t, J = 5.87 Hz, 2H) 3.58–3.69 (m, 2H) 4.12 (t, J = 5.75 Hz, 2H) 4.18–4.26 (m, 2H) 7.16–7.24 (m, 2H) 7.24–7.31 (m, 2H) M_n: 40KDa, PDI: 1.34, T_d: 273 °C, T_g: −16 °C.

2.3.2. Polymer Characterization

Structures of small molecules and polymers were confirmed by 300 and 500 MHz Nuclear magnetic resonance (NMR) proton spectra via a Varian NMRS instrument (Palo Alto, CA, USA). Deuterated chloroform was used as a solvent. Chemical shifts, δ (ppm), were referenced to the residual proton signal.

The molecular weight and polydispersity index for each custom polymer was measured via gel permeation chromatography (GPC). GPC analysis in tetrahydrofuran (THF) was performed on a Waters 150-C Plus instrument (Milford, MA, USA) equipped with refractive index and light scattering detector. Polystyrene was used as a standard. GPC analysis in DMF was performed on an HLC-8320 instrument (King of Prussia, PA, USA) equipped with refractive index and UV detectors using polystyrene as a standard. The flow rate of the eluent was 1 mL/min for both GPC instruments.

The polymer's decomposition temperature was measured by thermal gravimetric analysis (TGA) with a TA Q500 thermal gravimetric analysis instrument (TA Instruments, New Castle, DE, USA). Each polymer was heated in N_2 from room temperature to 600 °C with a heating rate of 10 °C /min. Alternatively, the glass transition temperature was tested by differential scanning

calorimeter (DSC) using TA Q2000 differential scanning calorimeter (TA Instruments, New Castle, DE, USA) with heating and cooling rates set at 10 °C/min.

ABVF putties were fabricated similarly to our previous molded formulations [55–57] with a couple of critical distinctions to produce a material with a putty-like consistency. Four of the putty formulations contained Pro Osteon 500R™ (Biomet, Irvine, CA, USA) morselized and sieved to between 150 and 425 micrometers; a combination of polymer binders Poly(d,l-lactide-*co*-glycolide) (PLGA-50:50, Sigma Aldrich, St. Louis, MO, USA) dissolved in *N*-Methyl-2-pyrrolidone (NMP, Fisher, Pittsburg, PA, USA), Poly ethyleneglycol (PEG-5kD, Fluka, St. Louis, MO, USA); and polycaprolactone (PCL-10kD); calcium chloride as a porogen, and vancomycin. Note that vancomycin from two different manufacturers was used in different formulations: (1) Vancomycin HCl Sterile Lyophilized Powder for Injection (Hospira, Inc., Lake Forest, IL, USA); and (2) Vancomycin HCl; Research Products International (RPI) (Mount Prospect, IL, USA). PLGA was dissolved in NMP (200 μL) and added to a homogenous mixture of molten PCL and PEG at ~75 °C. BVF, calcium chloride and vancomycin were mixed into the polymer composition and 20 μL of 1x phosphate buffered saline (PBS) was added to produce a putty-like composite. Additional, ABVF putty formulations were created using custom-made polymers (as described above). Briefly, polymers were heated to ~120 °C and Pro Osteon 500R™, calcium chloride, and vancomycin were added. Pro Osteon 500R™ is a cancellous bone like, osteoconductive matrix consisting of calcium carbonate and hydroxyapatite. The addition of NMP and PBS were not necessary to create a putty-like composite from the custom polymers. With the exception of formulation 2, which was shaped into a single large sphere, all formulations were made as single batches and partitioned into replicates (as indicated in Table 1)

using 2 mm diameter × 1.7 mm depth adhesive silicone isolators to form small ABVF disks. One large sphere was also made for formulation 2. Formulations are detailed in Table 2.1.

Table 2.1. Formulations prepared with different polymers.

Formulation (number of replicates)	Geometry	Polymer(s)	NMP	CaCl2	Vancomycin (10% w/v)
1 (n=6)	disk	PLGA/PCL/PEG	x	x	RPI
2 (n=1)	sphere	PLGA/PCL/PEG	x	x	RPI
3 (n=6)	disk	PLGA/PCL/PEG	x	x	Hospira
4 (n=4)	disk	p(FD-C10)		x	Hospira
5 (n=2)	disk	p(SC-C6)		x	Hospira
6 (n=3)	disk	p(A-C4)		x	Hospira
7 (n=2)	disk	p(A-C10)		x	Hospira

The source of vancomycin is noted in the last column. All formulations had the same ratio of components in the final formulation. The first two letters of the custom polymers (4–6) indicate the amino acid mimic (A—Alanine, F—Phenylalanine, D—Aspartic acid), whereas the second part denotes the number of carbon atoms in the diacid. The polymer p(SC-C6) contains two non-natural pendant groups.

2.3.3. Imaging

Both the small cylindrical disk as well as the larger sphere were imaged using scanning electron microscopy imaging. Additionally, the cylindrical disk was imaged using micro computed tomography (µ-CT) at the North Dakota State University (NDSU) Electron Microscopy Center core facility (Fargo, ND, USA).

2.3.4. Micro Computed Tomography (µ-CT)

The sample was hot glued to a glass rod and placed into a GE Phoenix v|tome| xs X-ray computed tomography system with a 180 kV high power nanofocus X-ray tube xs|180 nf, high contrast GE DXR250RT flat panel detector, and molybdenum target (GE Sensing & Inspection Technologies GmbH, Wunstorf, Germany). One thousand projections were acquired at a voltage of 80 kV and a current of 300 µA. Voxel size was 6.4 µm. Acquired images were reconstructed

into a volume data set using GE datos|x 3D computer tomography software Version 2.2 (GE Sensing & Inspection Technologies GmbH, Wunstorf, Germany). The reconstructed volume was then viewed and manipulated using VGStudio Max (Volume Graphics Inc., Charlotte, NC, USA).

2.3.5. Scanning Electron Microscopy (SEM)

Samples for scanning electron microscopy (SEM) were cut with a razor blade to expose the interior surfaces, attached to cylindrical aluminum mounts with colloidal silver paint (Structure Probe Inc., West Chester, PA, USA) and coated with gold (Cressington Inc., Redding, CA, USA) or with carbon (Cressington Inc.). Images were obtained with a JEOL JSM-6490LV scanning electron microscope or JEOL JSM-7600F field-emission scanning electron microscope (JEOL USA, Inc., Peabody, MA, USA).

2.3.6. In Vitro Drug Release

Three molded ABVF cylindrical disks from both putty formulations 1 and 3 were released after curing 24 h at 4 °C, whereas the three remaining ABVF disks were released after one week at 4 °C. The ABVF putty cylindrical disk released after 24 h weighed an average of 45.6 mg (STDV (standard deviation): 4.925). Cylindrical disks were placed in individual 2 mL microcentrifuge tubes containing 2 mL of PBS for six weeks at a constant temperature of 37 °C. PBS was replaced at 24, 48, and 72 h and every week thereafter for a total of six week as previously described [55,63]. At the end of 6 weeks, the remaining ABVF putty samples were dissolved in 1 mL of dichloromethane and 500 µL water, vortexed for 15 s, and centrifuged for 5 min at 15,000 rpm to separate the aqueous layer. The aqueous layer was then collected, to determine presence of unreleased vancomycin. The extracted PBS samples and residual vancomycin in the aqueous layer were then analyzed to determine the amount of vancomycin

released and its bioactivity. Alternatively, the large sphere from the entire formulation 2 batch (710 mg) was placed in a 50 mL conical tube and the drug was released into 5 mL of PBS as described for the smaller cylindrical disks.

2.3.7. In Vitro Vancomycin Release Kinetics

The amount of vancomycin released into PBS or the amount of residual vancomycin left in the device after release was determined using a custom-built detector as previously described [64]. Briefly, a 280 nm wavelength light emitting diode (LED) and a photodiode were mounted in a cuvette holder, machined from aluminum such that light from the LED passed through the chamber and into the photodiode aperture. Light that reaches the photodiode was converted into a voltage and read by an analog to digital converter (ADC). A computer, along with supporting circuitry, controlled the entire system. The amount of vancomycin was calculated based on a standard curve. The data were then fitted to different pharmacokinetic models [65].

2.3.8. Kirby Bauer Zone of Inhibition Assay (ZOI)

A standard Kirby Bauer zone of inhibition (ZOI) assay was performed [56,66]. In addition, 100 µL of release solution from each time point was dried on filter paper disk (6.5 mm diameter) before being placed on Trypticase Soy Agar plates (TSA) with an average depth of 4.7 mm [63] and spread with a uniform bacterial field of *Staphylococcus aureus* strain 49230 (12×10^7 CFU). Standard vancomycin concentrations (8 mg/mL serially diluted to 0.0625 mg/mL) and PBS blanks were prepared in same fashion as release solution. Plates were inverted and incubated at 37 °C for up to 20 h before diameter of zone of inhibition was recorded via electronic calipers.

2.3.9. Mechanical Characterization

ABVF constructs from formulation 1 with (n = 3) and without (n = 3) vancomycin and from formulation 4 (n = 2) were assessed for their putty-like characteristics using a Bose 3200 load frame (TA Instruments, New Castle, DE, USA) with supplied compression surfaces. A 225N load cell with Wintest software (TA Instruments, New Castle, DE, USA) was used for data collection. Supplied Bose compression surfaces were used in the compressive tests. However, a custom designed and built fixture was used to test the tackiness of the samples in a tensile lap test. This fixture consisted of two 16 gauge 304 stainless blanks, which were placed in grips. The blank held in the bottom grip had a toggle clamp bolted to it, which provided consistent sample thicknesses. The toggle clamp had a foot, which used a roller bearing to provide clamping force but provide minimal drag to the test. Each sample (26–41 mm^3) was compressed to create a uniform cylinder of 2.45 mm in diameter and 4.8–8.9 mm in height. Samples were tested on the same day they were fabricated.

2.3.9.1. Compression Testing

Compression tests were run at a rate of 0.1 mm/s. Samples were pressed in the longitudinal direction while the load frame measured strain and load. True stress, which calculates stress based on a changing area, was calculated by solving for the changing contact area in relation to the changing height, assuming constant sample volume. The average and standard deviation was calculated for each formulation.

2.3.9.2. Tensile Lap Testing

Each material was compressed in the aforementioned lap-testing fixture. Each sample was placed on the upper stainless plate and the lower plate with toggle clamp was clamped

compressing the sample to a thickness of 0.77 mm. Each test was conducted at a rate of 0.1 mm/s.

2.3.10. Statistical Analysis

Averages and standard error mean are reported. Any pairwise comparisons presented were done via ANOVA with significance of $\alpha < 0.05$.

2.4. Results

Combinations of common biomedical polymers or four custom-designed, pendant-functionalized polyesters were used to create seven different ABVF putty formulations (Table 1). ABVF putty formulations 1–3 were made as a composite of polymers (i.e., PEG, PCL, PLGA) generally regarded as safe (GRAS) for biomedical applications. To develop an ABVF device with putty-like consistency, previously described methods [55–58] were modified to include NMP [67]. Alternatively, customized polyesters were synthesized with appropriate pendant groups to enable optimum hydrophobicity or specific interactions to obtain desired release and degradation properties over a 6–8 weeks period. Polymers were synthesized as shown in Figures 2 and 3 and characterized as outlined in Materials and Methods. ABVF putties made with these custom polymers did not require the use of NMP or other co-polymer binders. μ-CT and SEM imaging was done to assess (1) the homogeneity of composition; (2) percentage of pro osteon particles in the ABVF composition; and (3) qualitative porosity (Figure 2.4). By adjusting the grey-scale contrast and setting a threshold, the volume of mineral composition was calculated to be ~28.3% v/v from the μ-CT. The actual composition of the formulation was 63% w/w. The composition seems homogeneous by looking at pro osteon particles distribution in polymers matrix.

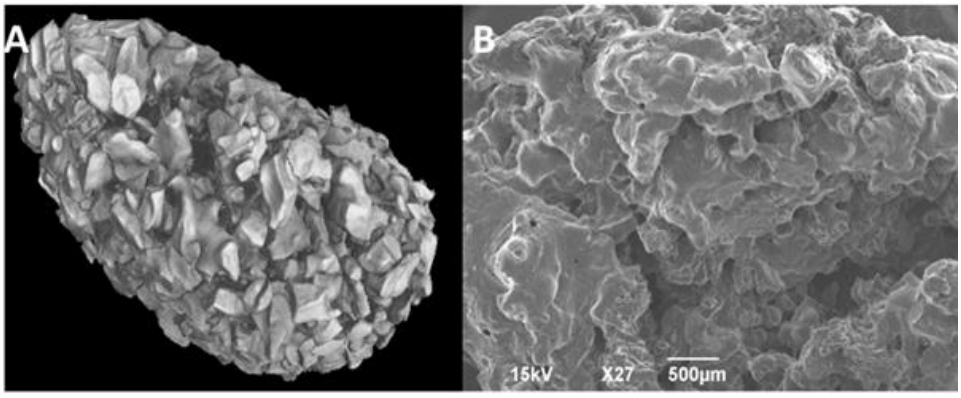

Figure 2.4. µ-CT image of ABVF putty.
The homogeneity of the composition, percent of ABVF, and the porosity of the ABVF putty was determined for a model formulation of a PCL/PEG/PLGA putty using microCT on a small cylindrical disk (A); and SEM through the center of a large sphere (B).

In each of the custom polymers (4–6, Table 1), the first two letters indicate the pendant amino acid mimic (A—Alanine, F—Phenylalanine, D—Aspartic acid), whereas the second part denotes the number of carbon atoms in the diacid. Polymer p(SC-C6) contains two non-natural pendant groups. The amounts of pendant-functionalized polymers were limiting, and thus all other components of the BVF putty composition were altered to maintain the ratios previously reported [63] in these pilot scale formulation. p(FD-C10) had a honey-like consistency and was light sensitive; thus, it was protected from light until it was used in ABVF fabrication. These samples were released or tested the same day and were protected from light during release. Duplicate formulations without vancomycin were made as a negative control (data not shown). There was no bioactivity from any of the control formulations without drugs. Incorporating polymers with different pendant groups and therefore various physical properties as the bulk matrix of an antibiotic-loaded BVF device showed (i) that there was no intrinsic antimicrobial activity for this set of polymers; (ii) p(FD-C10), p(SC-C6), and p(A-C4) were all able to release vancomycin for over one month, with p(SC-C6) (formulation 5) exhibiting the lowest burst release (Figure 2.5) and zero order drug release kinetics (Table 2.2); and (iii) unlike the

commercially available polymer formulation, and ABVF formulation with custom polymers displayed evidence of a heterogeneous composition (appendix A, Table A1).

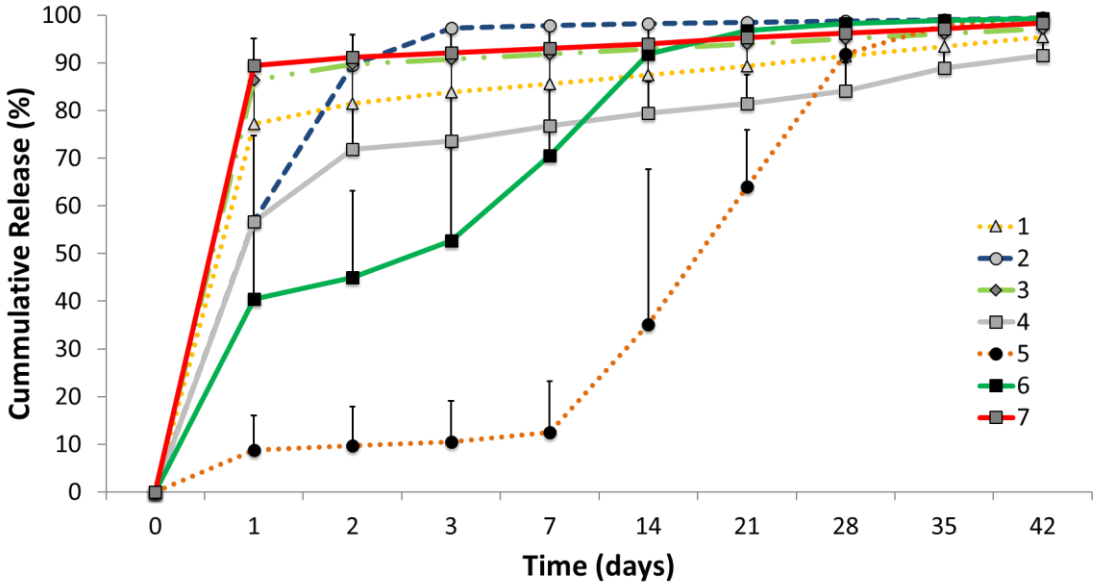

Formulation	3P (disk)	3P (sphere)	3P (disk)	pF10	pS6	pA4	pA10
% released in the first 24 hours	77.2	56.8	86.4	56.7	8.7	40.5	89.4

Figure 2.5. Vancomycin release kinetics for each formulation are shown in the line graph. One of the major distinctions in the formulations is the percent of drug released in the first 24 h. Note that formulation 2 was a larger sphere while all other formulations are smaller cylindrical disks. Standard error mean is shown for each formulation.

Vancomycin was released in vitro from a newly developed bone void filling putty that used a varied composition of polymer binders for up to six weeks, a time point considered critical by the orthopedic community for infection prevention [46]. The cumulative percent of vancomycin released was plotted over time (Figure 2.5). Formulation 1 and formulation 3 only differed in the source of vancomycin incorporated. However, based on the kinetics and bioactivity data, there is no statistical difference between different sources of vancomycin. Formulations 1 and 2 only differ in the geometry and size of the device. The larger spherical device released a little more than half as much drug in the first 24 h as its smaller cylindrical disk counterpart. Additionally, bioactivity of vancomycin released from the larger sphere was

extended from three days to two weeks (data not shown), likely as a result of the increased amount of drugs in the larger device. The cumulative percent of vancomycin released at each time point was averaged to produce an average pharmacokinetic curve (Figure 2.5), which was subsequently evaluated against zero-order, first-order, Korsmeyer–Peppas, Higuchi, and Hixon–Crowell models and the best fit, based on R^2 value, was used to determine the mode of release and the importance of geometry and polymer composition (Table 2.2). A similar analysis was performed for each individual replicate (Appendix A Table A1).

Formulations 1 and 3, which only differ in the source of vancomycin used, showed no significant difference and displayed homogeneous composition as each individual replicate as well as the average all followed the Korsmeyer–Peppas model, which indicated that vancomycin was released from the matrix by both erosion and diffusion. Formulation 2, which only varied in its size and geometry from formulation 1, fit a first-order kinetic model more than any other model. This may indicate that dissolution from the matrix is dependent on the concentration of the dissolving species; however, this supposition remains to be confirmed with additional replicates. The average vancomycin release from formulation 4 is most closely modeled by the Korsmeyer–Peppas equation; however, individual replicates vary between first order and Korsmeyer–Pappas, indicating a lack of homogeneity (Appendix A Table A1). Formulation 5 closely follows both zero order and Hixon–Crowell with zero order kinetics being slightly favored. This observation again likely reflects that the individual replicates vary between zero order and Hixon–Crowell release models. Nevertheless, this particular formulation provided consistent bioactivity throughout the experimental time course. Formulation 6, which also provided bioactivity throughout the experimental time course, followed both first order and Korsmeyer–Peppas models individually, favoring first order kinetics slightly on average.

Table 2.2. Vancomycin release kinetics from different ABVF formulation fitted into different drug release kinetics model

Formulation	Zero Order (R2)	First Order (R2)	Korsmeyer-Peppas (R2)	Higuchi (R2)	Hixson-Crowell (R2)
1	0.15	0.45	0.93	0.30	0.28
2	0.26	0.61	0.51	0.46	0.45
3	0.14	0.42	0.88	0.29	0.25
4	0.28	0.68	0.92	0.45	0.52
5	0.92	0.88	0.86	0.84	0.91
6	0.70	0.97	0.96	0.88	0.90
7	0.16	0.59	0.96	0.32	0.33

For calculation, the amount of vancomycin was plotted against time on the *x*-axis. The average of each formulation was then fitted to each of the common pharmacokinetic models to identify the best fit.

ZOI assay determined the bioactivity of released vancomycin against *S. aureus* over time. Using the "standard" polymer formulation of PCL, PEG, and PLGA that provided sufficient duration of bioactivity from a solid molded BVF form [55–57] was insufficient to provide bioactivity past seven days as a BVF putty formulation (Figure 2.6). However, when the polymer matrix and drug-releasing barrier was a custom, pendant-functionalized polymer, bioactivity could be extended to between 35 and 42 days, dependent on the identity of the polymer and geometry of the putty (Figure 2.6).

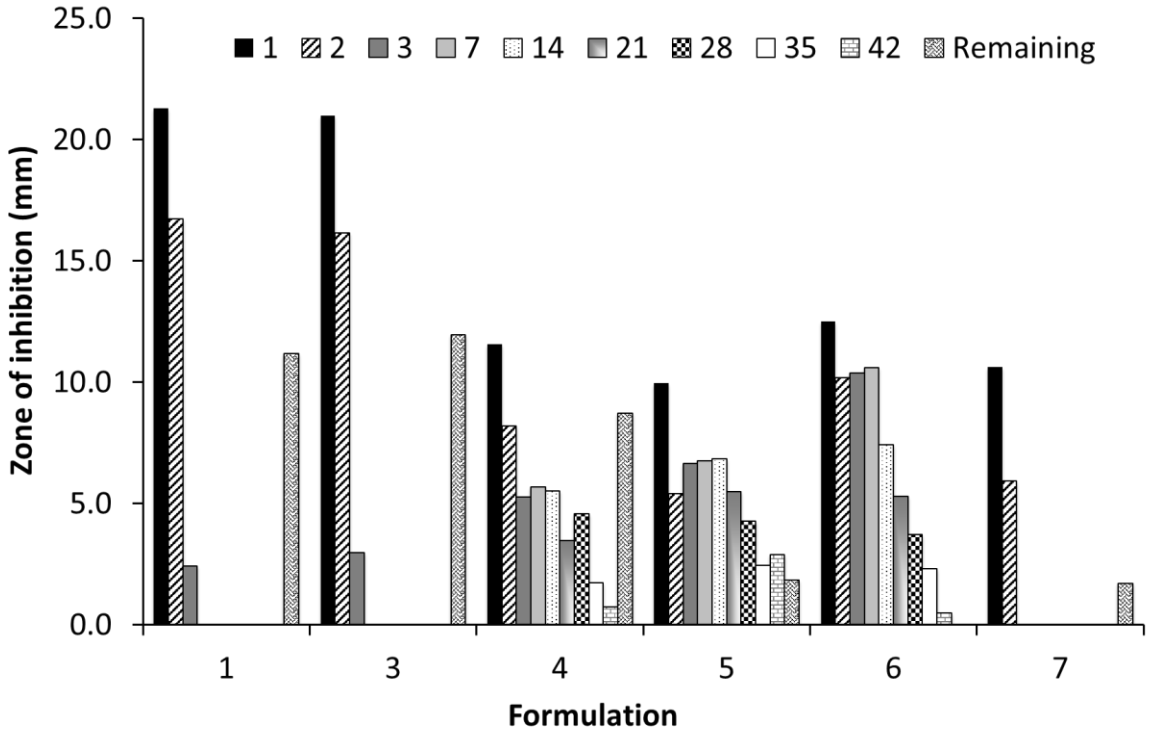

Figure 2.6. The bioactivity of released vancomycin was determined via a Kirby Bauer zone of inhibition study.
Release studies were done for six weeks. At the conclusion of the study, the remaining drug was extracted from the putty. Bioactivity was seen throughout the experimental time course in formulations 4–6.

ABVF from the two most qualitatively disparate formulations based on their stiffness: the commercial polymer formulation (formulation **1**) and custom polymer p(FD-C10) (formulation 4), were mechanically evaluated as model formulations to characterize the new composition as a putty. Each sample was compressed into a cylinder prior to testing as described in Materials and Methods. A combination of compression (Figure 2.7) and tensile lap testing (Figure 2.8) were used to assess the composition's plastic deformation and adhesion, critical elements in putty-like behavior. Qualitatively, formulation **1** without drugs was very easy to manipulate into shape and was the softest of the three materials, whereas formulation **1** with drug was firmer and did not deform as easily. Interestingly, despite its viscous honey-like consistency, formulation **4** was the hardest to deform and did not compress into the uniform cylinders as easily. Additionally,

formulation 1 with or without the addition of vancomycin kept their shape after being compressed into a cylindrical shape but formulation **4** expanded in a longitudinal direction and did not hold its shape after being removed from the cylindrical mold. Compression of formulation **1** with or without drugs shows how easily deformable the material was, with very low stresses being required to produce deformation. As shown in Figure 2.7 A, formulation **1** with drugs had a proportional, elastic-like, stress-strain relationship to a strain of 0.1. The material then exhibited plastic deformation past strains of 0.1. Surprisingly, compressive behavior changed in the absence of vancomycin and higher strain or 0.8 was required to plastically deform the cylindrical material (Figure 2.7 B). Formulation **4** gave a linear elastic stress-strain relationship to a strain of approximately 0.4 at which time the response changed to plastic deformation (Figure 2.7 C). Tensile lap testing, which assessed the "stickiness" of the composition, showed that formulation **4** was able to maintain almost twice the amount of force when compared to formulation **1** either with or without drugs (Figure 2.8).

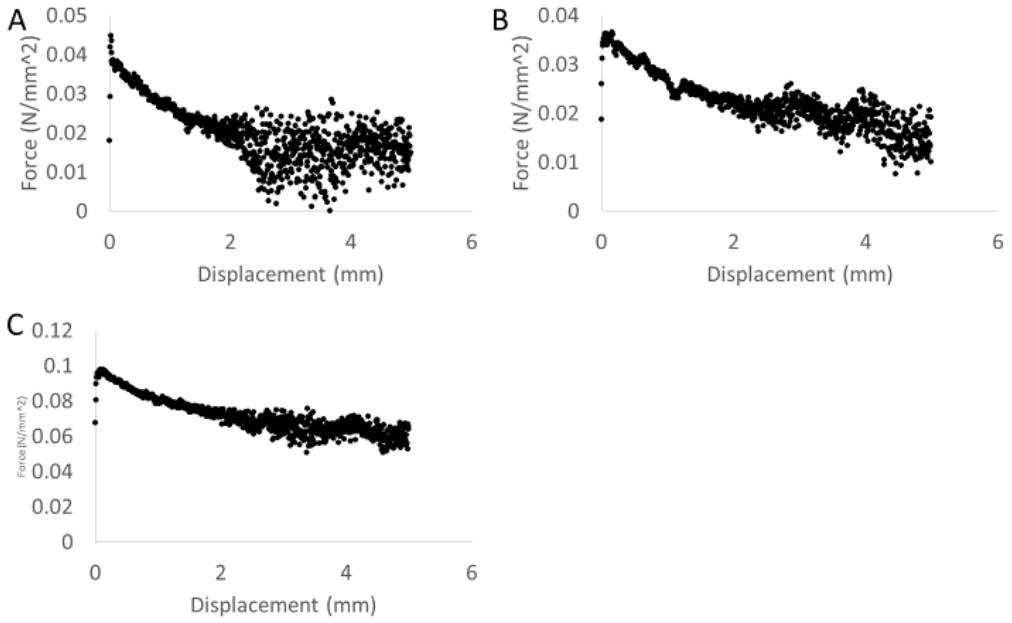

Figure 2.7. Compression tests with different formulations.
Formulation 1 with drugs (A) and without drugs (B) as well as formulation 4 with drugs. Notice that the compression behavior of the composition changes quite a bit in the absence of vancomycin and can withstand more stress prior to plastic deformation.

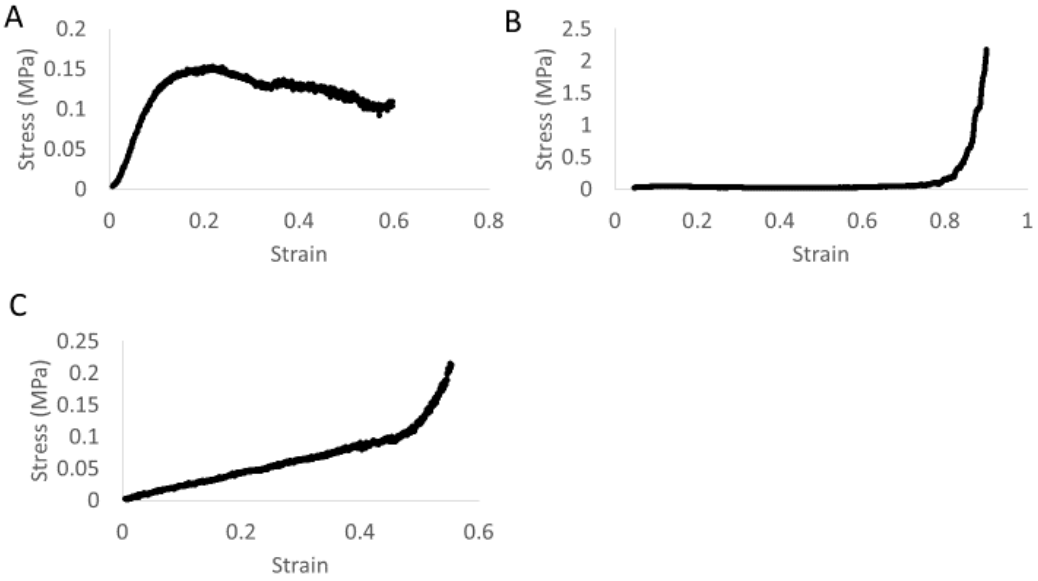

Figure 2.8. Tensile lap tests with different formulations.
Formulation 1 with drugs (A) and without drugs (B) as well as formulation 4 with drug to assess the "stickiness" of the composition. Notice that formulation 4 can withstand almost twice the stress with a corresponding strain.

2.5. Discussion

Osteomyelitis is a complex condition with multiple etiologies that necessitate new, tailorable strategies (Figure 2.9). Previously, polymer-controlled, antibiotic-releasing, moldable BVF devices proved effective in preventing infection in a rabbit radial defect model. Unfortunately, the solid polymer BVF composite material did not provide intimate contact with the host bone and little cellular infiltration was noted. Thus, a putty composition with similar drug release kinetics was produced. Current bone cements used for orthopedic procedures requiring some mechanical robustness, such as methyl methacrylate in TJR, contain acrylic oligomers or monomers to provide low viscosity pliable composites [68]. The high heat of reaction from these materials can cause tissue necrosis. Alternatively, the use of synthetic polymers such as those previously used to create a solid, moldable, BVF formulation [55–58] may not be suitable for BVF putties due to their high modulus. Hence, we assessed four custom pendant-functionalized polyesters. Formulations 4 and 5 seemed to have particularly useful pharmacokinetics and will be followed up with a more rigorous statistically significant study. Clinically accepted polymers previously used for BVF drug delivery have a specific set of physical properties that cannot be tuned to the application. Therefore, polymers whose physical and chemical properties can be tailored to the in vivo environment are desperately needed.

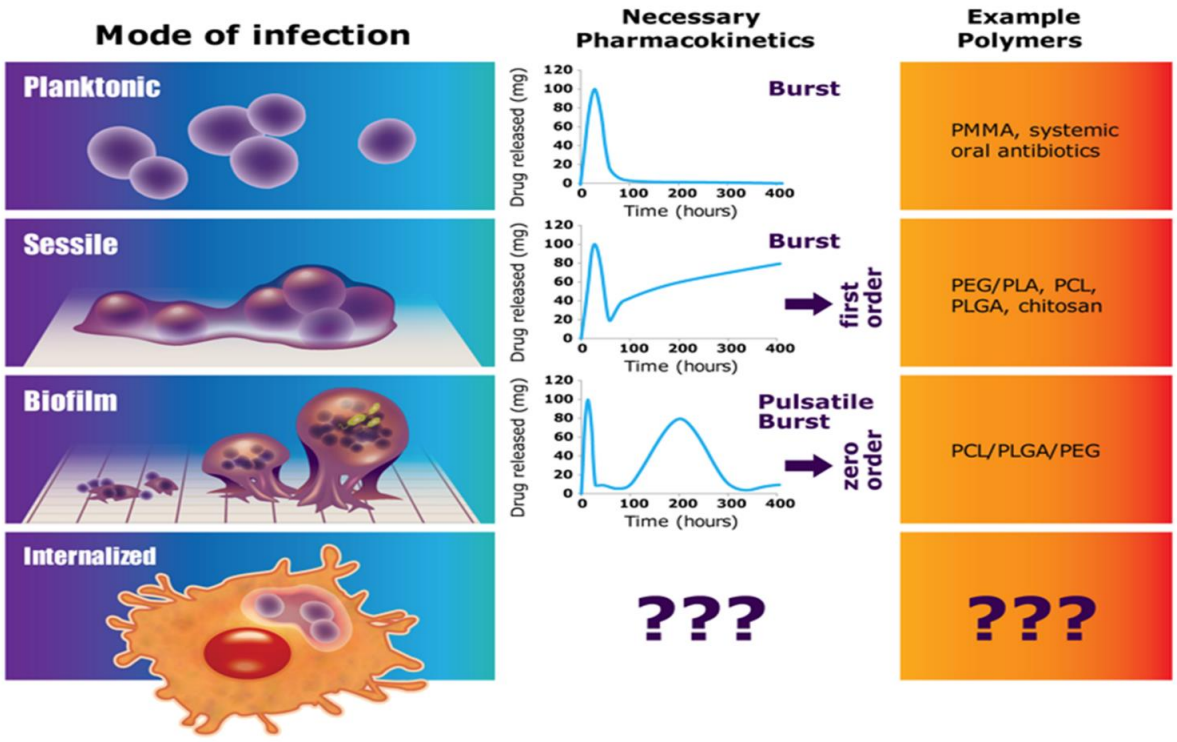

Figure 2.9. Osteomyelitis etiologies and relevant drug release pattern for treatment graphical representation.
There are four relevant modes of infection related to total joint replacement. Planktonic bacteria-sourced infections can be combatted with simple burst release kinetics such as that provided by bone cements (i.e. poly(methyl methacrylate, PMMA) or systemic antibiotics. After attaching to a surface, sessile bacteria are slightly more difficult to treat and typically require a first-order or zero-order sustained release after the burst. To combat biofilm resident bacteria, a pulsatile burst with zero-order kinetics are thought to be essential. Such sustained release formulations may be provided using combinations of polymers such as that described here. The most challenging orthopedic infections, recurring chronic osteomyelitis, will require distinctly new approaches with new polymer compositions (e.g., pendant-functionalized polymers, etc.).

Previously, a platform of peptidomimetic polyesters whose physical and chemical properties can be modulated over a wide range of properties was developed [62]. These polyesters are characterized by the presence of "peptide-like" pendant functional groups at every repeat unit, providing a set of tailorable polymers with functionality to suit the application need. The polyesters were designed to mimic the functional diversity of peptides. The currently reported polymers have significantly lower glass transition temperatures (Tg) than the previous polyesters and hence allow fabrication of drug-encapsulated putties at lower temperatures. This

is critical for future efforts, which may encapsulate heat sensitive drugs. The polyester, p(SC-C6), with pendant groups having long aliphatic chains lead to polymers with very low T_g. Additionally, the nature of the diacid also influences the T_g of the polymers. Polymerization of the functionalized diols with long chain diacids such as sebacic acid lowers the T_g of the polyesters such as p(A-C10). However, unlike polypeptides, the ester backbone ensures hydrolytic degradation and bioresorption, the rate of which can be tuned by the identity of the pendant group. In addition, the polyesters were designed to avoid any hydrogen bonding, which makes the polymers easier to process. The modular synthesis of the polyester platform has enabled the design of such polymers for various applications such as thermoresponsive polymers [61]; polyesters for room temperature 3D printing (accepted, in press); wet adhesives (submitted) and extracellular matrix (ECM) mimetic electron spun matrices for controlled release applications (unpublished).

The physical properties of the polyesters can be engineered by polymerization of appropriately functionalized monomers to provide low-viscosity materials. To achieve the range in properties needed for these studies, the choice of pendant-functionalized diols and the nature of diacids was varied. The identity of the pendant functionalized diol influences the hydrophobic/hydrophilic balance of the polymer and gates the release rate of the encapsulated drug. For example, polyesters having succinic acid (C_4) will be more hydrophilic and have a higher modulus than the corresponding polyesters made from sebacic acid (C_{10}). Therefore, these high molecular weight polymers can be mixed with the bone filler without the use of any organic solvent. The release profiles of a putty-encapsulated therapeutic can be gated utilizing polyester pendant groups (Figures 2.5 and 2.6) and provide altered pharmacokinetic and bioactivity profiles, unattainable using single composition common biomaterials such as PCL or PLGA.

Importantly, in each formulation 10% *w/w* of vancomycin was added. Thus, the amount of vancomycin varied with the weight of the BVF composite device. However, except for the larger formulation 2 sphere, all replicates weighed roughly 50 mg, providing an accurate comparison of the pharmacokinetics. Nevertheless, variation in the amount of vancomycin incorporated cannot be completely ruled out as a contributing factor to the varied pharmacokinetic profiles seen, particularly considering the apparent heterogeneity of certain formulations.

Using a mix of commercial polymers to create an ABVF putty allowed for a good comparison with previously formulated moldable ABVF fabricated from the same polymer composition. In vitro pharmacokinetics from the moldable ABVF provided antimicrobial activity for up to six weeks [56,58], whereas the analogous composition formulated as a putty only provided effective antimicrobial activity for three days (Figure 2.6). Although the mechanical criteria to identify a composite as a putty is not clear, putties are generally agreed to have temperature dependent viscoelastic properties and undergo plastic deformation. For the purpose of this study, a putty is defined by its low stress/low strain plastic deformation as well as a "tacky" or "sticky" texture. Due to the high deformability of each sample, true stress was used as opposed to engineering stress as it was determined to be more accurate since the cross-sectional area of the ABVF changes under stress. Although stress-strain curves in each of the three samples differed (Figure 2.7), each material exhibited putty like behavior. Samples required relatively low stress to result in measurable strain. Formulations **1** and **4** had the most disparate properties of all formulations; thus, they were evaluated to (1) confirm that they should be classified as putty and (2) define protocols and procedures for putty characterization. Importantly, in tensile tests of formulation 1 with and without drugs, the force fluctuated a lot in displacements above 2. Additionally, the maximum force at the beginning of the test seemed to

drift, necessitating additional replicates. Nevertheless, the methodology was able to reveal differences and indicated that the putty used in formulation 4 was stickier (Figure 2.8) than the polymer combination used in formulation 1.

The PCL/PEG/PLGA composition seemed susceptible to the effect of geometry, as evidenced by a shift from the Korsmeyer–Peppas model (formulations **1** and **3**) [69] to a first-order kinetic model (formulation **2**) although even this R^2 value is not high and may indicate a mixed mode of release, not uncommon in composite polymers. The Korsmeyer–Peppas model indicates release of the drug from a matrix by a combination of diffusion and erosion. The Higuchi model describes the release of a drug from a matrix tablet by diffusion, whereas the Hixson–Crowell model describes release by erosion. Based on the average of formulation **5**, a zero-order release model, which is typically associated with long-duration sustained drug release, is slightly favored, but the Hixson–Crowell model is also closely followed; this closely follows the disparity between individual replicates, which indicate that despite efforts to create a homogenous composition, there was variability. Variability was a common issue for the replicates of formulation 6 as well, which, on average, slightly favored a first-order release model. Additional replicates are necessary to verify which model is more closely followed. Additionally, future efforts must control heterogeneity of composition. Formulations 4 and 7 clearly followed the Korsmeyer–Peppas model more closely.

Using a combination of confirmed and in silico derived models is a powerful approach in controlled-drug delivery formulation development, providing a mechanism to consider each element of the composition (i.e., drug, polymers and additives) to attain a particular pharmacokinetic profile by theoretical means [70]. Unfortunately, even though they are useful to describe drug release kinetics in terms of a classic pharmacokinetic model, these theoretical

models lack predictive use. Alternatively, using in silico tools such as Quantitative Structure–Activity Relationship (QSAR) analysis and other molecular modeling tools [71–73] (e.g., Schrodinger, Monte Carlo simulations, Molecular Docking, etc.) to quantitatively correlate relationships between trends in chemical structure alterations and respective changes in biological endpoints (i.e., which chemical properties are determinants of biological activities), the number of compounds to be synthesized can be minimized by selecting the most promising candidates [72], [73], [74]. In silico modeling of drug release kinetics may streamline formulation optimizations to address the most challenging clinical cases of TJR-associated infection (Figure 2.9) where *S. aureus* enters the osteoblast to avoid antibiotics and the host immune system. Currently, in silico efforts are underway using Schrodinger software (NY, USA) to create relevant polymer models of vancomycin release.

2.6. Conclusions

The work presented here represents a logical extension of our previous moldable antibiotic-releasing, polymer controlled BVF device [56]. By including either NMP or using low T_g custom polymers, a promising putty-like composition was created to locally deliver bioactive vancomycin over 42 days, ultimately facilitating effective treatment for orthopedic *S. aureus* infection. Using the strategies presented here, additional polymers can be developed to tailor the pharmacokinetic profile of vancomycin release and begin to tackle the most challenging chronic and invasive infections.

3. AN ANTIBIOTIC RELEASING BONE VOID FILLER (ABVF) PUTTY FOR THE TREATMENT OF OSTEOMYELITIS[2]

3.1. Abstract

Not only is the number of Total Joint Replacements (TJR) on the rise, but there is a corresponding increase in the number of infected TJRs, which are the major cause of revision surgeries. Unfortunately, the rate of recurring infection after a primary infected TJR revision is much higher (20% -30%). Current treatments with either antibiotic releasing PMMA based bone cement or systemic antibiotic after surgical debridement do not provide effective treatment due to fluctuating antibiotic levels at the site of infection. In addition, non-biodegradable PMMA needs to be removed by additional surgery. Here we report a biodegradable, easy to use "press fitting" Antibiotic-Releasing Bone Void Filler (ABVF) putty that not only provides efficient antibiotic pharmacokinetics at the site of infection but also allows efficient osseointegration. The ABVF formulation was homogenous, had a porous structure and showed putty like mechanical properties. Furthermore, the ABVF putty showed in vitro antibacterial activity for up to 6 weeks. Finally, the ABVF putty was biodegradable in vivo and showed effective infection control with the ABVF treatment group showing significantly higher bone growth ($p<0.009$) compared to the control group. The potential of infection treatment and osseointegration makes ABVF putty a promising treatment option for osteomyelitis after TJR.

---

[2] The material in this chapter was co-authored by Raquib Hasan, Abbey Wohlers, Jacob Shreffler, Pranothi Mulinti, Hunter Schleske, Codi Schaper, Benjamin Brooks and Amanda Brooks. Raquib Hasan and Amanda Brooks conceived and designed the experiments. Raquib had primary responsibility to conduct all the experiments listed in the section, analyze the data and write the manuscript. Abbey Wohlers and Pranothi Mulinti collected drug release samples and helped with in vitro antibacterial activity experiment. Jacob Shreffler, Hunter Schleske, Codi Schaper helped with animal care and in vivo study. µ-CT and SEM imaging was done by Jayma Moore and Dr. Scott Payne, Dr. Lisa Christenson helped with X-ray imaging. Dr. Ganesh Balasubramanian performed the HPLC analysis. Bradley Hoffmann helped with rheology. Dr. Pawel Borowicz helped with microscopy. Raquib Hasan analyzed the data and Amanda Brooks verified the data. Raquib Hasan wrote the manuscript, Amanda Brooks checked and revised the document.

Keywords: Osteomyelitis; total joint replacement; bone void filler; antibiotic release; controlled drug delivery; bone regeneration

3.2. Introduction

Currently, in the United States over a million people undergo Total Joint Replacements (TJR) each year [5] [6] [7]. This number is projected to exceed 4 million primary procedures each year by 2030 [6]. Although, TJRs, including Total Knee Replacements (TKR) and Total Hip Replacements (THR), are arguably some of the most successful surgical practices to improve quality of life, secondary or revision surgeries are becoming commonplace. Furthermore, with the success of TJR, primary TJR procedures are occurring at an earlier age [75] [76], often necessitating a revision during the patient's lifetime as the synthetic TJR materials age. According to the American Academy of Orthopedic Surgeons (AAOS), there is an increase in revision surgery. In fact, 365,000 secondary or revision procedures are projected by 2030 [6]. Aseptic loosening, implant age, and infection are major contributors to the rate of revision. Among the list of contributing factors, infection is a major, and perhaps the most concerning, cause for TJR revision, responsible for 18% of revision THR and 26.8% of revision TKR. Infection also causes the majority of early implant failures (within 3 months of primary surgery) (18.9% for THR and 44.8% for TKR) [77] [78] . Regardless of the underlying cause of the revision, the complexity of a revision procedure makes it less successful than primary TJR surgery [79]. Risk of infection after revision surgery is alarmingly high at 21%, after septic revision; whereas, in case of aseptic revisions the risk sits at 5.4% (compared to 1-2% after primary TJR) [8]. Unfortunately, implant removal and hardware replacement drives the risk of infection to a staggering 20-30% [9,10].

Osteomyelitis, or a deep, progressive bone infection, is a clinically difficult to treat condition [80]. *Staphylococcus aureus* is the most common causative pathogen of prosthetic joint infection (PJI) after TJR, responsible for ~ 65% of total cases, out of which 20% are methicillin resistant *S. aureus* (MRSA) [81] [78]. Current clinical treatment strategies include thorough surgical debridement followed by 4-6 weeks of parenteral antibiotic therapy as well as antibiotic-loaded Polymethylmethacrylate (PMMA) based bone cement for local antibiotic delivery [82]. Surgical debridement almost always leaves residual bacteria necessitating continuous, local antibacterial activity for a prolonged period of time [83]. Notably, local antibiotic therapy at the site of infection not only provides high local drug concentration but also helps avoid systemic side effects [82]. Such localized antibiotic therapy is often provided by antibiotic releasing PMMA. Unfortunately, antibiotic PMMA has several disadvantages such as: low antibiotic release rate (less than 10% antibiotic release), poor biocompatibility, lack of biodegradability, which may necessitate an additional surgery for removal. In fact, inadequate drug release kinetics and sub-therapeutic dug concentrations eluted from PMMA may lead to antibiotic resistance [17]. Importantly, there is a current impetus to move towards cementless TJR compared to cemented TJR due to the longevity, mitigated failure, and higher bone density around the implant in the case of cementless TJR [84]. Developing an antibiotic ABVF putty to fill defects created after debridement to prevent and cure infections after revision TJR [85] seems to be a necessity to fulfill the role of a local antibiotic release. A putty-like ABVF composition can meet this need and facilitate ease of use. Moreover, biodegradable bone void fillers can work as a scaffold to guide tissue regeneration and infection regression as they degrade [86].

Vancomycin, formerly a “last line of defense” antibiotic, is now common place in the treatment of osteomyelitis and its underlying pathogen, MRSA [87]. Unfortunately, when used

parenterally, vancomycin has poor bone penetration and only a fraction of the drug reaches the bone having a bone/serum ratio of 10%, with even lower penetration in osteomyelitic bone [88]. Furthermore, extended, high-dose intravenous therapy with vancomycin can lead to nephrotoxicity and red man syndrome [89]. Local release of vancomycin not only can achieve high local antibiotic concentrations but also avoids systemic side effects. The current study evaluated the in vitro vancomycin release and in vivo potential of ABVF putty to be used to treat osteomyelitis, demonstrating both antibacterial protection as well as osseointegration and healing of local bone tissue.

3.3. Materials and Methods

3.3.1. Materials

PLGA (90:10) (poly(D,L-lactide-co-glycolide)) was purchased from Polysciences, Inc., Warington, PA, USA; PEG (5 kD) (polyethylene glycol) was purchased from, Fluka, St. Louis, MO, USA); PCL (10 kD) (polycaprolactone) from Sigma-Aldrich, St. Louis, MO, USA; Vancomycin Hydrochloride (V-HCl) from Sagent Pharmaceuticals, Schaumburg, IL, USA, NMP (N-Methyl-2-pyrrolidone) from Fisher Sci, Pittsburg, PA, USA; $CaCl_2$ (calcium chloride) from EMD Chemicals Inc., Gibbstown, NJ, USA and PRO OSTEON 500R was kindly provided by BIOMET, Parsippany, NJ, USA, MTT (3-(4,5-dimethylthiazol-2-yl)-2,5-diphenyltetrazolium bromide) (VWR, Radnor, PA, USA), TRIzol reagent (Life Tech, Carlsbad, CA, USA), SuperScript™ VILO™ cDNA Synthesis Kit (Thermo-Fisher Scientific, Carlsbad, CA, USA).

3.3.2. Preparation of Vancomycin Free-Base (V-fb)

V-fb was made from V-HCl according to previously published method [90]. Briefly, V-HCl was dissolved in water at concentration of 70 mg/mL. NaOH (3N) was added to increase the pH to 8.00 and precipitate V-fb. After incubation of 30 minutes, the precipitated V-fb was

centrifuged at 3000 rpm for 10 minutes. After washing the V-fb in sequential 70% ethanol and methanol, the V-fb was suspended in water, frozen and lyophilized. Validation of V-fb was done by HPLC (appendix B, Figure B2.1). The bioactivity of V-fb and V-HCl was also compared via a Zone of Inhibition (ZOI) assay (appendix B, Figure B2.2).

3.3.3. Fabrication of ABVF Putty and In Vitro Characterization

3.3.3.1. Preparation of ABVF

PRO OSTEON 500R was crushed and sieved to get a particle size distribution of 175 to 425 μm. The PRO OSTEON particles (350 mg) were soaked in V-HCl solution (100 mg/mL) and were dried at 37 C. The polymers, PEG (21.2 mg) and PCL (42.5 mg), were melted and mixed at 65 C in a steel slide mold. V-HCL soaked and dried PRO OSTEON particles were added into the molten polymers to create a homogenous mixture. At this point, V-FB (vancomycin free-base) (55.5 mg) was added to the mixture. Subsequently, PLGA (85.5 mg) dissolved in 200 μL of N-Methyl-2-Pyrrolidone (NMP) and 22 mg $CaCl_2$ (used as porogen) were added to the mixture. Phosphate buffered saline (PBS) was added (20 μL) dropwise to produce a putty-like consistency. This master mix was put into a 3D printed mold to get the desired size and cylindrical shape (4 mm diameter x 3.5 mm height) to be used for further studies.

3.3.3.2. Scanning Electron Microscopy (SEM) of the ABVF Putty

SEM was done on the putty to observe the morphological characteristics of outer and inner surface of ABVF. SEM images of the surface and the inside (exposed by cutting the ABVF with razor blade) of the ABVF putty were taken after fabrication, one week of incubation in PBS and four weeks of incubation in PBS to observe the degradation of the putty. The samples were attached to cylindrical aluminum mounts with colloidal silver paint (Structure Probe Inc., West

Chester, PA, USA) followed by gold coating (Cressington Inc., Redding, CA, USA). Images were taken with a JEOL JSM-6490LV scanning electron microscope.

3.3.3.3. Micro Computed Tomography (µ-CT) of ABVF Putty

The sample was hot glued to a glass rod and placed into a GE Phoenix v|tome| xs X-ray computed tomography system with a 180 kV high power nanofocus X-ray tube xs|180 nf, high contrast GE DXR250RT flat panel detector, and molybdenum target (GE Sensing & Inspection Technologies GmbH, Wunstorf, Germany). One thousand projections were acquired at a voltage of 80 kV and a current of 300 µA. Voxel size was 6.4 µm. Acquired images were reconstructed into a volume data set using GE datos|x 3D computer tomography software Version 2.2 (GE Sensing & Inspection Technologies GmbH, Wunstorf, Germany). The reconstructed volume was then viewed and manipulated using VGStudio Max (Volume Graphics Inc., Charlotte, NC, USA).

3.3.3.4. Mechanical Characterization

Mechanical compliance was characterized using a rheometer (ARG2, TA Instruments, New Castle, DE, USA). ABVF putty-like material was used to cover the bottom plate of the rheometer (25 mm diameter). Frequency was increased from 6.283 and 628.3 rad/s, and strain within the viscoelastic region (determined by strain sweep) was applied. A demonstration of its putty-like characteristic was also determined by press-fitting the material into different 3D printed shapes.

3.3.3.5. In Vitro Drug Release Kinetics

Drug release was determined by incubating ABVF putty in PBS as drug release media. ABVF (4 mm x 3.5 mm) was put into 2 mL of PBS (1x) and was incubated at 37 C. At different time points (day 1, day 2, day 3, day 7 and every week after that through 6 weeks), all of the

release media was collected and replaced with fresh PBS. The vancomycin concentration in the release was measured by UV-vis spectrometer (Spectramax m5, Molecular Devices, Downingtown, PA, USA) at 280 nm.

3.3.3.6. In vitro Antibacterial Activity

In vitro antibacterial activity of the released drug was assessed against *Staphylococcus aureus* (ATCC 49230) using a Kirby-Bauer ZOI assay [91]. Briefly, 100 μL of the collected drug release media was dried on a 6.5 mm diameter filter paper disk. An overnight *S. aureus* culture was prepared and diluted in PBS to get a 10^7 CFU/mL bacterial concentration. The bacteria solution was streaked on TSA plates and the drug impregnated filter paper disks were placed on the plates (within 15 minutes of streaking) and incubated for 20 hours at 37 C. The ZOI around the disk was measured using a digital caliper.

3.3.3.7. In vitro Cytocompatibility of ABVF Putty

In vitro cytocompatibility of ABVF putty was assessed via MTT assay. Briefly, 100,000 MG-63 osteoblast cells (ATCC, Manassas, VA) were seeded in each well of a 24-well plate. Cells were grown in Dulbecco's Modified Eagle Media (DMEM) containing 10% fetal bovine serum (FBS) and 1% penicillin-streptomycin-fungizone (Lonza, Walkersville, MD, USA). Cells were incubated at 37 C and 5% CO_2. After reaching 60% confluence, 500 μL of release media from ABVF was added to each well. Control wells received PBS. After 48 hours of incubation with ABVF release media, cells were washed with PBS 3 times and the MTT reagent (0.5mg/mL in PBS) was added. Subsequently, wells were incubated at 37C for 4 hours. After incubation, the cells were washed with PBS and dimethyl sulfoxide (DMSO) was added followed by 20 minutes of incubation in the dark. After this final incubation, the absorbance was read at 570 nm (Spectramax m5, Molecular Devices, Downingtown, PA, USA). Alternatively, to determine the

direct effect of drug release on cells, ABVF was placed in transwell inserts in wells of 24 well plates and enough cell culture media was added to submerge the ABVF in the inserts. Putty containing no antibiotic was used as control. After 48 hours of incubation, the MTT assay was done to determine the cell viability as the described method above.

3.3.4. In Vivo Assessment

3.3.4.1. Rat Osteomyelitis Model

A rat osteomyelitis model was performed under the supervision of the Institutional Animal Care and Use committee at North Dakota State University (A19019). Sprague-Dawley rats (>350 grams) were used for the in vivo study. Briefly, rats were anesthetized with isoflurane inhalation. Buprenorphine hydrochloride was injected subcutaneously as an analgesic. The right hind leg was shaved and sterilized using alcohol and iodine pads, repeatedly. A small incision of ~ 12 mm was made below the knee over the tibial metaphysis. A 4.2 mm hole was drilled until it penetrated the marrow space of the tibial metaphysis using an orthopedic drill (Stryker, Kalamazoo, MI, USA). *S. aureus* (10^8 CFU) in sterile saline was inoculated through the drill hole defect into the marrow space using a 25 μL Hamilton syringe followed by implantation of the ABVF putty. The incision was closed using a series of mattress sutures followed by application of surgical glue (Vetbond Tissue Adhesive, 3M, MN, USA). The control group underwent the same surgical procedure but only received the putty without antibiotic. Rats were monitored daily for signs of discomfort and infection. After 10 weeks, the rats were sacrificed, and the tibia was harvested for further study. Blood and kidney were also collected for further study.

3.3.4.2. Serum Creatinine

Blood collected from the rats at the time of euthanasia was centrifuged at 2000g (Allegra X-14R, Beckman Coulter, Brea, CA, USA) to collect the serum. Serum was used to measure the

creatinine level using an enzymatic rat creatinine assay kit (Crystal Chem, IL, USA) following the manufacturer's protocol.

3.3.4.3. X-ray and µ-CT

Radiographic analyses of bone were done after disarticulating the limb and harvesting the bone following euthanasia. X-ray was done using IDEXX CR Digital Radiography System (Westbrook, Maine, USA) following standard protocols. Briefly, lateral and cranial-caudal radiographic images were obtained of each limb at mAs: 4 and kVp: 40. µ-CT of the bone was done following similar procedure as described in section 2.3.3 with slight adjustment of current to 400 – 500 µA.

3.3.4.4. Bone Volume

Bone volume was determined based on the µ-CT scanned bones using VGStudio Max (Volume Graphics Inc., Charlotte, NC, USA) software. A region of interest (ROI) was set on each of the scanned bones. Adjusting the contrast to highlight the bone in the ROI and comparing the ROI from the infection control group and the treatment group determined the amount of regenerated or new bone growth.

3.3.4.5. Histology

Rats were euthanized after 10 weeks. The bone was harvested by fixing it in 10% neutral buffered formalin for 72 hours. Immersing it in EDTA solution for 2 weeks, with solution exchange every other day, decalcified the bone. Taking an x-ray of the bone ensured the decalcification endpoint. The bone was sectioned after embedding it in paraffin wax. The sections were mounted on glass slides and stained with either H&E stain or gram stain according to standard protocols. Briefly, the sections were deparaffinized in Clear Rite 3 (Thermo Fisher Scientific, Kalamazoo, MI, USA). Subsequently, the tissue was rehydrated with a decreasing

gradient of ethanol. After H&E staining (Scy Tek Lab., Logan, Utah, USA), the tissue section was covered with a glass coverslip using synthetic resin. Alternatively, gram staining was done according to the manufacturer's protocol for the BD gram staining kit (Sparks, MD, USA) with slight modification. Briefly, the slide was dipped in gram crystal violet for 20 seconds followed by washing in cold tap water. Subsequently, slides were dipped into stabilized gram iodine for 20 seconds followed by washing in tap water. Gram decolorizer was used until the slide was colorless followed by washing in cold tap water. Slides were dipped in gram safranin for 15 seconds followed by washing in cold tap water. Slides were bolted to dry, and a cover slip was added.

3.3.4.6. Bacterial Colony Count

Collected bone was flash frozen in liquid nitrogen, followed by pulverization using a custom-made bone crusher (details in Appendix B, Figure 2.4). The pulverized bone was weighed and suspended in 500 μL of PBS. Serial dilutions were made [90] and 10 μL of suspension was plated on blood agar plates (Fisher Sci, Pittsburg, PA, USA). Subsequently, plates were incubated for 48 hours at 37 °C and bacterial colonies were counted. To get the total number of bacteria in the total sample, the number of colonies were multiplied by the dilution factor and normalized per gram of bone.

3.3.4.7. Polymerase Chain Reaction (PCR)

PCR was done to identify the presence of inoculated bacteria. Bacterial RNA was isolated from the pulverized bone samples using TRIZOL according to the manufacturer's instructions for RNA isolation [92] [93]. The extracted RNA was used to synthesize first strand cDNA using SuperScript™ VILO™ cDNA Synthesis Kit according to manufacturer's protocol. Primers (Forward primer: GCACATCTTGACGGTACCTAAT and reverse primer:

CGGGACTTAACCCAACATCTC) were designed to amplify 16s RNA specific for S. aureus 49230 (PCR program: 95 °C (2 min) for initial denaturation, 40 cycles of 95 °C (30 sec), 54 °C (30 sec), 72 °C (30 sec), and final extension at 72 °C (5 min)). Primers were synthesized by Integrated DNA Technologies, Inc., Coralville, IA, USA. PCR was run using Go-Taq green master mix (Promega, Madison, WI, USA) on a MultiGene™ OptiMax thermal cycler (Labnet Inc., Edison, NJ, USA). For each PCR reaction, 240 ng of cDNA was used. PCR products were examined by electrophoresis in a 1% (w/v) agarose gel and visualized by ethidium bromide.

3.4. Results

3.4.1. Scanning Electron Microscopy (SEM) of the ABVF Putty

SEM was done to see the morphology of both the outer and inner surfaces of the ABVF putty. SEM images show that ABVF has a rough outer surface (Figure 3.1 a) while the inner surface has both macro and micro porous structures (Figure 3.1 a). In vitro degradation of the ABVF putty over time was also monitored via SEM. SEM was done at day 0, day 7 and day 28 after incubation in PBS (Figure 3.1 a). The SEM images show continuous degradation of ABVF after exposure to PBS. The outer surface showed signs of degradation at day 7. At day 28 there were signs of erosion and pore formation on the outer surface due to degradation. The inner surface also showed signs of degradation and pore formation.

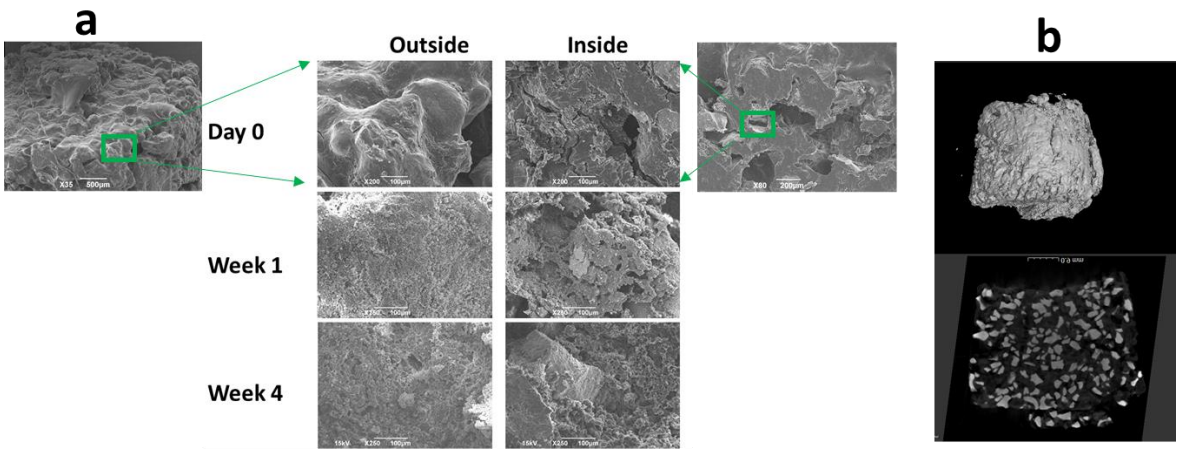

Figure 3.1. SEM and μ-CT images of ABVF putty.
(a) SEM image of ABVF after manufacturing. The outer surface is rough (top left corner) and the inner surface has pores (top right corner). SEM images of ABVF degradation in PBS at different time points, showing increasing signs of degradation on both the outer and inner surfaces of the ABVF. (b) μ-CT of ABVF shows homogenous distribution of the Pro-Osteon particles in the polymer matrix.

3.4.2. μ-CT of ABVF Putty

In vitro μ-CT was done to see the homogeneity of the formulation. Images show that the Pro-Osteon particles are homogenously mixed and distributed within the polymeric matrix (Figure 3.1 b). The v/v percentage of the pro-osteon particles in the polymer matrix is 28.23%. The percentage weight of Pro-Osteon is ~52% of the total weight of the ABVF putty. The images ensured that not only does the manufacturing of the ABVF putty produce a homogenous mixture of the ingredients but also that the process is reproducible.

3.4.3. Putty-like Mechanical Property

To evaluate the putty-like property of the ABVF, rheology was done (n=3). From Figure 3.2 a, it is clear that the loss modulus (G”) increases as the angular frequency increases, which is characteristic of a putty-like material [94]. As frequency continued to increase, the storage modulus G’ also increased. This increasing G’ signifies an elastic-solid like behavior [95]. The

ABVF putty also could be easily molded into different 3D printed shapes (Figure 3.2 b), demonstrating good press fitting, an important handling property for clinical use. During press fitting, the sticky ABVF stayed in place and maintained its structural integrity. Later, to simulate in vivo bone void space filling, a defect was made in a 3D printed rat tibia and ABVF putty was press-fitted into the defect without leaving any visible void space.

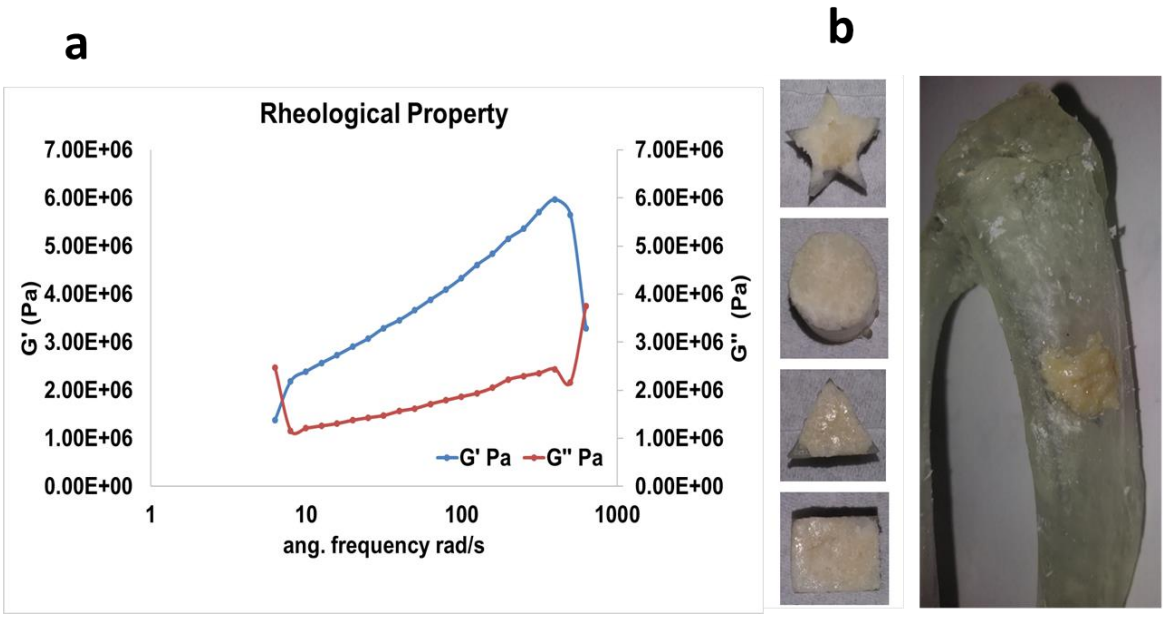

Figure 3.2. Mechanical (rheology) property and press-fitting demonstration of ABVF putty. (a) Storage (G') and loss modulus (G'') of ABVF putty at increasing angular frequency at room temperature (25 C). (b) Press-fitting of ABVF putty in different 3D printed shapes and in a defect created in a 3D printed rat tibia. The ABVF putty could be easily press-fitted into shapes and seemed to contact the surrounding surfaces completely, without leaving any void spaces.

3.4.4. In Vitro Vancomycin Release Kinetics

An in vitro drug release study was done to assess drug release over the desired six-week period. The cumulative drug release curve from the formulation described (Figure 3.3 a), which best fit the Korsemeyer-Peppas model (appendix B, Table B.1), shows desired drug release kinetics over 6 weeks. It was observed that an initial burst release of ~40% occurred during the first day of release. That may be due to the drug present near the surface of ABVF. Later, a more

sustained release was observed. There was a small burst release between day 7 and day 14, indicating that the vancomycin released from the ABVF putty through both erosion of the polymer matrix and diffusion as the release media penetrates into the putty [91]. Erosion is also evident from the SEM images of degradation where erosion and degradation created pores (Figure 3.3 a), which also might be conducive for diffusion.

3.4.5. In Vitro Antibacterial Activity

In vitro antimicrobial activity was assessed via ZOI assay against *S. aureus* (ATCC 49230). The released vancomycin showed antimicrobial activity during the study period of 6 weeks (Figure 3.3 b). Notably, vancomycin-HCl and (V-fb) showed similar bioactivity at the same concentration in ZOI assay (appendix B, Figure B2.2).

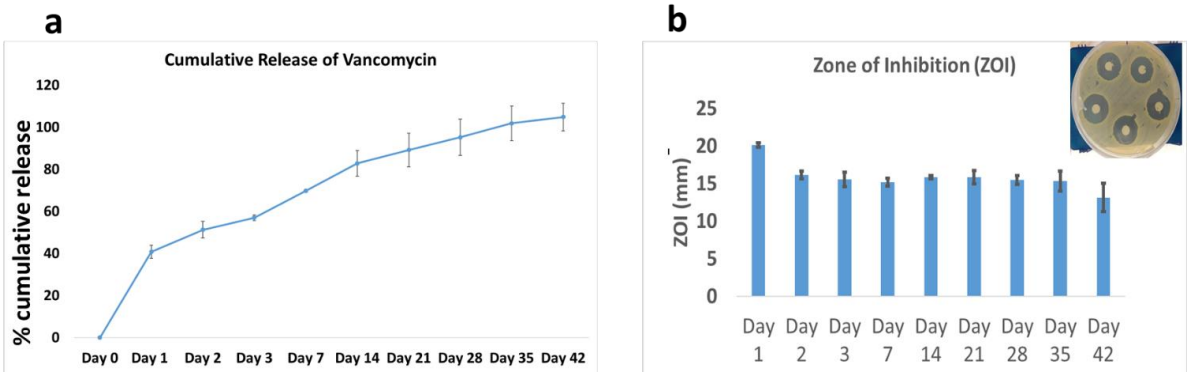

Figure 3.3. Cumulative drug release curve and Zone of Inhibition (ZOI) of released vancomycin from ABVF.
(a) Drug release kinetics of vancomycin from ABVF putty shows drug release up to 42 days (6 weeks). (b) The bioactivity of released vancomycin was determined via a Kirby Bauer zone of inhibition study against Staphylococcus aureus (strain 49230: 1.0 x 10^7 CFU/mL).

3.4.6. In Vitro Cytocompatibility of ABVF Putty

To assess whether released vancomycin is tolerated by the osteoblast cells, cytocompatibility was evaluated via the MTT assay. The MTT assay showed there was no significant difference in cell viability between the control and drug release group (Figure 3.4 a). Furthermore, when ABVF putty was placed in transwell culture with MG63 osteoblasts, cell

viability assays showed that no significant difference was found in cell viability between ABVF and the control group (Figure 3.4 b), indicating that the amount of vancomycin released is well tolerated by MG63 osteoblasts cells.

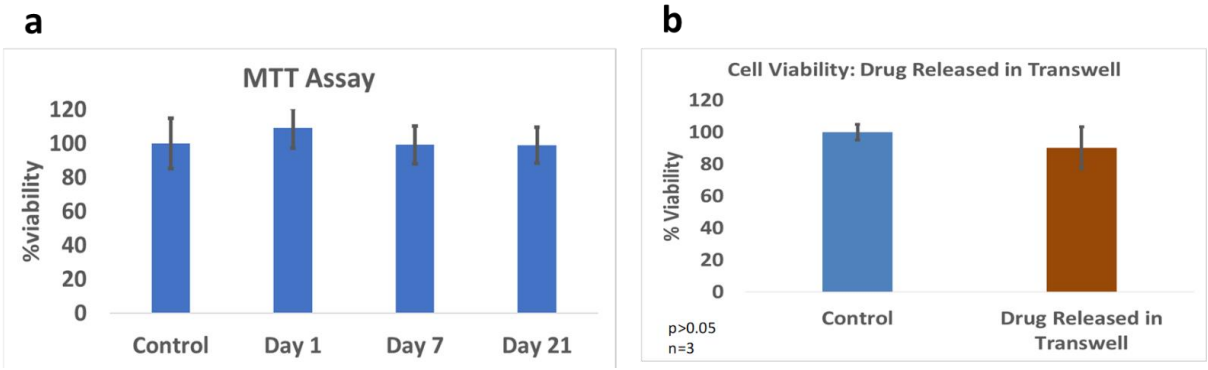

Figure 3.4. Cell viability of MG63 osteoblast cells when exposed to ABVF drug release. (a) There was no significant decrease in either cell viability of MG63 cells when the cells were exposed to different drug release samples from different time points ($\alpha = 0.05$, n= 4) or, (b) drug released from transwell inserts containing ABVF ($\alpha = 0.05$, n=3).

3.5. In Vivo Study Results

Following extensive in vitro characterization and validation, ABVF putty was implanted into a rat orthopedic drill hole defect model. Thirteen rats were implanted with ABVF putty while twelve rats were implanted with BVF putty with no antibiotic. Spontaneous fracture was seen in 3 rats (within a week of the surgery) necessitating euthanasia and removal from the study cohort. All of these 3 rats were in the control group. On an average, surgeries took about 15 minutes from incision to suturing the wound. In the case of treatment group, swelling and/or redness at surgical site seemed to resolve about a week post-surgery. However, in the control group, some rats showed drainage from the wound. Nevertheless, the temperature of all the rats seemed to be normal, and all the rats were weight bearing and steadily gained weight during the experiment.

3.5.1. Serum Creatinine

Although there was no evidence of cytotoxicity in vitro, vancomycin can potentially cause nephrotoxicity [96], especially in the case of prolonged intravenous (IV) treatment, during elimination. Thus, serum creatinine levels were measured to assess if locally released vancomycin at the surgical site would have any nephrotoxicity [97]. Serum creatinine levels in the infection treatment, infection control and no surgery control groups were within the previously reported range of 0.3-0.6 mg/ dL (Figure 3.5) [98] [99], and there were no significant difference between the groups.

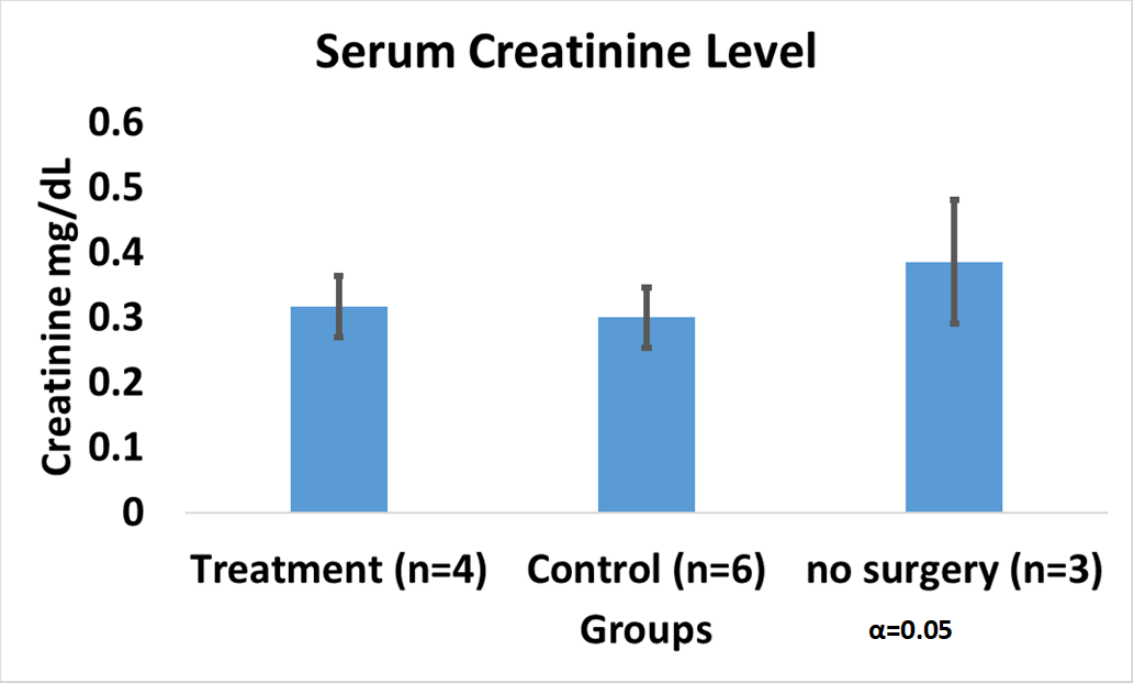

Figure 3.5. Serum creatinine level in rats of different cohorts.
Serum creatinine level shows no significant difference between infection treatment, infection control and no surgery control groups. The serum creatinine level seems to be within normal limits.

3.5.2. Radiographs – X-ray and µ-CT

Macroscopically the bones of the infection control group showed the presence of purulent discharge and sinus tracts formation. Bone deformity, periosteal reaction, narrowing of marrow

space and presence of fibrous tissue was also visible around the surgical sight (Figure 3.6 a & b). All of the observations corresponded to presence of osteomyelitis in the infection control group. In the treatment group (Figure 3.6 c & d), signs of a healing callous, no visible implant, and ongoing bone remodeling were visible. Additionally, no fibrous tissue or the presence of inflammation or purulent discharge was observed. μ-CT images show that the bone was remodeling, and the marrow space was re-established.

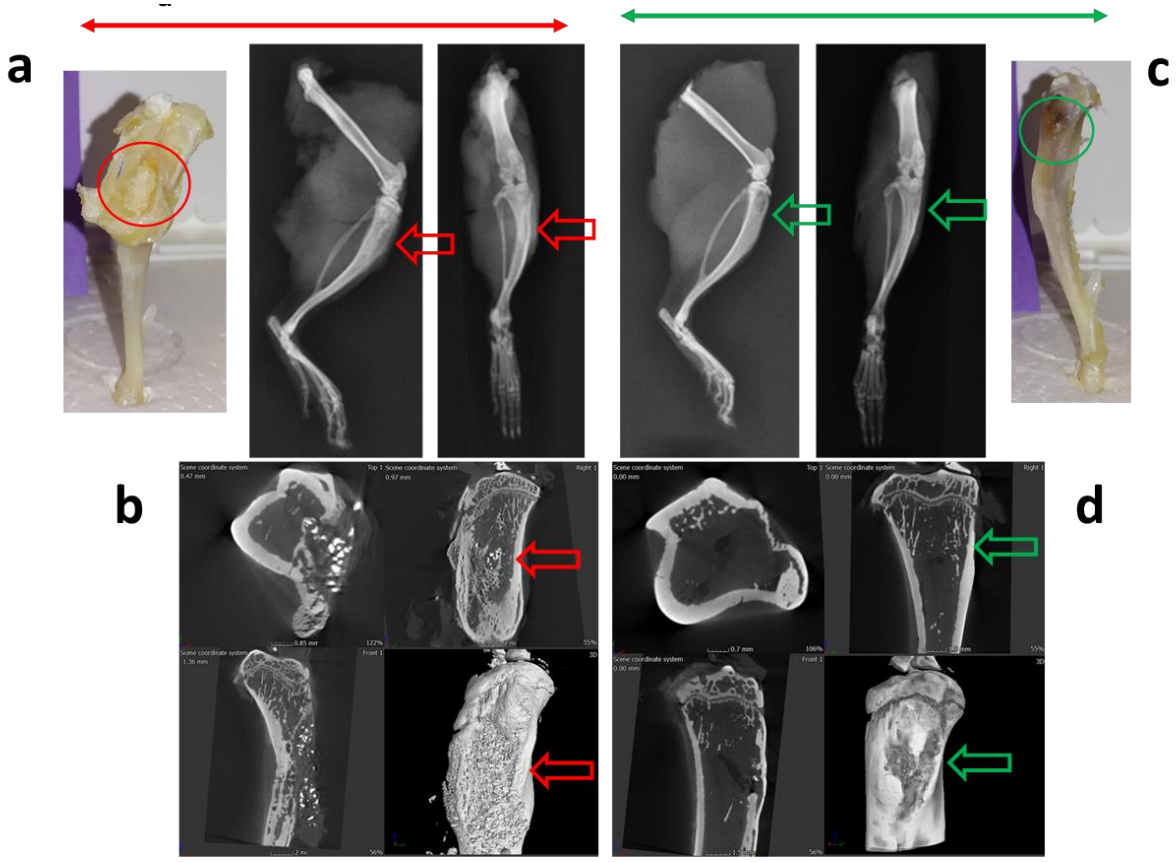

Figure 3.6. X-ray and μ-CT images of rat bones.
(a) Images under the red bar show osteomyelitic bone in infection control group. The macroscopic view (in red circle) and x-ray images (red arrow) show signs of osteomyelitis and sinus formation to drain puss. (b) μ-CT images show deformed bone and narrowing of marrow space in this control group. (c) Images under the green bar show treatment group animals with no apparent signs of osteomyelitis (green circle). (d) μ-CT images show signs of bone healing and remodeling (green arrows).

3.5.3. Bone Volume Measurement

Bone volume was measured after selecting the surgical site as the region of interest (ROI). In the ROI, the treatment group had a significantly higher amount of bone volume compared to the infection control group ($p<0.009$, Figure 3.7 e). ABVF caused eradication of infection signs and functioned as a scaffold for host bone integration and growth.

3.5.4. Histology

H&E staining shows signs of osteomyelitis in the infection control group (Figure 3.7 a & b). Major bone destruction, narrowing of the marrow space, and fibrous tissue formation is abundant. In the treatment group (Figure 3.7 c & d), no signs of osteomyelitis were visible. The ABVF putty seemed to have degraded, leaving space for host bone ingrowth and facilitating osteointegration and bone healing.

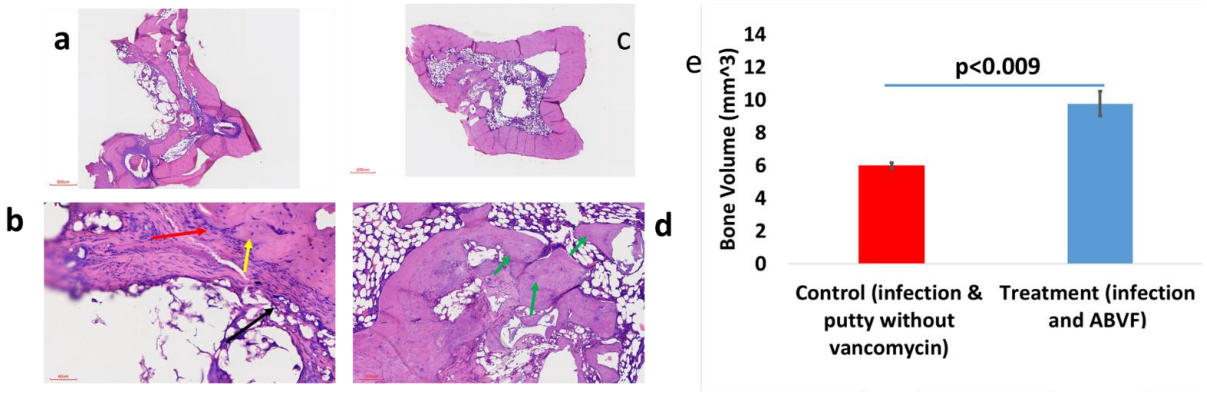

Figure 3.7. H&E staining of rat tibia and bone volume measurements.
Images a & b are from the infection control group showing signs of osteomyelitis. Narrowing of the marrow space and destruction of bone is visible. In image b, the red arrow indicates an inflammatory response; whereas, the yellow arrow shows an osteoclast and the black arrow shows fibrosing with granulation. In images c & d, the treatment group shows no signs of osteomyelitis. The bone seems to be healing and the implanted ABVF is degraded. The new bone grew into the space that was occupied by ABVF. The green arrow in image d is showing new bone growth. (e) The bone volume in treatment group (calculated from µ-CT image) was significantly higher compared to the control group (n=3).

3.5.5. Bacterial Load

Based on colony counts, the bacterial load per gram of bone was found to be significantly lower in the treatment group compared to the control group (Figure 3.8a). There was a 3-log reduction in the bacterial load in the treatment group, which is clinically significant. Histology and radiographs did not show any signs of infection in the treatment group animals even after the 10-week experimental time course, although a minimal number of colonies were still visible.

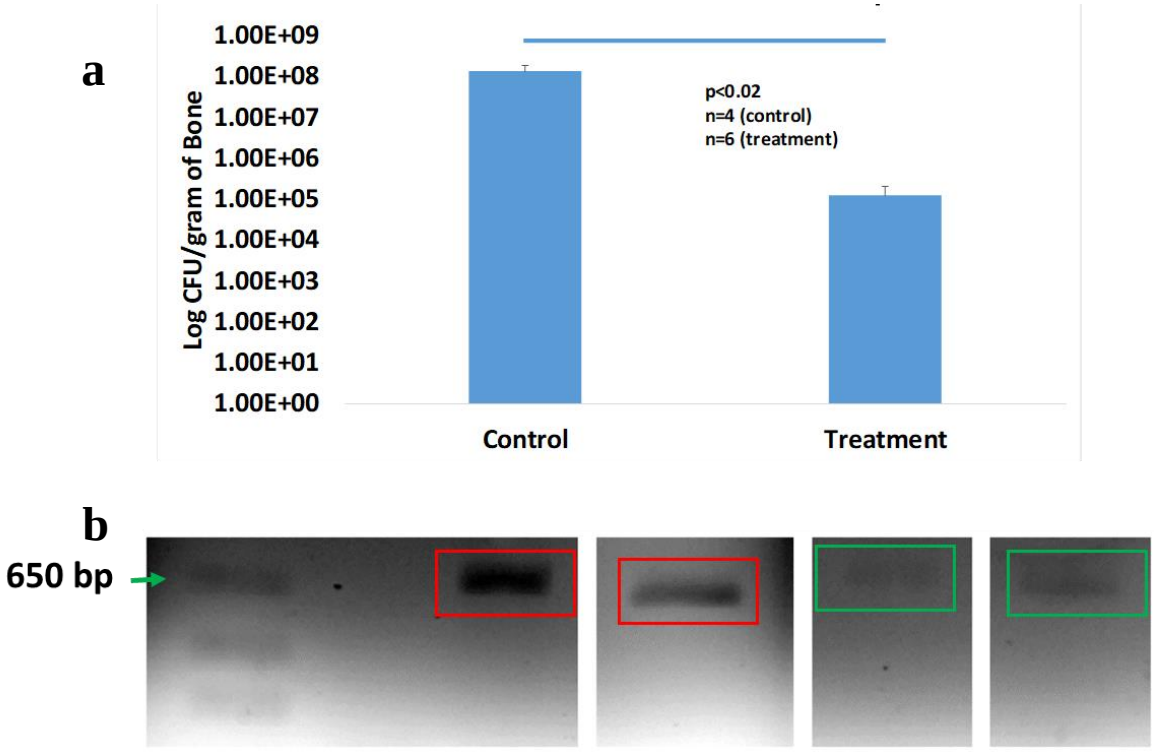

Figure 3.8. Bacterial load count and PCR image of bacteria isolated from rat bones.
(a) Bacterial load per gram of bone in control and treatment groups. At $p<0.02$ the bacterial load is significantly lower in treatment group (n=6) than in control group (n=4). (b) DNA gel images of PCR amplified 16S from S. aureus. The red boxes show DNA bands from control group animals and the bands in the green box are from the treatment group.

3.5.6. PCR

Furthermore, PCR was done to confirm the strain of pathogenic bacteria in the bone and the inoculated species were one in the same. After extracting RNA and creating first strand

cDNA, SA-1 primers, specific for 16S rRNA of S. aureus 49230 were used to amplify a 600 bp pair band and confirm the presence of *S. aureus* 49230. The band was clearly seen in the control culture as well as the control animals and only lightly seen in the test animals (fig. 3.8b), potentially an indication of decreased bacterial load, although it must be noted that this technique cannot assess the viability of the bacteria present.

3.6. Discussion

Osteomyelitis after TJR is a difficult clinical challenge due to poor pharmacokinetics in bone; additionally, the presence of hardware can lead to stress shielding and bone necrosis and prevalent sequestra that provide a safe environment to harbor pathogenic bacteria, allowing almost unfettered proliferation [100]. PMMA based bone cements and beads are the standard of care for revision surgeries to treat osteomyelitis after TJR despite several drawbacks, including high temperature of processing, non-biodegradability, and poor pharmacokinetics. The polymerization of the methymethacrylate monomers to create PMMA cement produces an exothermic reaction reaching high temperature (115.2 C) during the curing process, [101] not only limiting the candidate biomolecules that can be incorporated but also potentially causing surrounding tissue necrosis. Alternatively, ABVF putty fabrication as described herein, is not an exothermic process, allowing an expanded repertoire of drugs to potentially be added. In the current study, two different forms of vancomycin were incorporated into the ABVF putty and sustained drug release was achieved (Figure 3.3a). Furthermore, inadequate antibiotic pharmacokinetics can also lead to the development of resistant bacteria and exacerbate an already challenging clinical treatment. The literature has reported that antibiotic releasing PMMA based systems have a high burst release with little sustained release. In fact some reports indicate that only about 10% of the drug gets released [102] with the remaining drug leaching

below the antibiotic's minimal inhibitory concentration for prolonged period, potentially leading to antibiotic resistance [103]. Finally, while PMMA is not biodegradable, often either requiring additional invasive surgery to remove the beads or acting as a foreign body and nidus of subsequent infections, the ABVF putty reported here is both biodegradable and allows for host bone integration.

Vancomycin, which used to be a "last line of defense" antibiotic, has become an increasingly popular alternative to treat orthopedic infections, especially when MRSA (Multi-drug Resistance *Staphylococcus aureus*) is suspected [104]. Hence, the clinical life of vancomycin must be preserved by appropriate prescribing and patient compliance [105]. Local and complete release of vancomycin from ABVF putty is a safer option. Local release may also avoid some of the systemic, extended-use toxicities of vancomycin (e.g., nephrotoxicity, ototoxicity and poor venous compatibility) [106]. Nevertheless, the toxicity of locally released vancomycin from the ABVF putty was assessed by assaying serum creatinine (Figure 3.5), which indicated no nephrotoxic effects. Importantly, the cytotoxicity of released vancomycin on host cells did not extend to pathogenic bacteria where released vancomycin was shown to not only be bactericidal in vitro for 6-weeks (Figure 3.3 b), but also was able to provide at least a 3-log reduction in bacteria in the treatment group in vivo throughout the 10-week study course (Figure 3.8 a). Previous studies with implantable/ injectable biodegradable polymer-based vancomycin delivery systems showed varying results. Le Ray *et al.* used vancomycin-loaded PCL particles to treat osteomyelitis in a rabbit model (10^7 CFU *S. aureus* inoculation) with 2 log reduction in bacterial count after 110 days of treatment [106], although no osseointegrating material was used in this study. In another study by Inzana *et al*. the authors reported that when vancomycin-loaded calcium phosphate was implanted, it resulted in around 1 log reduction in

bacterial count in bone [107]. Notably, a minimal number of colonies were evident in some of our replicates, likely due to contamination from the normal skin flora during sample preparation. The majority of colonies though the bacteria were identified via PCR as *S. aureus* 49230 (Figure 3.8 b), the species inoculated into the defect. Other studies containing vancomycin HCl and vancomycin free based in polyurethane scaffolds, also shown remnant bacteria in the bone although the bacterial load used in those studies was much lower (10^5 CFU *S. aureus*) than in our study (10^8 CFU *S. aureus*) [108] [90]. In the current study, even after 10 weeks in the treatment group, no signs of infection were observed in radiology and histology (Figure 3.6 and 3.7). It can be argued that absence of clinical signs of infection such as inflammation, bone destruction, pus formation etc. can be considered as an effective treatment against the infection as active infection would have compromised the bone regrowth [109], which we did not observe in our study.

The treatment of osteomyelitis aims not only to manage infection but also to achieve bone regeneration [110]. These two goals must be matched as they are intimately connected by the "race for the surface" [111] with delayed integration being associated with increased infection [112]. BVF containing antibiotics, a clinically standard treatment for TJR revisions, often embodied by PMMA bone cement or antibiotic soaked calcium phosphate based bone fillers, has shown efficiency as an antibiotic carrier; however, a biodegradable scaffold can help in osseointegration. Current antibiotic containing BVFs frequently suffer from limitations in their ability to integrate with host bone, either based on their biodegradation, particle size, or contact with the host bone. An osseointegrating, biodegradable ABVF putty offers a viable and promising alterative.

Osseointegration can be limited by the particle size of the mineral composition in other hyaluronic acid (HA) and calcium phosphate (CP) based BVFs as the particle size in ceramic/

polymer composite BVF plays an important role in bone healing. Previously, it was thought that small bone graft particle of <105 μm would provide better healing due to the greater surface area. However, in a recent study, it was found that BVFs with particle sizes ranging between 100 – 500 μm showed 12 – 16% more new bone growth compared to BVF with smaller (<105 μm) particles in a rabbit femoral condyle defect model [113]; an observation corroborated by other studies. In another study, particles between 100 - 300 μm showed significantly more new bone formation and faster resorption compared to particles ranging from 1000 – 2000 μm in size when used in a femoral defect model in rhesus monkeys [114]. Finally, in a study on the effect of particle size on bone healing in a rabbit femoral condyle defect model, it was shown that animals receiving particles in the range of 250 – 500 μm experienced significantly more new bone growth when compared to groups receiving larger (1000 – 2000 μm) or smaller (90 – 125 μm) particles in a composite BVF [115]. In the ABVF putty reported here, the Pro Osteon BVF component of the putty was morselized and sieved to 175 – 425 μm to maximize bone regrowth and host bone integration.

Beyond particle size, which affects degradable natural and synthetic BVFs, PMMA osseointegration is limited not only by a lack of degradation but also by the inability of host bone to adhere to PMMA filler, causing a layer of fibrous tissue between the PMMA and bone [116]. Alternatively, with the ABVF putty composition, bone regeneration and ingrowth were significantly higher in the treatment group compared to the control group ($p<0.009$) (Figure 3.7). This integration may have resulted from the intimate contact between the host bone and the ABVF putty composition. In recent years, injectable or settable BVFs have gained popularity [113] as they are easy to use and when applied can settle and harden at the site of application. Our ABVF composition demonstrated a desirable, putty-like behavior that allowed easy press-

fitting (Figure 3.2), which was demonstrated by the increasing loss modulus (G") indicative of a viscous response and flow of the material [117]. Furthermore, the increasing loss modulus G' signifies an elastic-solid like behavior [95] or a stiffening over time. The increase in G' was also higher than G" as the sheer stress increased showing a shift towards stiffening under higher stress corresponding to putty like behavior [117]. The in situ hardening behavior of the ABVF putty is also desirable as it would remain in the defect site. Finally, hardening overtime was also observed during in vitro release in an aqueous environment. Theoretically, this phenomenon may be accounted for by PLGA dissolved in NMP, which shows phase inversion. In an aqueous environment, the NMP diffuses out of the polymer leaving a hardened matrix behind [118], eliminating the need for ex vivo curing prior to wound closure.

3.7. Conclusion

ABVF putty has shown sustained vancomycin release for 6 weeks and antibacterial activity *in vitro*. In a rat osteomyelitis model, it also showed infection control as well as supported osseointegration. ABVF putty degraded *in vivo* after 10 weeks, allowing good host bone ingrowth. Ultimately, ABVF putty is a promising new alternative for treating osteomyelitis after revision TJR. Future work will consider the use of ABVF putty in the presence of a biofilm-seeded k-wire and the release of multiple drugs.

4. EXTENDED RELEASE COMBINATION ANTIBIOTIC THERAPY FROM A BONE VOID FILLING PUTTY FOR TREATMENT OF OSTEOMYELITIS[3]

4.1. Abstract

Despite advances in Total Joint Replacements (TJR), infection remains a major concern and a primary causative factor for revision surgery. Current clinical standards treat these osteolytic infections with antibiotic-laden poly(methyl methacrylate) (PMMA) based cement, which has several disadvantages, including inadequate local drug release kinetics, antibiotic leaching for prolonged period and additional surgical interventions to remove it, etc. Moreover, not all antibiotics (e.g., such as rifampicin, a potent antibiofilm antibiotic) are compatible with PMMA. For this reason, treatment of TJR associated infectious complications remain a significant concern. The objective of this study was to develop a polymer-controlled, combination antibiotic releasing bone void filler (ABVF-C) with an underlying osteoconductive substrate to treat the TJR implant associated biofilm infections. An ABVF-C putty was designed to provide sustained vancomycin and rifampicin antibiotic release for 6 weeks while concurrently providing an osseointegrating support for regrowth of lost bone. The reported ABVF-C showed efficient antibacterial and antibiofilm activity *in vitro*. In a rat infection model the ABVF-C showed complete bacterial elimination and supported bone growth. Furthermore, in

[3] R. Hasan et al., "Extended Release Combination Antibiotic Therapy from a Bone Void Filling Putty for Treatment of Osteomyelitis," Pharmaceutics, vol. 11, no. 11, p. 592, Nov. 2019, doi: 10.3390/pharmaceutics11110592. The material in this chapter was co-authored by Raquib Hasan, Kambri Schaner, Meredith Schroeder, Abbey Wohlers, Jacob Shreffler, Codi Schaper, Hariharaputhiran Subramanian and Amanda Brooks. Raquib Hasan and Amanda Brooks conceived the project and along with Meredith Schroeder designed the experiments. Raquib had primary responsibility to conduct all the experiments listed in the section, analyze the data and write the manuscript. Kambri Schaner and Abbey Wohlers collected drug release samples and helped with in vitro antibacterial activity experiment. Jacob Shreffler and Codi Schaper helped with animal care and in vivo study. µ-CT and SEM imaging was done by Jayma Moore and Dr. Scott Payne, Dr. Lisa Christenson helped with X-ray imaging. Dr. Hariharaputhiran Subramanian performed the HPLC analysis. Jordan Flaten made the histology slides. Raquib Hasan analyzed the data and Amanda Brooks verified the data. Raquib Hasan wrote the manuscript, Amanda Brooks checked and revised the document.

an *in vivo* k-wire based biofilm infection model the ABVF-C putty also was able to eliminate the biofilm infection while supporting osseointegration. Retrieved k-wire implants were also free from biofilm and bacterial burden. ABVF-C putty demonstrated that it can be a viable treatment option for implant related osteomyelitis and may lead to retention of the hardware while enabling a single stage surgery.

Keywords: osteomyelitis, total joint replacement, biofilm, infection, vancomycin, rifampicin, combination antibiotic delivery, bone void filler, drug release

4.2. Introduction

Although Total Joint Replacements (TJR), including Total Knee Replacements (TKR) and Total Hip Replacements (THR), are arguably one of the most successful surgical interventions to improve quality of life, there is a growing trend in the number of secondary or revision surgeries being done in the United States according to the American Academy of Orthopedic Surgeons (AAOS). Of the more than a million people undergoing a Total Joint Replacements (TJR) each year in the United States with projections of more than 4 million procedures a year by 2030 [5] [6] [7], an estimated 365,000 secondary or revision procedures will be performed [6]. These numbers do not necessarily reflect a failure in the TJR procedure as much as a indication of (1) surgical intervention at an earlier age [75] [76], often necessitating a revision surgery later in their life as the TJR implants materials wear out and(2) rising obesity leading to osteoarthritis, which is reported to account for >90% of TKR procedures, and infection. Despite its low incidence in primary TJR (1-2%), infection is perhaps the most concerning cause for TJR revision, accounting for 18% and 26.8% of revision THR and TKR, respectively. Responsible for ~ 65% of total cases, *Staphylococcus aureus* is the most common causative pathogen associated prosthetic joint infection (PJI) after TJR. Almost 20% of these *S.*

aureus infections are classified as methicillin resistant (MRSA) [81] [78]. Not only do these infected TJR surgeries impose a significant socioeconomic and mortality burden, but they also predispose the implant to further threats from infection, driving the risk of recurrence to a staggering 21%. Implant removal and hardware replacement can propel the risk of infection to a threatening 20-30% [9,10]. Importantly, non-infected revision TJR also has a modestly increased infection risk of 5.4% [8].

Osteomyelitic, deep bone infections, are clinically difficult to treat, often due to the development of a biofilm associated with the implanted hardware [80] and infiltration of the surrounding soft tissue [119]. The Centers for Disease Control estimates that 80% of all bacterial infections are caused by biofilms, including those associated with medical devices such as joint prostheses, catheters, and heart valves etc [120]. Biofilm resident bacteria often require up to a 1000 fold more antibiotic to eradicate the infection when compared to their planktonic counterparts [121]. The current clinical treatment regimen for revision TJR, particularly those due to infection, centers around implantation with antibiotic loaded polymethylmethacrylate (PMMA) bone cement for local antibiotic delivery after thorough debridement of infected and necrotic tissue. Importantly, due the leaching of low concentration antibiotic from PMMA bone cements over an extended period of time, antibiotic-releasing PMMA can be associated with higher incidence of localized antibiotic resistant bacteria [105].

Alternatively, an concurrent or sequential extended course of systemic antibiotics may also be used [82]. Often vancomycin is the physician's chosen systemic treatment for osteomyelitis due to the threat of MRSA [87], despite the risk of nephrotoxicity and red-man syndrome [89] associated with high-dose intravenous therapy. Unfortunately, not only does systemic vancomycin have poor bone penetration with only a fraction of the drug reaching the

bone to provide a bone/serum ratio of 10%, with even lower penetration in osteomyelitic bone [88], but vancomycin also has limited activity against bacterial biofilms [122]. Rifampicin, which has a variable ability to penetrate bone (from 8% to 56%) has demonstrated superior activity against both biofilm and slow growing bacteria [123]. In multiple clinical trials, the use of rifampicin in conjunction with another antibiotic resulted in infection cure and implant salvage in the majority of cases [119], [124]. Importantly, monotherapy with rifampicin, particularly as a prolonged oral therapy (up to 6 months), was ill-advised as there was a higher possibility of resistant infection [123] and toxicity (i.e., gastrointestinal, hepatic, renal symptoms and red-man syndrome [125]) in patients. Despite its potential for biofilm infections, local delivery of rifampicin, specifically from PMMA, has been hindered by the fact that rifampicin can act as a scavenger of reactive oxygen species, thereby preventing the polymerization of PMMA [126]. The utility of rifampicin as an adjunct antibiotic therapy combined with the uselessness of PMMA bone cement to locally deliver rifampicin to bone necessitates the development of an alternative ABVF-C with the potential to treat biofilm infections. Moreover, developing a biodegradable bone void filler with degradation matched antibiotic release kinetics can provide scaffold like support to guide bone tissue regeneration [86].

The current study evaluated not only the *in vitro* kinetics of dual vancomycin and rifampicin release from a developed press-fitting, ABVF-C putty but also the *in vitro* antibacterial and anti-biofilm activity of the released combination. Additionally, *in vivo* host bone integration and antibiotic protection of the ABVF-C putty was evaluated in a pilot rat model of biofilm-seeded osteomyelitis. Both *in vitro* and *in vivo* results support the use of our developed ABVF-C putty for the local delivery of vancomycin and rifampicin to combat biofilm-associated osteomyelitis while avoiding systemic side effects. This effective

osteomyelitis treatment will increase the rate of implant salvage, thereby reducing the socioeconomic burden of TJR infections on our healthcare system.

4.3. Materials and Methods

4.3.1. Materials

Poly(D,L-lactide-co-glycolide) 90:10 (PLGA) (Polysciences, Inc., Warington, PA, USA); Polyethylene Glycol (5kD) (PEG) (Fluka, St. Louis, MO, USA) and Polycaprolactone (10 kD) (PCL-Sigma-Aldrich, St. Louis, MO, USA) were used as received. Rifampicin (EMD Millipore, Darmstadt, Germany), N-Methyl-2-pyrrolidone (NMP) (Fisher Sci, Pittsburg, PA, USA), Calcium Chloride ($CaCl_2$) (EMD Chemicals Inc., Gibbstown, NJ, USA), alamarBlue (Bio Rad, CA, USA), Kirschner wire (K-wire) (Key Surgical, Eden Prairie, MN, USA) were all used as received from the manufacturer. Vancomycin Hydrochloride (V-HCl) (Sagent Pharmaceuticals, Schaumburg, IL, USA) and PRO OSTEON 500R (kindly provided by Zimmer Biomet, Warsaw, IN, USA) were processed, as outlined below, after received.

4.3.2. Preparation of Vancomycin Free-Base (V-fb)

V-fb was prepared from V-HCl following previously published method [23]. Briefly, V-HCl was dissolved in water at concentration of 70 mg/mL. To precipitate V-fb at pH 8.00, NaOH (3N) was added until pH 8.00 was achieved. After incubation for 30 minutes at ambient temperature and humidity, the precipitated V-fb was centrifuged at 3000 rpm for 10 minutes followed by sequential washes in 70% ethanol and methanol. Subsequently, V-fb was suspended in water, frozen and lyophilized.

4.4. Fabrication and In Vitro Characterization of ABVF Putty Containing Combination Antibiotics

4.4.1. Preparation of ABVF-C

ABVF-C putty was prepared according to our previously published method with few modifications [91]. Briefly, Pro Osteon 500R was morselized using a mortar and pestle, and sieved to yield a particle size distribution of 175 to 425 μm. 350 mg of ProOsteon particles were soaked with agitation (100 rpm) in a 1 mL solution of V-HCl/rifampicin (80 mg/mL of vancomycin and 20 mg/mL rifampicin, in 50:50 water : DMSO solvent) for 1 hour at room temperature. The solution was subsequently evaporated to dryness at 37 C under vacuum. To fabricate the ABVF putty, PEG (21.2 mg) and PCL (42.5 mg), were melted and mixed at 65 C. The prepared Pro Osteon particles were added to the molten polymers to create a homogenous mixture. Powdered V-fb (30 mg) and rifampicin (25.5 mg) was added to the mixture. PLGA (85.5 mg) dissolved in 200 μL of NMP and $CaCl_2$ (22 mg) were combined with the molten mixture to create a homogenous putty base. Phosphate buffered saline (PBS) was added dropwise to the putty base to give a putty-like consistency. Subsequently, the putty mix was manually compressed into a 3D printed mold to get the desired size and cylindrical shape (4 mm diameter x 3.5 mm height) for surgical implantation into a rat drill hole model.

4.4.2. In Vitro Drug Release Kinetics

An ABVF-C putty cylinder was submerged in 2 mL of PBS (1x) release media and was incubated at 37 C. At different time points (day 1, day 3, day 7 and every week after that until week 6), release media was collected and replaced with fresh PBS. The amount of drug in the sample was assessed via high-performance liquid chromatography (HPLC) analyses on a Waters e2695 separation module (254 nm) with an Empower workstation. The standard samples

(Vancomycin, Vancomycin free-base, or Rifampicin dissolved in PBS) were separated on a XTERRA RP 18 5μm 4.6x250 mm column using 0.1% TFA in water and 0.1% TFA in acetonitrile as mobile phases.

4.4.3. In Vitro Antibacterial Activity

In vitro antibacterial activity of the released drugs was assessed against *Staphylococcus aureus* (ATCC 49230) using a Kirby-bauer zone of inhibition (ZOI) assay [24]. Briefly, 100 μL of the collected drug release media was dried on filter paper disks (6.5 mm diameter) in a 96 well-plate. An overnight culture of *S. aureus* was diluted in PBS to get a bacterial concentration of 10^7 CFU/mL. The bacteria culture was streaked on LB (Luria-Bertani) agar plates and the filter paper disks with adsorbed drug were placed on the plates immediately. Agar plates were incubated for 20 hours at 37 C. The ZOI around the disk with no bacterial growth was measured using a digital caliper.

4.4.4. In Vitro Antibiofilm Assay

An overnight culture of *S. aureus* was adjusted to OD_{600} of 0.5 in LB broth. 1 mL of adjusted bacterial culture was added to each well of a 24-well plate and was incubated for 24 hours at 37 C with gentle shaking (100 rpm). After incubation, the broth was aspirated, and the remaining bacterial film was washed with 1X PBS three times. After washing, 500 μL of fresh broth and 500 μL of drug release media from day 1 was added to the wells. Control wells received only PBS without drug and broth. Wells were incubated for 24 hours at 37 C with gentle shaking (100 rpm), and the liquid was aspirated. Each well was again washed with 1X PBS three times. The bacteria in the remaining biofilm were extracted from the surface and suspended in 1X PBS for colony counts. Briefly, serial dilutions were made, and the bacteria were plated on Tryptic Soy Agar (TSA). After incubating 20 hours at 37 C, bacteria colonies

were counted. Alternatively, a similar procedure was followed with modifications to assess the antibiofilm capability of the drug release milieu in the presence of a k-wire.

K-wire (1.4 mm diameter) was cut into 12 mm lengths and autoclaved. Subsequently, sterilized k-wires were immersed into LB broth and dried at 50 C to produce a film-like coating of nutrients on the wire. An overnight culture of *S. aureus* was adjusted to OD_{600} = 0.5 in LB broth. The prepared k-wires were put into 24 well plates at an angle and 1.5 mL of bacterial culture was added to the wells to completely submerge the k-wires. After incubating 24 hours at 37 C and 100 rpm, the media was removed, and the k-wires were washed in 1X PBS three times, leaving on the adherent biofilm bacteria attached. After washing, 500 µL of fresh broth and 500 µL of drug release media from day 1 was added to the wells and the biofilm covered k-wires were incubated at 37 C (100 rpm) for 24 hours. In control wells 500 µL of fresh broth and 500 µL 1X PBS without drug was added. After incubation, k-wires were removed and again washed in 1X PBS to remove loosely adherent bacteria. The wire was vortexed in 1 mL 1X PBS for 60 seconds to dislodge the biofilm and create a bacterial suspension. Serial dilutions of the suspension were made, and bacterial dilutions were plated on LB agar plates. After 24 hours of incubation at 37 C, bacterial colonies were counted.

4.4.5. In Vitro Cytocompatibility

Cytocompatibility of ABVF-C putty was assessed via a standard alamarBlue assay, according to the manufacturer's protocol. Briefly, 10,000 MG-63 osteoblast cells (ATCC, Manassas, VA) were seeded in each well of a 96-well plate. Cells were grown in Dulbecco's Modified Eagle Media (DMEM) containing 10% fetal bovine serum (FBS) and 1% penicillin-streptomycin-fungizone (Lonza, Walkersville, MD, USA). Cells were incubated at 37 C and 5% CO2. After reaching 60% confluence, 100 µL of release media from ABVF-C was added to each

well. Control wells received 1X PBS only. After 48 hours of incubation, cells were washed with 1X PBS three times. Fresh media was added to the wells followed by addition of alamarBlue to a 10% final concentration. Subsequently, wells were incubated at 37 C for 4 hours. After the incubation, absorbance was read at 570 nm and 600 nm (Spectramax m5, Molecular Devices, Downingtown, PA, USA). Cell viability was calculated using the following equation:

$$\%\text{cell viability} = ((O2 \times A1) - (O1 \times A2)) / ((O2 \times P1) - (O1 \times P2)), \quad (1)$$

Where, O1 = molar extinction coefficient (E) of oxidized alamarBlue (Blue) at 570 nm, O2= E of oxidized alamarBlue at 600 nm, A1 = absorbance of test wells at 570 nm, A2 = absorbance of test wells at 600 nm, P1 = absorbance of positive growth control well (cells plus alamarBlue but no test agent) at 570 nm, P2 = absorbance of positive growth control well (cells plus alamarBlue but no test agent at 600 nm).

4.5. In Vivo Assessment

4.5.1. Rat Osteomyelitis Model

Twenty-three, skeletally mature, male Sprague-Dawley rats (>350 grams) divided into 4 cohorts (Table 4.1) were used for *in vivo* studies (approved by the NDSU IACUC protocols A16016 and A19019). Briefly, rats were anesthetized with isoflurane inhalation. Buprenorphine hydrochloride (0.01mg/kg) was injected subcutaneously as an analgesic. The right hind leg was shaved and sterilized using repeated swabs of alcohol and iodine. A small incision of ~12 mm was made below the knee and over the tibial metaphysis. A 4.2 mm hole was drilled in the exposed bone until it penetrated the marrow space of the tibial metaphysis. *S. aureus* (10^8 CFU) in sterile saline was inoculated through the drill hole defect into the marrow space using a 25 μL Hamilton syringe followed by implantation of the cylindrical ABVF-C putty into the drill hole. Alternatively, as a preliminary study to assess the in vivo antibiofilm activity, a biofilm-seeded

k-wire (12 mm length x 1.4 mm diameter), prepared according to method 2.3.6, was pushed inside the marrow space followed by implantation of the cylindrical ABVF-C putty. The incision was closed using a series of mattress sutures followed by application of surgical glue (Vetbond Tissue Adhesive, 3M, MN, USA). The control group underwent the same surgical procedure but received the putty without antibiotic regardless of the form of bacterial inoculation (i.e., planktonic or biofilm). Rats were monitored daily for signs of discomfort and infection. After 10 weeks, the rats were sacrificed by isoflurane overdose, and the tibia was harvested for further study. Importantly, cohorts implanted with a biofilm-seeded k-wire were kept for 6 weeks prior to sacrifice, and the k-wire was extracted from the bone for further analysis.

Table 4.1. Description of the cohorts used in this study

Cohort	**Implant**	**Surgery Model**	**Infectious Dose**	**Time to Sacrifice (Weeks)**	**Cohort Purpose**	**Morbidity/ Infection**	**Cohort Size**
1	BVF putty without antibiotics	Drill-hole Osteomyelitis	10^8 CFU	10	Positive Infection control	Local infection	12
2	ABVF-C with vancomycin and rifampicin	Drill-hole Osteomyelitis	10^8 CFU	10	Infection treatment	No infection	5
3	BVF putty without antibiotics	K-wire biofilm osteomyelitis model	Biofilm on k-wire	6	Positive Infection control	Local infection	3
4	ABVF-C with vancomycin and rifampicin	K-wire biofilm osteomyelitis model	Biofilm on k-wire	6	Infection treatment	No infection	3

4.5.2. X-ray and Microcomputed Tomography (μ-CT)

Radiographic analyses of bone were done after disarticulating the limb and harvesting the bone following euthanasia. X-ray imaging was performed on an IDEXX CR Digital

Radiography System (Westbrook, Maine, USA) following standard protocols. Briefly, lateral and cranial-caudal radiographic images were obtained of each limb at mAs: 4 and kVp: 40. For μ-CT, the bone was hot glued to a glass rod and placed into a GE Phoenix v|tome| xs X-ray computed tomography system with a 180 kV high power nanofocus X-ray tube xs|180 nf, high contrast GE DXR250RT flat panel detector, and molybdenum target (GE Sensing & Inspection Technologies GmbH, Wunstorf, Germany). One thousand projections were acquired at a voltage of 80 kV and a current of 300 μA. Voxel size was 6.4 μm. Acquired images were reconstructed into a volume data set using GE datos|x 3D computer tomography software Version 2.2 (GE Sensing & Inspection Technologies GmbH, Wunstorf, Germany). The reconstructed volume was then viewed and manipulated using VGStudio Max (Volume Graphics Inc., Charlotte, NC, USA).

4.5.3. Bone Volume

Bone volume was determined based on the μ-CT scans using VGStudio Max (Volume Graphics Inc., Charlotte, NC, USA) software. A region of interest (ROI) was set on each of the scanned bones according to where the drill hole was made. The amount of regenerated bone was determined by adjusting the contrast to highlight the bone and comparing the ROI from the infection control group and the treatment group. Regenerated bone was the bone in the ROI where the drill hole was made and filled up by new bone.

4.5.4. Histology

After euthanasia, the bone was harvested by fixing it in 10% neutral buffered formalin for 72 hours. Subsequently, bone was decalcified by immersing it in an EDTA solution (10% solution at pH 7.4) for 2 weeks, with solution exchange every other day. Once the bone was decalcified it was embedded in paraffin wax and sectioned (5 μm). Sections were mounted on

glass slides and stained with hemotoxin and eosin stain (H&E stain - Scy Tek Lab., Logan, Utah, USA) according to standard protocols. Briefly, the sections were deparaffinized in Clear Rite 3 (Thermo Fisher Scientific, Kalamazoo, MI, USA). Subsequently, tissue was rehydrated with a decreasing gradient of ethanol. After H&E staining, the tissue section was covered with a glass coverslip using synthetic resin. Stained slides were imaged at 40x using MoticEasyScan Digital Slide Scanning microscope (Motic Digital Pathology, San Francisco, CA, USA).

4.5.5. Bacterial Colony Count

Harvested bone was flash frozen in liquid nitrogen, followed by pulverization using a custom-made bone crusher. The pulverized bone was weighed and suspended in 500 μL of PBS. Serial dilutions were made [23] and 10 μL of suspension was plated on blood agar plates (Fisher Sci, Pittsburg, PA, USA). The plates were incubated for 48 hours at 37C and bacterial colonies were counted. To determine the total number of bacteria in the bone, the number of colonies were multiplied by the dilution factor and normalized per gram bone samples. For the extracted k-wires, the k-wire was put in 1 mL of PBS and vortexed for 1 minute. Serial dilutions were made and 10 μL of suspension was plated on blood agar plates (Fisher Sci, Pittsburg, PA, USA). The plates were incubated for 48 hours at 37C and bacterial colonies were counted.

4.6. Results

4.6.1. In Vitro Drug Release Kinetics

HPLC detected both vancomycin and rifampicin in the release media through 2 weeks of release. ABVF-C showed sustained release of both drugs (Figure 4.1). Approximately 30% of the incorporated vancomycin was released within 2 weeks, while 14% of the rifampicin was released in the same timeframe. The current HPLC method was unable to detect drugs beyond

week 2, likely due to interference from the degrading polymer matrix; hence, consideration of the bioactivity of the system may prove more useful.

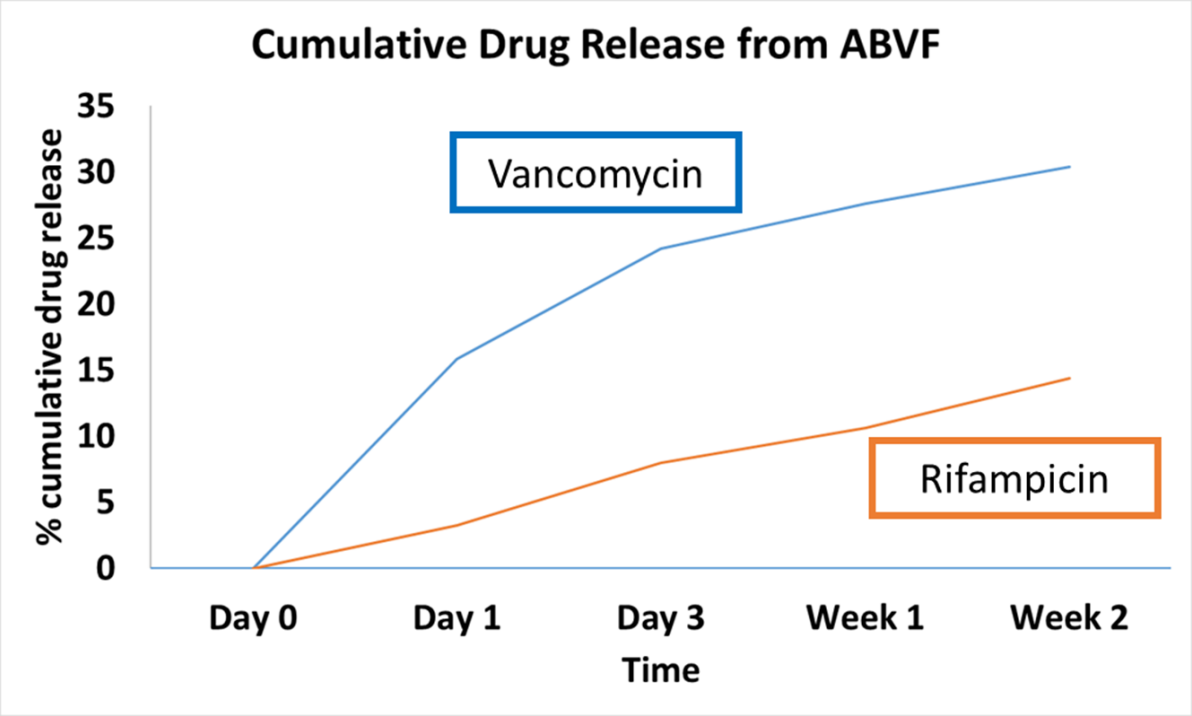

Figure 4.1. Drug release curve of ABVF-C.
HPLC showed sustained release of vancomycin and rifampicin from ABVF-C. There was an initial burst release of vancomycin at day 1. Rifampicin showed release in a sustained manner.

4.6.2. In Vitro Antibacterial Activity

Using a standard ZOI assay, efficient antibacterial activity was evident throughout the 6-week study time-course (Figure 4.2). Day 1 release samples showed the highest ZOI (40.35 ± 0.75 mm) against *S. aureus*. At week 6, the ZOI remained robust at 21.71 ± 1.23 mm. To ensure that sink conditions were maintained and did not impact the results, samples were also released in 5 mL of PBS and the ZOI study was replicated, yielding the same results (appendix C, Figure C1).

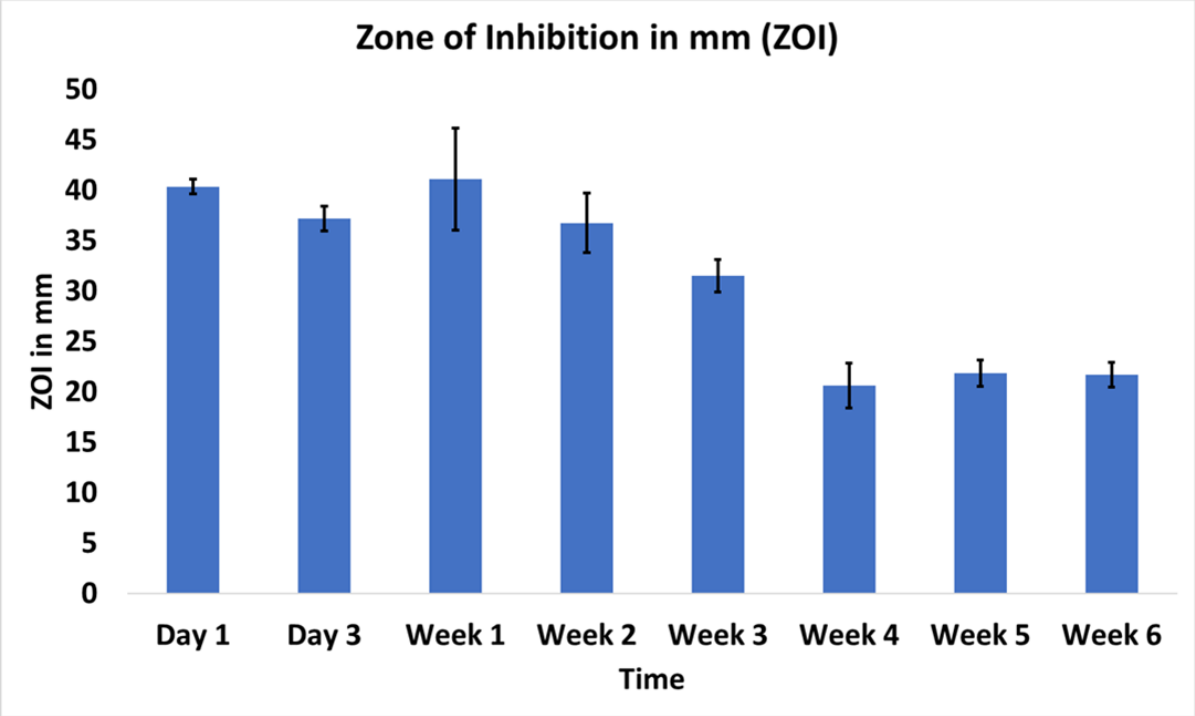

Figure 4.2. The zone of inhibition of released drugs from ABVF-C against *S. aureus*. Released drugs from ABVF-C showed excellent antibacterial property over 6 weeks.

4.6.3. In Vitro Antibiofilm Assay

Since the majority of bacterial contaminants, particularly in the presence of biomedical implants, are found in a biofilm, the ability of the dual release ABVF-C was evaluated against a biofilm. The biofilm was determined to have $4.05x10^6 \pm 9.81x10^5$ bacterial colony forming units per mL (CFU/mL). Complete obliteration of the bacteria in the biofilm was seen when the biofilm was exposed to drug release milieu from ABVF-C, with no bacterial growth evident in a colony forming assay. Alternatively, the control without antibiotics showed robust colony growth ($p<0.005$, Figure 3.3 a). Furthermore, the ability of a dual drug releasing ABVF-C to eliminate biofilm formation on a k-wire was also assessed. Biofilm formation on the k-wire was evident in the control group with $2.80x10^6 \pm 4.65x10^5$ CFU of bacteria per mm length of k-wire. On the contrary, the treatment group had significantly less bacteria ($p<0.002$) along the length of

the k-wire, with many samples showing no evidence of colony forming units, indicating effective eradication of bacteria in biofilm (Figure 4.3 b).

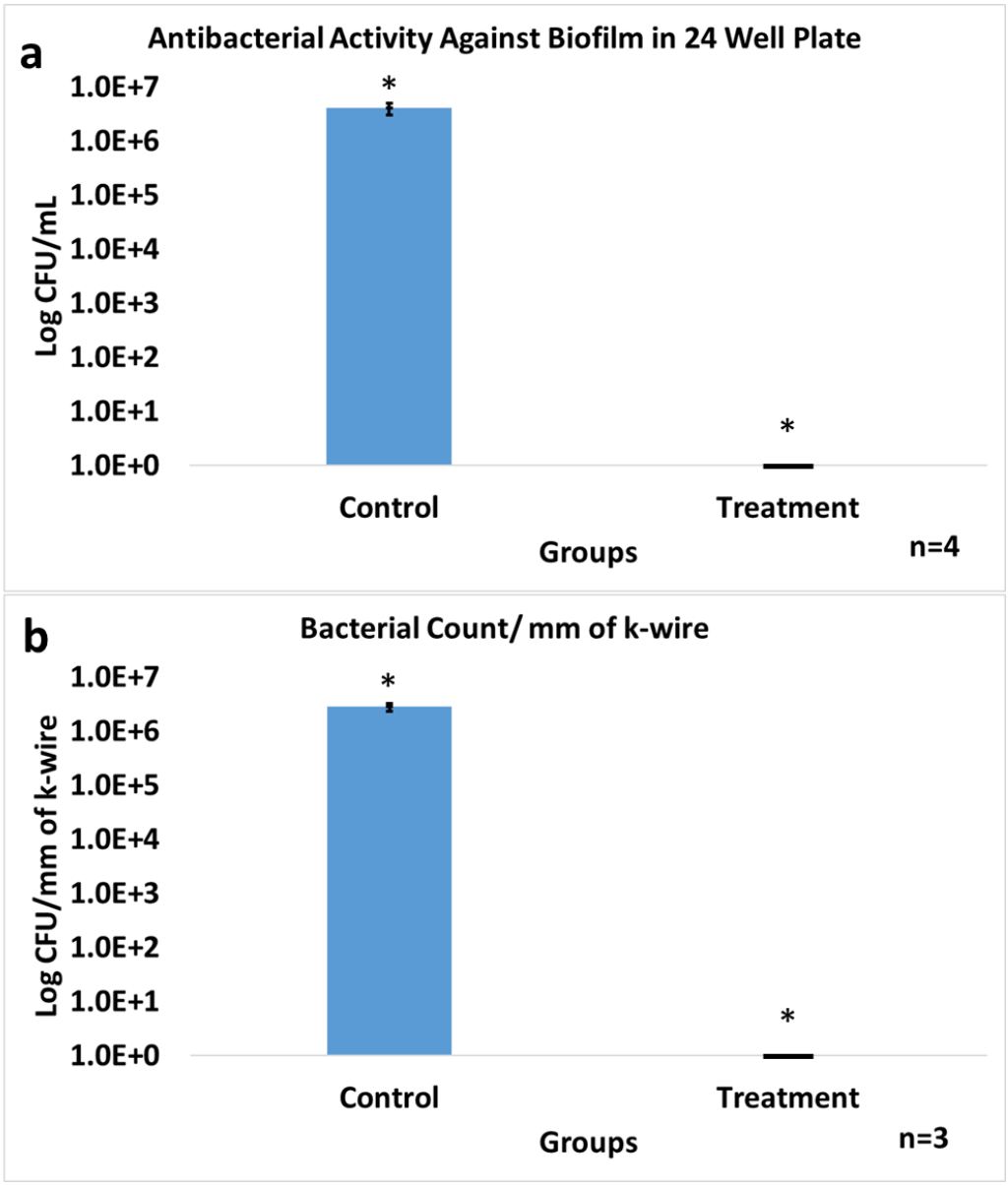

Figure 4.3. Antibiofilm activity of released drugs from ABVF-C against biofilm grown on 24-well plate and k-wire.
(a) The released drug showed excellent antibiofilm activity property against S. aureus biofilm grown in a 24 well plate. The Treatment group (treated with day 1 release media) showed complete wipeout of the biofilm, whereas, the control group that didn't receive the release drug showed high bacterial content in the biofilm, *$p<0.005$. (b) S. aureus biofilm grown on k-wire in-vitro was completely eradicated in the treatment group treated with released antibiotics (day 1 release media) from the ABVF, while the control group showed high bacterial count in the biofilm grown on k-wire, *$p<0.002$.

4.6.4. In Vitro Cytocompatibility

A standard alamarBlue assay was run to assess the cytotoxicity of the dual releasing ABVF-C putty on MG-63 osteoblasts. The viability of the treatment cells appeared to be less than the control cells, and statistically significant difference ($p<0.05$) was seen in cell viability (Figure 4.4). Cells exposed to week 3 release media showed significantly higher viability than week 1. This may indicate lower amount of drug caused less impact on viability of the cells.

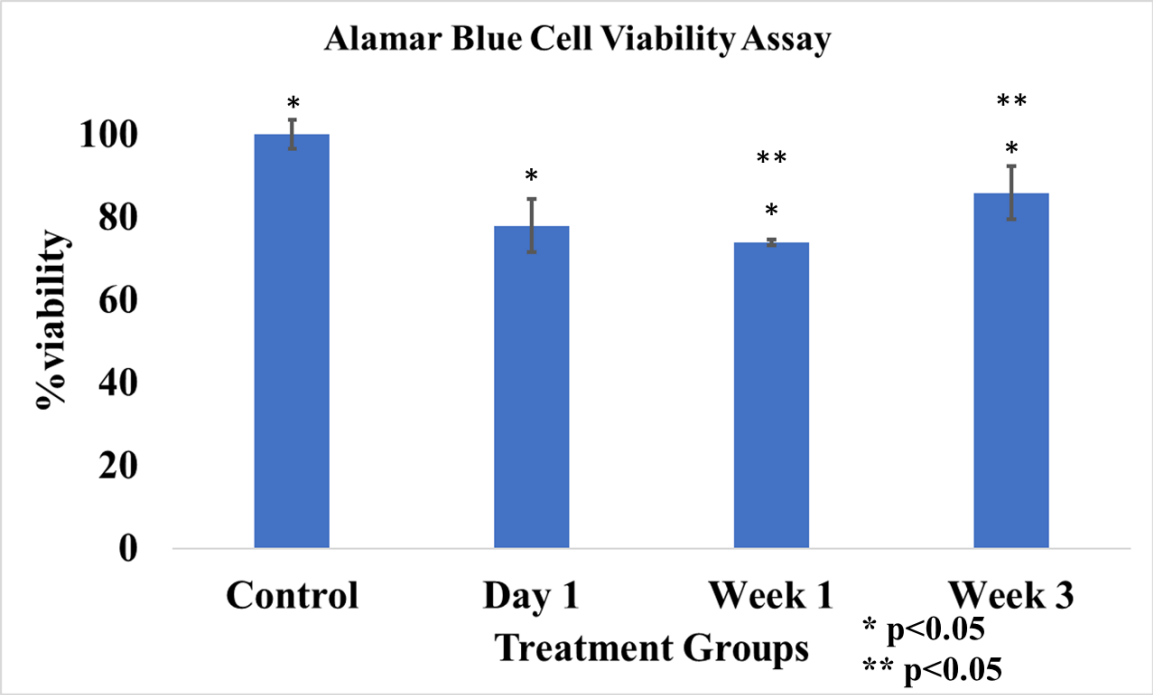

Figure 4.4. Viability of MG63 osteoblast cells when exposed to released drugs from ABVF-C. The alamarBlue cell viability assay showed a significant difference in cell viability between the control and the treatment groups with day 1, week 1 and week 3 drug release milieu ($p<0.05$). There was also a significant difference between viability when cells were exposed to release milieu from week 1 and week 3 ($p<0.05$), but no significant difference was seen between day 1 and week 1 and day 1 and week 3. * $p<0.05$, ** $p<0.05$

4.6.5. Rat Drill-hole Osteomyelitis Model

Infection was seen in all the animals of cohort 1 (i.e., the control cohort - Table 4.1). Macroscopic evaluation of the affected bone revealed purulent drainage and formation of sequestra and fibrous encapsulated, pus-filled regions in the tibial bone, although the rats did not

show any overt behavioral changes and did not lose weight over the experiment period (in fact they gained weight) or show any increase in body temperature. Importantly, spontaneous fracture was seen in 3 rats of cohort 1 within 3 days of surgery, and they were excluded from the study. None of the ABVF-C treatment rats in cohort 2 showed any signs of infection nor did they show any changes in behavior. Furthermore, they looked healthy. In addition to assessing the dual releasing ABVF-C putty against planktonic bacteria, a preliminary assessment of the effect of the ABVF-C putty on a biofilm infection was also evaluated. As in the planktonic control cohort, infections developed in all cohort 3 control rats, as evidenced by formation of purulent pus, pus filled fibrous capsule, and deformed bone with thickening at different places, although, again, no behavioral changes, weight loss or temperature increase was observed. Healing without any signs of infection was observed in the cohort 4 animals containing ABVF-C treatment. Similar to cohort 2, no behavioral changes were seen in the cohort 4 rats, and they gained weight over the experimental period while maintaining normal body temperature of ~36 C.

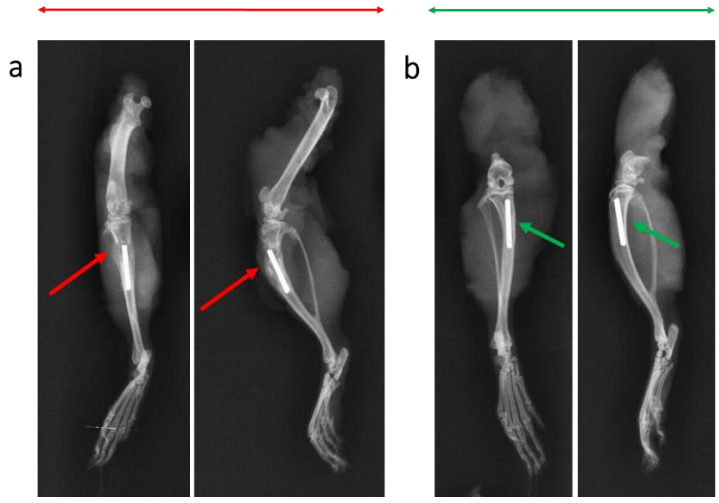

Figure 4.5. X-ray image of rat bones from k-wire biofilm infection model.
(a) The x-ray radiograph of k-wire rat control group demonstrated signs of osteomyelitis (i.e., osteolysis, periosteal thickening and formation of sequestrum). (b) The k-wire treatment group showed no such signs of osteomyelitis and the bone appeared to be healed.

4.6.6. X-ray and Microcomputed Tomography (μ-CT)

X-ray and μ-CT were done to assess the bone health. X-ray of cohort 1 animals showed signs of osteomyelitis with formation of sequestra, abscess, lytic regions and periosteal thickening (appendix C, Figure C2). Similar radiologic features were seen in the k-wire control group, with clear signs of osteomyelitis through regions of periosteum in addition to lysis of bone, loss of cortical bone and presence of necrotic bone (Figure 4.5 a). By contrast, x-ray images of rats in the k-wire treatment group in cohort 4, did not show any sign of infection (Figure 4.5 b). Regardless of the cohort, the k-wire seemed well positioned in the intramedullary space. No adverse events were observed. μ-CT of the cohort 1 (Figure 4.6 a) showed widespread signs of infection. Specifically, these images showed the presence of sinus tracts and fibrous material (red arrows). Finally, infection looked to have spread with the posterior tibia showing signs of osteolysis and cortical destruction. Similarly, bones in cohort 3 rats (Figure 4.6 c) also displayed sinus tract formation and a narrowing of the marrow space. Cortical bone growth with periosteal thickening was evident at places. A large fibrous capsule was noticeably covering the bone defect. Conversely, cohort 2 rat bones (Figure 4.6 b) showed healing of bone and cortical bridging. The bone appeared to be undergoing remodeling. Likewise, cohort 4 rat bones (Figure 4.6 d) appeared to have new bone integrated with implanted ABVF-C (i.e., osseointegration). Alternatively, in this cohort, bone healing seemed more advanced.

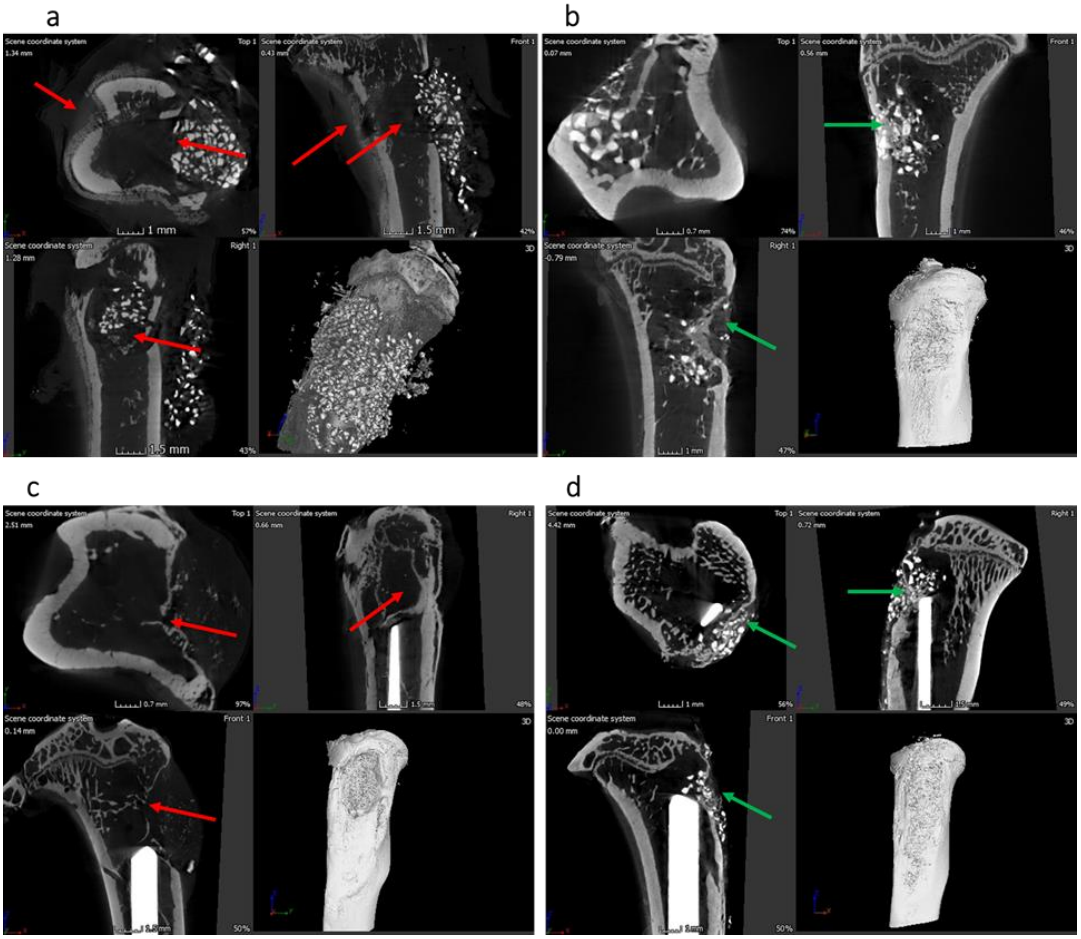

Figure 4.6. μ –CT images of rat bones from drill hole model and k-wire biofilm infection model. (a) The μ –CT images of drill-hole rat control group demonstrated signs of osteomyelitis through signs of infection, decreased bone formation and formation of sinus tract. Infection seems to be spread to the posterior of the bone. (b) The drill-hole treatment group showed no signs of osteomyelitis and the bone appeared to be healed with new bone formation and cortical bone bridging. Bone seems to be undergoing remodeling. (c) The μ –CT images of k-wire rat control group demonstrated signs of osteomyelitis through signs of infection, decreased bone formation and formation of sinus tract. (d) The k-wire treatment group showed no signs of osteomyelitis and the bone appeared to be healed with new bone formation. Bone seems to be undergoing remodeling.

4.6.7. Bone Volume of Newly Formed Bone

Bone volume of cohorts 1 and 2 was measured due to higher sample size and longer duration of the study period that allowed a more accurate interpretation of the comparison. The treatment group showed significantly higher ($p < 0.02$) bone volume at the ROI compared to the

control group (Figure 4.7). The bone volume of cohort 1 was 5.98 ± 0.18 mm^3. In contrast, the cohort 2 treatment group exhibited much higher bone volume of 10.65 ± 1.03 mm^3.

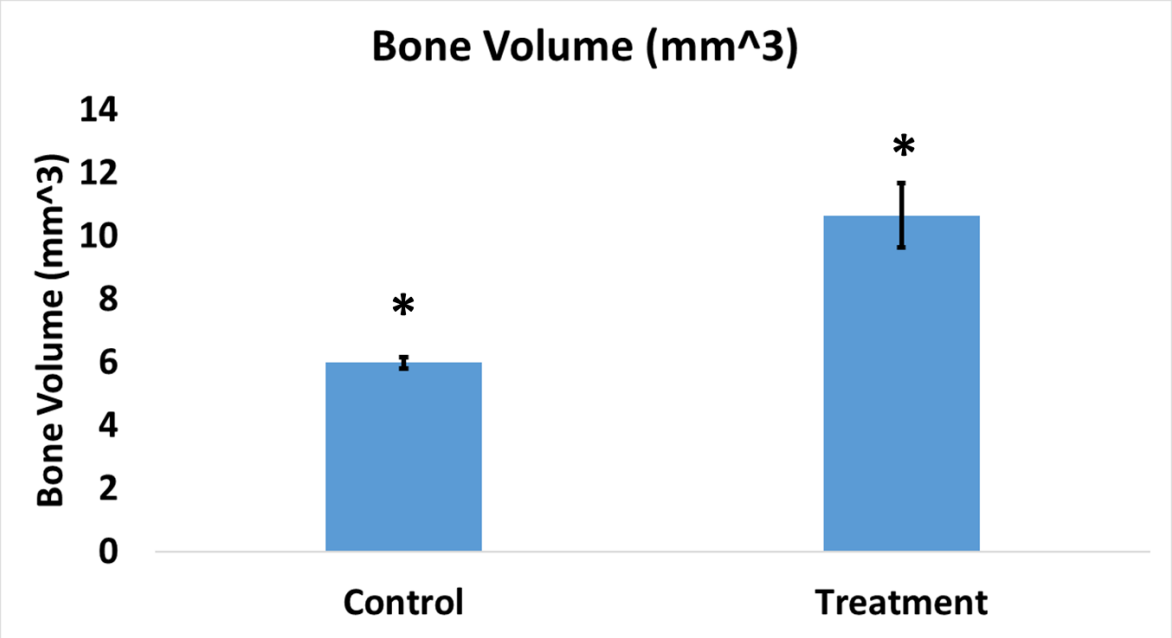

Figure 4.7. Bone volume measurement of newly formed bone in drill hole model rats.
Bone volume in the infection control group of drill-hole model was significantly lower compared to the treatment group. *p<0.02.

4.6.8. Histology

To assess histological features of the bone at the surgical site, H&E staining was done. Cohort 1 showed unhealed bone, lack of new bone growth, and presence of fibrous tissue as a consequence of infection (red arrows, Figure 4.8 a). On the contrary, cohort 2 showed healed bone with cortical bridging, new bone growth and osseointegration, likely resulting from the absence of infection (Figure 4.8 b). Accordingly, cohort 3 animals were consistent in showing signs of massive infection. Osteomyelitis was evidenced by large fibrous capsules with an abundance of inflammatory cells, narrowing of the marrow space, and a combination of thickening and destruction of boney structure (red arrows, Figure 4.9 a). Conversely, histology of the cohort 4 showed new bone formation, ongoing bridging of newly formed bone and limited

mature collagen structure (green arrows, Figure 4.9 b). These signs are consistent with the documented healing process of bone and absence of infection.

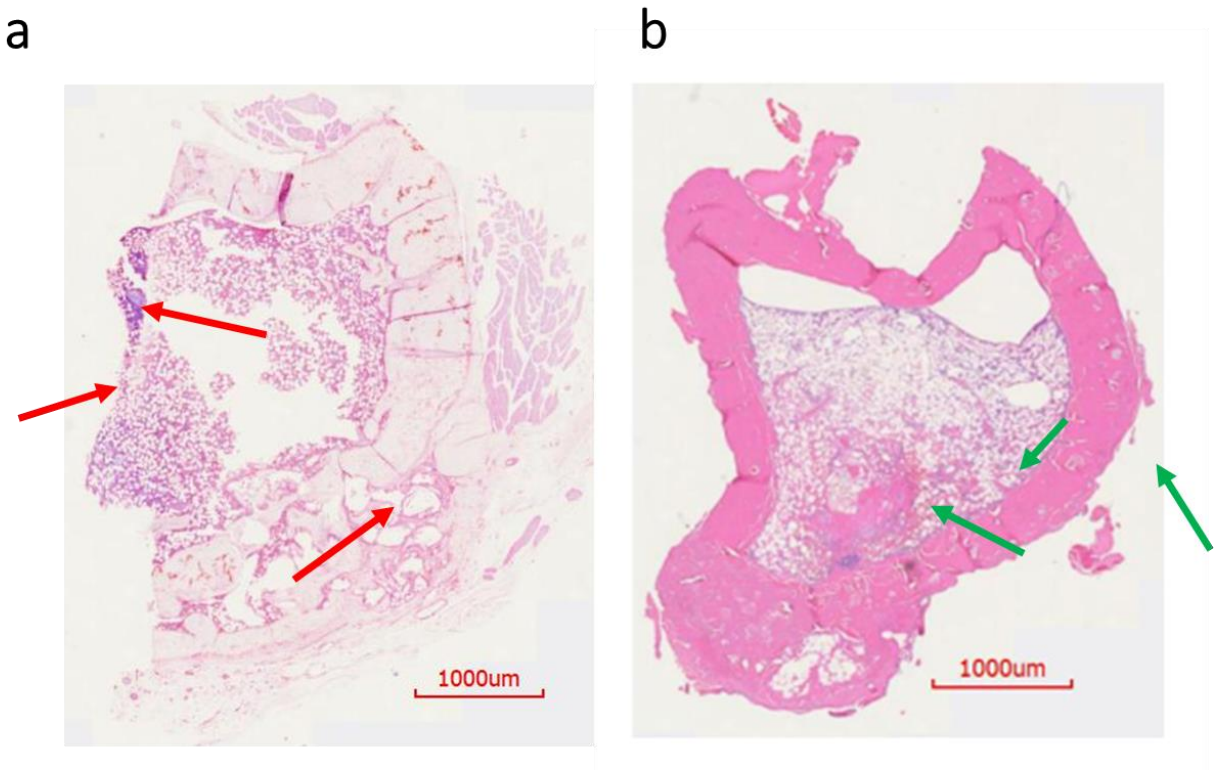

Figure 4.8. H&E staining of rat bones from drill-hole model.
(a) H&E staining of control rat bone. There is a lack of bone growth at the dilled site. There is some destruction of the bone. (b) Bone from treatment group rat shows healing of the bone and cortical bridging with new bone growth.

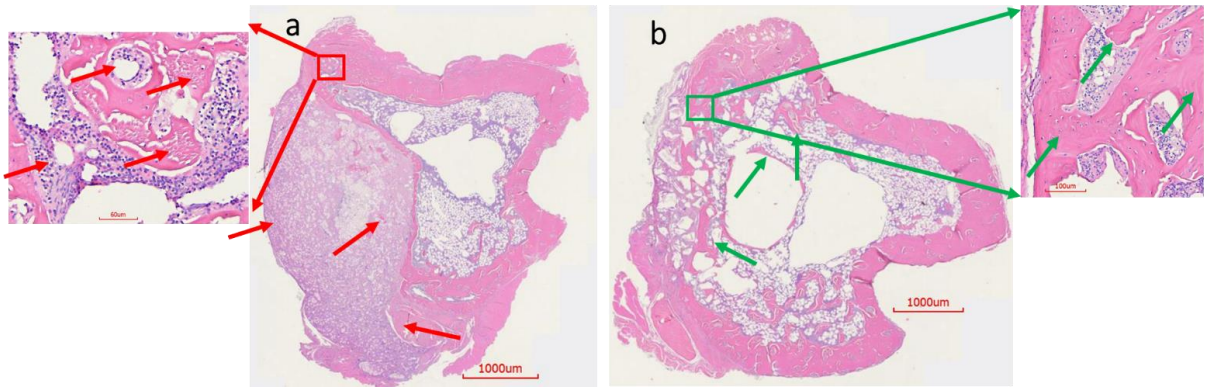

Figure 4.9. H&E staining of rat bones from k-wire osteomyelitis model.
(a) H&E staining of control rat bone. There is growth with narrowing of marrow space. In places there are thickening of bone. A big fibrous capsule with inflammatory cells is visible. (b) Bone from treatment group rat shows ongoing healing of the bone. New bone formation is visible in the defect. New bone growth was seen as the degradation of the ABVF-C allowed new bone to grow in.

4.6.9. Bacterial Colony Count

Bacterial colony counts revealed a high bacterial content (1.33E+08 ± 5.56E+07 CFU/ gm bone) in cohort 1 rats that didn't receive ABVF-C (Figure 4.10 a). Whereas, complete obliteration of bacteria was seen in cohort 2 rats; no bacterial colonies were observed after culturing (Figure 4.10a), showing a statistically significant reduction in bacterial content ($p<0.05$). Similarly, high bacterial loads were also present in cohort 3 rats (Figure 4.10 b), in contrast to a distinct lack of bacteria and infection in the treatment group (cohort 4, Figure 4.10 b). Bacterial content on the k-wire extracted from cohort 3 showed high bacterial content of with a mean bacterial load of 2.03×10^6 CFU/ k-wire (ranged between 1×10^5 to 3.95×10^6 CFU/ k-wire) (Figure 4.10 c). No bacteria were able to be grown from the k-wires extracted from cohort 4 rats (Figure 4.10 c), indicating absence of bacteria and infection.

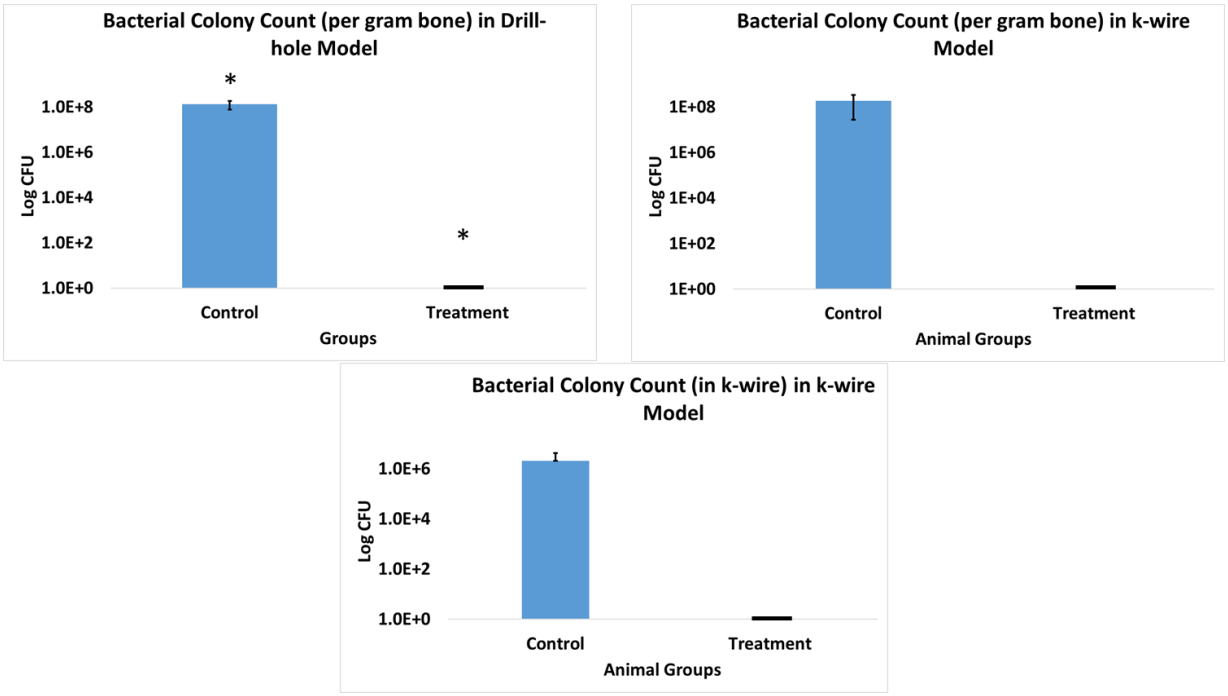

Figure 4.10. Bacterial colony count with bacteria extracted from rat bones and k-wire of different cohorts.
(a) The bacterial count in drill-hole model control group showed very high bacterial count in the bone, $p<0.05$. The treatment group did not show any presence of bacteria and the infection was eliminated. (b) The bacterial count in k-wire rat model control group showed very high bacterial count in the bone. The treatment group was free from any bacterial load and the infection was eliminated. (c) The bacterial count in k-wire rat model control group showed high bacterial count on the extracted k-wire. The k-wire extracted from the treatment group was free from any bacterial load.

4.7. Discussion

Despite of many disadvantages with PMMA-based bone cement, such as non-biodegradability, poor drug release kinetics, immune response and additional surgical removal etc., it is still the standard of care for treating infected TJR [127] [128]. FDA approved bone cements generally use tobramycin, gentamicin and vancomycin as the antibiotic payload [129], although none of these antibiotics are effective against bacterial biofilms [130] as their efficacy requires metabolically active bacteria. The presence of bacteria in low metabolic state in biofilm, which are not actively dividing may render vancomycin less effective and vancomycin

targets cell wall of bacteria by blocking cell wall synthesis [131]. Limited efficacy of vancomycin against biofilm is documented both in vitro and in vivo [130]. Local delivery of antibiotic is needed to effectively treat the TJR related osteomyelitis, as systemic antibiotic cannot reach high enough concentration in dense cortical bone as well as in avascular bone. No viable options to deliver antibiotic, apart from bone cements, are regularly used in patient treatment [129]. Moreover, antibiotics such as rifampicin, which is known to be active against biofilm, cannot be incorporated in bone cement as it hinders the polymerization of PMMA bone cement compromising the material property of PMMA [132].

The incompatibility of rifampicin with PMMA significantly limits the efficacy of PMMA in cases of implant-associated biofilm formation, a common occurrence in TJR. Previous studies have indicated that bacterial biofilm formation can happen within 5 – 10 hours following bacterial seeding in wound [133]. Moreover, the presence of blood plasma can potentially enhance the propensity of *S. aureus* to form a biofilm. Unlike vancomycin, which has limited or no activity against *S. aureus* biofilms[130] [134], active replication of bacteria is not needed for rifampicin activity making, it an effective alternative for biofilm bacteria [135]. Rifampicin not only active against *S. aureus* biofilms but also against *S. epidermis* biofilm bacteria, another common causative agent of implant related osteomyelitis [136]. Unfortunately, bacteria can readily develop resistance to rifampicin due to its mode of action. Thus, combination therapy with other antibiotics is necessary. Vancomycin, which is effective against planktonic *S. aureus* infection, can be delivered as a cocktail with rifampicin, which is active against the biofilm form of *S. aureus,* to provide better therapeutic outcome. The synergistic effect of rifampicin in combination with vancomycin is previously documented [137]. Other aminoglycoside antibiotics, like tobramycin showed no beneficial outcome with rifampicin, while others such as

gentamicin seem to be antagonistic [137]. A rifampicin-vancomycin combination could be a viable therapeutic arsenal against *S. aureus* biofilm infection.

As expected from other reports in the literature, the ABVF-C showed efficient bioactivity with good zones of inhibition (Figure 4.6) over 6 weeks. Based on our previous work in which we validated that a mature *S. aureus* biofilm could be reliably formed within 24 hours of bacterial seeding [131] [138], *S. aureus* biofilms were exposed to released drug from ABVF-C, which showed complete eradication of biofilm and viable bacterial load both in a well plate and on a k-wire. This result is supported by previous studies, where this antibiotic combination showed bacterial biofilm eradication [139] [140]. The in vivo experiments also showed complete eradication of the biofilm and bacterial load both in the bone and on the k-wire of cohort 4 (treatment group). In the cohort 3 control group, not only was the bacterial load very high in the bone, but it was also very high on the k-wire in all the rats. Although no statistically significant difference was found between cohorts 3 and 4 due to the preliminary nature of this part of the study, it can be noted that bacterial elimination was achieved in the cohort 4 treatment group in all rats. Additionally, it is worth noting that the standard deviation of colony counts on the k-wire was extremely high, likely the result of a partial.

delamination of the biofilm when extracting it from the intramedullary space. Nevertheless, in the absence of antibiotic treatment, all the k-wires had high bacterial load. Similarly, bones of the control cohorts showed high bacterial loads, although the variability of the load was high, ranging from 5.42×10^7 to 3.35×10^8 CFU/gram bone. Not only could delamination have impacted this range, but more importantly, the presence of an encapsulated, purulent-filled, cavity in the bone of several of the control animals, made “sterile” processing difficult, resulting in a puncture of the capsule and the loss of some CFUs. Nevertheless, all the

control animals showed infection; whereas, treated animals were free from infection. Finally, despite the clear difference in treatment and control animals in this preliminary study, statistical significance was not achieved, likely due to the factors outlined above. However, the study was extremely promising and based on the effect size in these cohorts (i.e., incidence of infection in cohort 3 = 90% and incidence of infection in cohort 4 = 0%) and a post hoc continuous power analysis of the means and standard deviations found in the colony counts, a sample size of 11 rats in each of cohort 3 and 4 would provide a statistically significant result (α=0.05 and power of 0.8).

Although the HPLC only detected the presence of drug until week 2 in a sustained manner, it is clear that the drug release was sustained until week 6 based on the bioactivity of the released drug in the ZOI study. The limited detection of the HPLC method was likely a reflection of interference from polymer degradation products. Nevertheless, HPLC detected the cumulative release of 30.41% of the total incorporated vancomycin and 14.38% of the incorporated rifampicin over the course of two weeks (Figure 4.1).

Although vancomycin has limited reported cytotoxicity and is well tolerated by osteoblasts even at high concentration, rifampicin has reported toxicity to osteoblast cells [141]. A decrease of up to 50% viability can be seen at 5mg/mL of rifampicin; whereas, vancomycin has no reported cytotoxicity at that concentration [141]. This may explain the reduced viability of osteoblasts when exposed to released drug from ABVF-C (Figure 4.4) and raises concerns that rifampicin may hinder *in vivo* bone regeneration. However, such an effect was not observed in our study. On the contrary, our ABVF-C putty was able to support bone healing and osseointegration (Figure 4.6, 4.8 & 4.9). Furthermore, this finding shows congruence with a recent study where application of rifampicin powder in a sterile wound did not result in reduced

healing of bone. In addition, rifampicin in an infected wound bed showed faster healing of bone compared to the no antibiotic control and the vancomycin only treated group previously reported by our lab [134]. Furthermore, the rifampicin/vancomycin cocktail showed absence of signs of infection in the biofilm infection model (Figure 4.6 & 4.9); whereas, vancomycin group and control group showed osteolysis and lucency and presence of bacteria in histology [134]. These findings highlight the lack of exact translation between *in vitro* and *in vivo* outcomes, perhaps because natural cellular turnover and renewal that provides some additional resistance to the cytotoxic effects observed *in vivo*. Importantly, the presence of bacteria can reduce the number of osteoblasts and increase osteoclastic resorption by inciting inflammation. Additionally, native pluripotent stem cells may lose the ability to differentiate into osteoblasts if exposed to bacteria [142]. Thus, it is wise to take measures to eliminate bacteria first as a treatment priority to allow the body's innate bone healing mechanisms in the absence of infection and inflammation.

Although vancomycin has limited to no known cytotoxicity, it can be source of nephrotoxicity during prolonged, systemic high doses. To validate that the local delivery of vancomycin in the ABVF-C putty did not also invoke such a response, in a previous study we carried out the serum creatinine assay (Chapter 3, Figure 3.5) and did not see any signs of increased creatinine in the rat's serum, suggesting the absence of nephrotic adverse response due to vancomycin released from ABVF-C. In literature, another antibiotic used in PMMA bone cement, tobramycin, showed significant nephrotoxicity at 80mg/kg/day [143]. This was not surprising based on the fact that 200mg/kg/day of vancomycin has been demonstrated to be safe without nephrotoxic effects [143], and the total vancomycin incorporated in our ABVF-C is well below the neurotoxic dose. Hence, local delivery of vancomycin not only prevents high systemic

exposure, but incorporation into ABVF-C resulted in much lower amount of vancomycin being used.

Alternatively, toxicity related to rifampicin dosing, including gastrointestinal, hepatic, renal, hematological, and central nervous system effects, have been reported with doses ranging from 9-15 g of drug. Furthermore, systemic dosed rifampicin is reported to be 70-80% protein bound and widely distributed throughout the body [125]. Nevertheless, rifampicin is a critical antibiotic for treating prostheses biofilm infections, especially when the hardware is retained [144]. Previous attempts to use rifampin alone on in combination with other antibiotic such as vancomycin showed better antibacterial activity but failed to totally eradicate the bacterial load both in bone and in biofilm [107] [145]. This may have been caused by insufficient drug release kinetics and in some cases the inability to incorporate sufficient amounts of antibiotic in the delivery device [132] [145]. In our study, ABVF showed complete eradication of both a planktonic bacterial load as well as a bacterial biofilm (Figure 4.3 & 4.10) both in vitro and in vivo.

4.8. Conclusions

The successful infection eradication in rats and obliterated biofilm on the k-wire shows the promise of a dual release ABVF-C to treat TJR related infections, enabling surgeons to retain the prosthetic implant. Furthermore, the developed dual release ABVF-C putty may also enable surgeons to perform single stage revision surgeries, reducing the immense burden on the healthcare system.

ABVF-C provided effective release of rifampicin and vancomycin showing in vitro and in vivo efficacy by eradicating the bacteria. ABVF-C was biodegradable and provided support

for new bone growth. No adverse effect on in vivo bone healing was observed. No apparent toxicity also seen in the rats.

5. BIOGLASS-BASED ANTIBIOTIC RELEASING BONE-VOID FILLER (ABVF-BG) PUTTY FOR THE TREATMENT OF OSTEOMYELITIS[4]

5.1. Abstract

Osteomyelitis, which is on the rise, remains a very difficult to treat condition despite newer treatment approaches and improved surgical techniques. Among other reasons, surgeries like Total Joint Replacements (TJR) and orthopedic trauma related surgeries, which are consider among the most successful modern surgical interventions to improve form, function, and quality of life, are projected to more than quadruple by 2030. While the infection rate after primary TJR sits at 1- 2% for trauma related surgery it can be as high as 3.6 to 21.2% based on the type of trauma. The risk of reinfection after revision surgery is even higher. Current treatments with antibiotic-releasing PMMA based bone cement and/or, systemic antibiotic after surgical debridement do not provide effective treatment due to fluctuating antibiotic levels at the site of infection, leading to insufficient local antibiotic concentration. In addition, non-biodegradable PMMA does not support bone regrowth in the debrided void spaces and often must be removed in an additional surgery. Here we report a bioactive glass or, bioglass (BG) substrate-based biodegradable, easy to use "press fitting" Antibiotic-Releasing Bone Void Filling (ABVF-BG) putty to provide effective local antibiotic release at the site of infection along with support for bone regeneration. The ABVF-BG putty formulation was homogenous, had a porous structure

[4] The material in this chapter was co-authored by Raquib Hasan, Kambri Schaner and Amanda Brooks. Raquib Hasan and Amanda Brooks conceived the project and designed the experiments. Raquib had primary responsibility to conduct all the experiments listed in the section, analyze the data and write the manuscript. Kambri Schaner and Pranothi Mulinti collected drug release samples and helped with in vitro antibacterial activity experiment. Kambri Schaner helped with in vivo experiment sample collection. Jacob Shreffler helped with animal care. µ-CT and SEM imaging was done by Jayma Moore and Dr. Scott Payne, Dr. Lisa Christenson helped with X-ray imaging. Dr. Hariharaputhiran Subramanian performed the HPLC analysis. Jordan Flaten made the histology slides. Greg Stommen helped with XRD. Raquib Hasan analyzed the data and Amanda Brooks verified the data. Raquib Hasan wrote the manuscript, Amanda Brooks checked and revised the document.

and showed putty like ease of handling. Furthermore, the ABVF-BG putty demonstrated in vitro antibacterial activity for up to 6 weeks. Finally, the ABVF-BG putty was biodegradable in vivo and showed 100% infection cure in the treatment group receiving ABVF-BG putty compared to the infection control group where all the rats had sustained osteomyelitis. The ABVF-BG putty also supported bone growth in the void space of bone. The potential for simultaneous infection treatment and bone healing using the developed BG based ABVF-BG putty is promising as an alternative treatment option for osteomyelitis.

Keywords: Osteomyelitis; vancomycin; bone void filler; antibiotic release; controlled drug delivery; bone regeneration; bioglass; biomaterial

5.2. Introduction

Despite the advances in treatments, osteomyelitis remains one of the most difficult orthopedic conditions to treat. There has been a steady increase of bone and joint infections leading to osteomyelitis due to high energy trauma and as a consequence of surgical procedures such as bone fracture surgery, total joint replacements etc. [146,147]. Majority of the infections are caused by *Staphylococcus aureus* [78,146,147]. Due to the poor penetration of antibiotics in poorly vascularized bone, surgical intervention is often necessary [148]. Surgical intervention includes removal of all implants, aggressive debridement of infected or necrotic bone, and any severely affected soft tissues [149]. It is important to fill up the void space after debridement to prevent further infection. Although, bone grafting is promising as they have higher bone regenerating property, they suffer from substantial failure rate due to the faster resorption in the presence of persistent local infection [148].

As a consequence, local antibiotic delivery through antibiotic loaded polymethylmethacrylate based bone cement became a standard treatment option to treat these

infections along with systemic antibiotic therapy for 4 -6 weeks. But the PMMA suffers from several drawbacks, such as potential degradation of antibiotics due to high polymerization temperature, second removal surgery due to non-biodegradability, as well as possibility of biofilm formation on the PMMA surface due to subtherapeutic level of antibiotic release [150].

Due to these issues, antibiotic loaded bone graft substitutes have become promising alternatives as no harvesting and processing needed and have unlimited availability as compared to bone grafts, they may provide support for bone healing, their biodegradability, the fact that they provide predictable antibiotic release kinetics and their promise to replace systemic antibiotic therapy [147,151].

Bone graft substitutes, such as calcium sulfate can be used as antibiotic carriers but shows faster resorption and local acidic environment [152]. Other like hydroxyapatite (HA), tricalcium phosphate, alone or as composites did not show effective antibiotic release past 21 days, where the antibiotic was vancomycin [152]. Moreover, HA was shown to have limited resorption in vivo [153]. On the other hand bioglass, a very promising bone graft substitute for its bone healing properties is not used as antibiotic carrier [152]. Studies with bioglass particles to treat osteomyelitis was also incorporated with systemic antibiotic therapy [154] [155]. An alternative can be to use bioglass in a bioglass-polymer composite, where polymer part would carry antibiotic and control drug release while the bioglass part would provide support for bone tissue regeneration.

In recent years, bioactive glass, or bioglass (BG), has garnered much attention for its biological activity, especially in the case of bone tissue engineering. Since its first inception, a variety of bioglass have been prepared and tested for their impact on bone and soft tissue engineering, 45S5 is the most widely studied among all [156] [157]. In today’s market, most of

the commercially available BG are used for trauma and bone injury treatment [158]. 45S5 bioglass is regarded as the gold standard in bone regenerative repair due to its bioactivity, biodegradability and bone bonding property [159]. BG shows higher quantity and quality of bone formation compared to synthetic hydroxyapatite (HA) [160]. Faster and higher onset of bone formation (17 times higher after week 1) and twice as much after 24 weeks was reported when bioglass was used in a rabbit femoral condyle defect model compared to when HA was used [161]. The 45S5 BG shows a higher degradation rate than HA [162], which is desirable to make space for growing bone proving overall better performance of BG in bone regeneration than commercial bioceramics available [158]. BG is also known to upregulate different genes such as insulin-like growth factor II (IGF-II), that induces osteoblast proliferation along with an increase in secretion of extra cellular matrix (ECM) [163] [164]. The upregulation may be due to the ions such as Calcium (Ca) and Silicon (Si) released from BG [165]. Moreover, ions such as Si, Ca, and inorganic Phosphate (Pi) play an essential role in bone tissue regeneration. Si plays a critical role in formation and calcification of bone tissue by HA precipitation, collagen I formation, and osteoblast differentiation [166] [167] [168]. Ca ion increases ECM formation, osteoblast differentiation and proliferation, and IGF activity [169] [170]. Pi ions increase matrix Gla protein (MGP) expression that regulates bone formation [171]. Although granular BG showed antibacterial properties, putty made with the bioglass granules did not show antibacterial properties [172]. This leaves room for developing putty like bone void filler made with bioglass that can treat infections as well as support bone healing.

Vancomycin still remains as the standard recommended antibiotic for treating osteomyelitis caused by *S. aureus* [148]. Moreover vancomycin is effective against methicillin-

resistant *Staphylococcus aureus* (MRSA) and the bacteria are slow to grow resistance against vancomycin [173].

Thus, the current focus of the study is to develop BG based antibiotic (vancomycin) releasing bone void filling putty (ABVF-BG) that provides antibiotic release for 4 to 6 weeks, can be easily press fitted into bone void space, biodegradable and provide support for bone growth to treat osteomyelitis.

5.3. Materials and Methods

5.3.1. Materials

Poly(D,L-lactide-co-glycolide) 90:10 (PLGA) (Polysciences, Inc., Warington, PA, USA); methylated Polyethylene Glycol (5kD) (mPEG) (Fluka, St. Louis, MO, USA) and Polycaprolactone (10 kD) (PCL-Sigma-Aldrich, St. Louis, MO, USA) were used as received. 45S5 BG powder (particles size d50 = 10μm) was obtained from Bonding Chemical (Katy, TX, USA), N-Methyl-2-pyrrolidone (NMP) from Fisher Sci (Pittsburg, PA, USA), alamarBlue from Bio Rad (Hercules, CA, USA) were all used as received from the manufacturer. Vancomycin Hydrochloride (V-HCl) was obtained from Sagent Pharmaceuticals (Schaumburg, IL, USA). Vancomycin free base (V-fb) was made from V-HCl as previously described [15].

5.3.2. Fabrication of Bioglass

Bioglass substrate (BG) was fabricated using a modification of a previously described method [174] [175]. Briefly, amorphous 45S5 BG particles of approximately 10μm were suspended (40 wt%) in a polyvinyl alcohol (PVA) – water solution (0.01 mol/L of PVA in water) by vigorously stirring to create a slurry. Subsequently, a polyester-based polyurethane (PU) foam with porosity of 90 ppi and dimensions of 1 cm x 1 cm x 0.5 cm was used as a sacrificial polymer template to fabricate a BG scaffold. The foam was dipped into the BG slurry, letting the

particles infiltrate and settle in the porous structure of the PU foam. After soaking for 15 minutes, excess PVA slurry was squeezed out and the foam was dried overnight. The dried foams were then heated and sintered in a kiln (Paragon Caldera XL Kiln, Clay-King.com, Spartanburg, SC, USA). To sinter the BG scaffolds, the kiln was heated at a rate of 2°C/min to 400°C and held at 400°C for 1 hour to burn out the polyurethane foam scaffold. Afterward, the kiln was heated to 1000°C at 2°C/min and held at 1000°C for 1 hour. At the conclusion of this incubation period, the kiln was cooled to room temperature at a rate of 5°C /min (figure 1). The resulting porous glass structure was collected for further use.

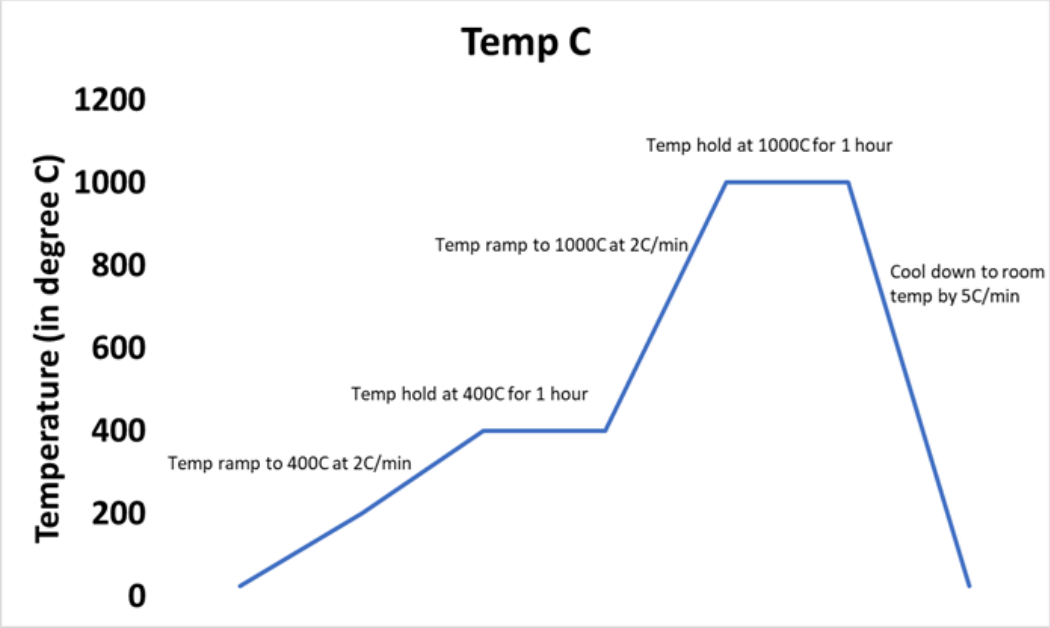

Figure 5.1. Heating and sintering temperature during BG scaffold fabrication.

5.3.3. Fabrication of ABVF-BG

The fabricated porous BG scaffold was crushed and sieved to get a particle size distribution of 150 to 425 μm. The BG particles, 350 mg, were soaked in 1mL of a vancomycin HCl solution (100 mg/mL in phosphate buffered saline) and dried in a controlled environment (37°C in a humidified incubator with 5% CO_2 flow for 48 hours, followed by 50 C at ambient

humidity on hot plate for 1 hour). The polymers (PEG, 21.2 mg, and PCL, 42.5 mg) were melted at 65 C in a steel slide. Antibiotic soaked and dried BG particles were added to the molten polymers and mixed to create a homogenous amalgamation. At this point, vancomycin free base (V-fb, 55.5 mg) was added to the mixture. Subsequently, PLGA, 85.5 mg, dissolved in 200 µL of N-Methyl-2-pyrrolidone (NMP) was mixed into the polymer/drug/BG composite. Later, 20 µL phosphate buffered saline (PBS) was added dropwise to produce a material with putty like consistency. This master mix was compressed into a 3D printed mold to yield a cylindrical shape of 4 mm diameter x 3.5 mm height for further study.

5.3.4. Characterization of Bioglass Scaffold and ABVF-BG

5.3.4.1. X-ray Diffraction (XRD)

The sintered BG scaffolds were crushed to powder using a mortar and pestle and used for XRD. As control the amorphous bioglass powder was also used for XRD. Bruker D8 advanced XRD machine (Bruker, Billerica, MA, USA) was used to run the XRD, employing Cu kα radiation (at 40 kV and 40 mA). Data were collected over the range of 2θ=0–90° using a step size of 15° and a counting time of 300 s per step.

5.3.4.2. Scanning Electron Microscopy (SEM) and Energy-dispersive X-ray Spectrometry (EDS)

SEM and EDS were run on the crushed bioglass particles (150 to 425 µm). SEM was also done on the ABVF putty to observe the morphology of it. For SEM, the samples were attached to cylindrical aluminum mounts with colloidal silver paint (Structure Probe Inc., West Chester, PA, USA) followed by gold coating (Cressington Inc., Redding, CA, USA). Images were taken with a JEOL JSM-6490LV scanning electron microscope. The microscope was equipped with Thermo Scientific UltraDry EDS detector for recording EDS spectra.

5.3.4.3. Assessment of In Vitro Bioactivity in Simulated Body Fluid (SBF)

This study was carried out by following standard method described earlier [176]. Briefly, the crushed BG particles were washed in deionized (DI) water followed by drying. Then in a 6-well plate, 100 mg of the BG particles were taken and 4 mL of SBF was added. The BG in SBF was incubated for 4 days at 37 C in an incubator with exchange of SBF every day. After 4 days, the particles were rinsed gently in DI water followed by drying. The dried particles were used for XRD to see the presence of hydroxyapatite (HA) crystal presence. XRD conditions were the same as described in method 5.3.4.1.

5.3.4.4. Micro Computed Tomography (µ-CT)

For µ-CT, the ABVF-BG or bone was hot glued to a glass rod and placed into a GE Phoenix v|tome| xs X-ray computed tomography system with a 180 kV high power nanofocus X-ray tube xs|180 nf, high contrast GE DXR250RT flat panel detector, and molybdenum target (GE Sensing & Inspection Technologies GmbH, Wunstorf, Germany). One thousand projections were acquired at a voltage of 80 kV and a current of 300 µA. Voxel size was 6.4 µm. Acquired images were reconstructed into a volume data set using GE datos|x 3D computer tomography software Version 2.2 (GE Sensing & Inspection Technologies GmbH, Wunstorf, Germany). The reconstructed volume was then viewed and manipulated using VGStudio Max (Volume Graphics Inc., Charlotte, NC, USA).

5.4. In Vitro Antimicrobial Activity Assay

Vancomycin was released by incubating ABVF-BG putty in PBS (phosphate buffered saline) release media. Cylindrical ABVF-BG (4 mm x 3.5 mm) was put into 2 mL of PBS (1x) in a centrifuge tube and was incubated at 37°C. At different time points (day 1, day 2, day 3, day 7 and every week after that through 6 weeks), all of the release media was collected and replaced

with fresh PBS. After 6 weeks of drug release, the ABVF-BG putty was dissolved in dichloromethane and residual vancomycin was extracted in DI water. In vitro antibacterial activity of the released and residual drug was assessed against *Staphylococcus aureus* (ATCC 49230) using a Kirby-Bauer ZOI assay [91]. Briefly, 100 μL of the collected drug release media was dried on a 6.5 mm diameter filter paper disk by incubating at 37°C. An overnight *S. aureus* culture was prepared and diluted in PBS to get a 10^7 CFU/mL bacterial concentration. The bacterial solution was streaked on Luria Bertani (LB) agar plates. Subsequently, drug-soaked filter paper disks were placed on the plates (within 15 minutes of bacteria streaking) and incubated for 20 hours at 37°C. The ZOI around the disk was measured using a digital caliper.

5.5. In Vitro Cell Viability Assay

Cytotoxicity of ABVF-BG putty was assessed via a standard alamarBlue assay, following the manufacturer's protocol. Briefly, 10,000 MG-63 osteoblast cells (ATCC, Manassas, VA) were seeded in each well of a 96-well plate. Cells were grown in Dulbecco's Modified Eagle Media (DMEM) containing 10% fetal bovine serum (FBS) and 1% penicillin-streptomycin-fungizone (Lonza, Walkersville, MD, USA) and were incubated at 37°C with 5% CO2. After reaching 60% confluence, 100 μL of release media collected at different time points from ABVF-BG was added to each well along with 100 μL of cell culture media. Control wells received 100 μL 1X PBS and 100 μL of cell culture media only. After 48 hours of incubation, cells were washed with 1X PBS three times. Fresh media was added to the wells followed by addition of alamarBlue to a 10% final concentration. Subsequently, wells were incubated at 37°C for 4 hours. After the incubation, the absorbance of the wells was read at 570 nm and 600 nm (Spectramax m5, Molecular Devices, Downingtown, PA, USA). Cell viability was calculated using the following equation:

$$\%\text{cell viability} = ((O2 \times A1) - (O1 \times A2)) / ((O2 \times P1) - (O1 \times P2)), \quad (1)$$

Where, O1 = molar extinction coefficient (E) of oxidized alamarBlue (Blue) at 570 nm, O2= E of oxidized alamarBlue at 600 nm, A1 = absorbance of test wells at 570 nm, A2 = absorbance of test wells at 600 nm, P1 = absorbance of positive growth control well (cells plus alamarBlue but no test agent) at 570 nm, P2 = absorbance of positive growth control well (cells plus alamarBlue but no test agent at 600 nm).

5.6. In Vivo Assessment

5.6.1. Rat Osteomyelitis Model

A rat osteomyelitis model was used to assess the in vivo performance of ABVF-BG according to approved protocol by the Institutional Animal Care and Use Committee (IACUC) at North Dakota State University (A19019). Sprague-Dawley rats, both male and female, (>280 grams) were used for the in vivo study. Briefly, rats were anesthetized by isoflurane inhalation. The right hind leg was shaved and sterilized using alcohol and iodine pads, repeatedly. A small incision of ~12 mm was made below the knee over the tibial metaphysis. A 4.2 mm hole was drilled using an orthopedic drill (Stryker, Kalamazoo, MI, USA) until it penetrated the bone and revealed the marrow space of the tibial metaphysis. Overnight S. aureus culture diluted in sterile saline to achieve concentration of 10^8 CFU/10 μL was injected (10 μL) through the drill hole defect into the marrow space using a 25 μL Hamilton syringe followed by implantation of the ABVF-BG putty to fill up the drilled hole. The incision was closed using a series of mattress sutures followed by application of surgical glue (Vetbond Tissue Adhesive, 3M, MN, USA). Following the surgery, buprenorphine hydrochloride (Hospira, Inc., Lake Forest, IL, USA) was injected (0.01 mg/kg) subcutaneously as an analgesic. The control group underwent the same surgical procedure but received putty without antibiotic (BVF putty). Rats were assigned

randomly to the control and treatment group. Rats were monitored daily for signs of discomfort and infection. After 8 weeks, the rats were sacrificed, and the tibia was harvested for further study.

5.6.2. X-ray and μ-CT

Following euthanasia, radiographic analyses of bones were done after disarticulating the limb and harvesting the bone by removing soft tissue. X-ray was done using IDEXX CR Digital Radiography System (Westbrook, Maine, USA) following standard protocols. Briefly, lateral and cranial-caudal radiographic images of each limb were obtained at mAs: 4 and kVp: 40. μ-CT of the bone was done following similar procedure as described in section 5.3.1.4 with slight adjustment of current to 400 – 500 μA.

5.6.3. Bacterial Colony Count

Collected bone was flash frozen in liquid nitrogen, followed by pulverization using a custom-made bone crusher. The pulverized bone was weighed and suspended in 500 μL of PBS. Serial dilutions were made [90] and 10 μL of suspension was plated on blood agar plates (Fisher Sci, Pittsburg, PA, USA). Subsequently, plates were incubated for 48 hours at 37°C and bacterial colonies were counted. To get the total number of bacteria in the total sample, the number of colonies were multiplied by the dilution factor and normalized per gram of bone.

5.6.4. Histology

After euthanasia, the bone was harvested and fixed in 10% neutral buffered formalin for 72 hours. Subsequently, bone was decalcified by immersing it in an EDTA solution (10% solution at pH 7.4) for 2 weeks. The EDTA solution was exchanged every other day. Once the bone was decalcified, it was embedded in paraffin wax and sectioned (5 μm). Sections were mounted on glass slides and stained with hematoxylin and eosin stains (H&E stain - Scy Tek

Lab., Logan, Utah, USA) according to standard protocols. Briefly, the sections were deparaffinized in Clear Rite 3 (Thermo Fisher Scientific, Kalamazoo, MI, USA). Subsequently, tissue was rehydrated with a decreasing gradient of ethanol. After H&E staining, the tissue section was covered with a glass coverslip using synthetic resin mounting media (Cytoseal XYL, Thermofisher, Kalamazoo, MI, USA). Stained slides were imaged at 40x using MoticEasyScan Digital Slide Scanning microscope (Motic Digital Pathology, San Francisco, CA, USA).

5.6.5. Statistical Analysis

The statistical package in Microsoft Excel 2016 was used for all calculations and statistical analyses. A student's T-test using $\alpha=0.05$ was done to determine statistical significance.

5.7. Results

5.7.1. XRD of Bioglass

XRD was done to assess the crystallinity of sintered BG. XRD of non-sintered BG shows amorphous XRD spectra (Figure 5.2 a). The sintered BG showed partially crystalline structure with mostly crystalline peaks related to crystalline $Na_2Ca_2Si_3O_9$ (Figure 5.2 b) [159,174]. The SBF exposed BG particles showed the presence of HA crystals (Figure 5.2 c). It can be noted from the changing XRD pattern of the SBF exposed BG particles that there is reduced crystallinity compared to sintered only BG particles (Figure 5.2 b).

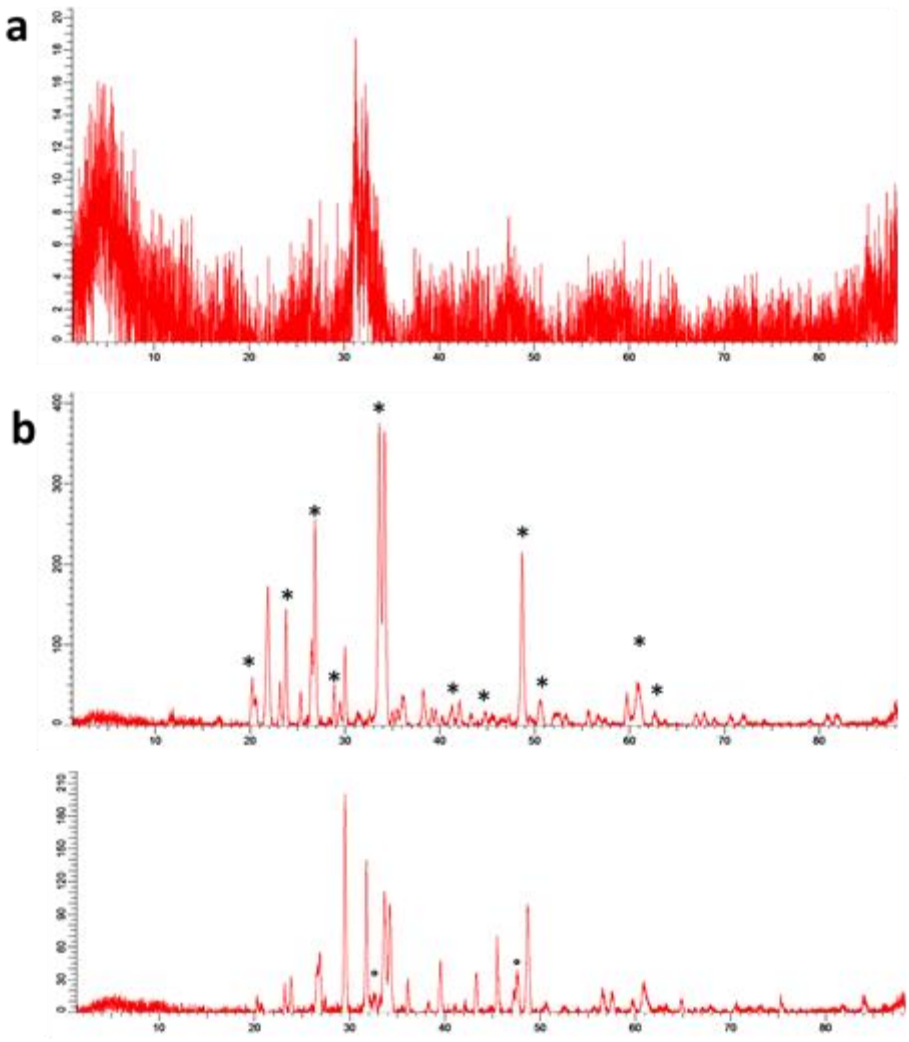

Figure 5.2. XRD spectra of amorphous bioglass powder, sintered BG particles and SBF exposed sintered BG particles.
a) XRD of amorphous bioglass particles before sintering. b) XRD of partially crystalline BG after sintering. Major peaks corresponding to crystalline phase containing Na2Ca2Si3O9 are marked with *. c) BG after been immersed in simulated body fluid for 4 days. Presence of HA can be seen, indicated by °.

5.7.2. SEM and EDS of Sintered Bioglass and ABVF-BG

SEM of sintered BG scaffold showed porous structure with pores ranging from 80 μm to 223 μm (Figure 5.3). The strut of the scaffold structure ranges from 81 μm to 242 μm (Figure 5.3). The strut provided the scaffold like structure resulting from the partial crystallinity of the bioglass that provided the support for holding the structure by providing increased mechanical

strength [174]. The SEM of particles of crushed bioglass scaffold showed particles of different width (Figure 5.4 a). It corresponds to the struts of different width seen in the scaffold (Figure 5.3). A close image of the strut showed densification after sintering along with micropores ranging from 1 – 4 μm on the particles. EDS spectra of the sintered BG showed the presence of Ca, P, Na and Si in the sintered BG (Figure 5.5). SEM of the ABVF-BG showed porous inner structure (Figure 5.6).

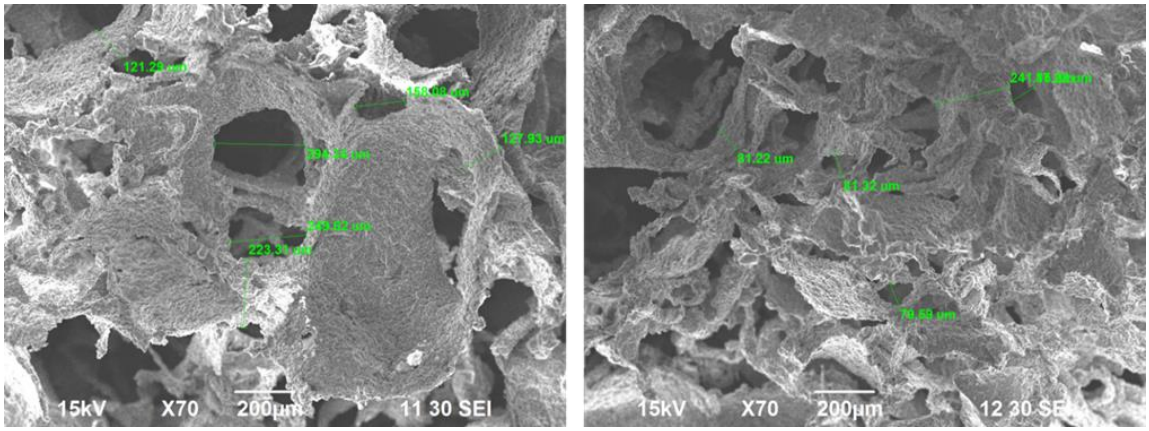

Figure 5.3. SEM image of BG scaffold after sintering.
The porous structure is visible in the images.

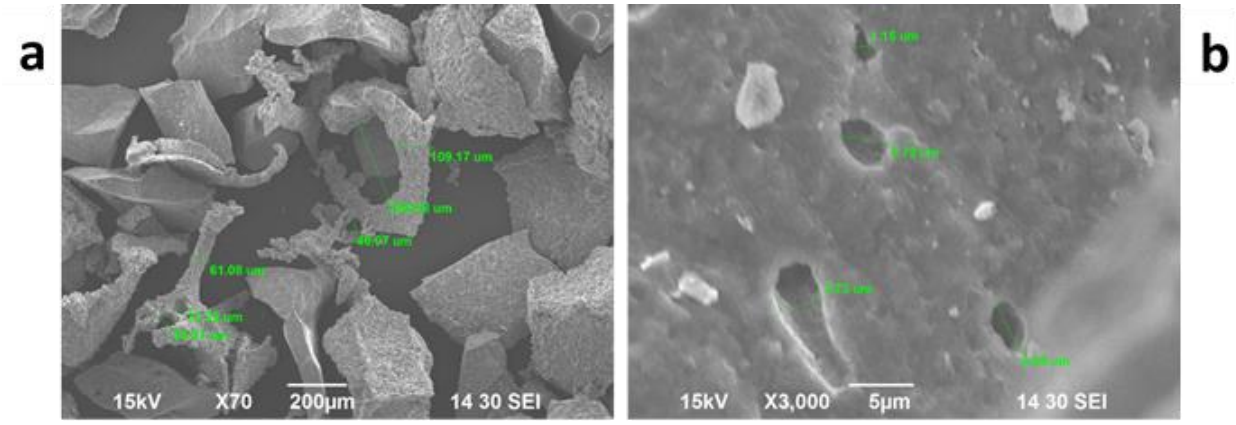

Figure 5.4. a) SEM images of crushed sintered BG particles.
Sturt of different width are seen. Micropores are also visible on the struts. b) The densified strut morphology is also seen.

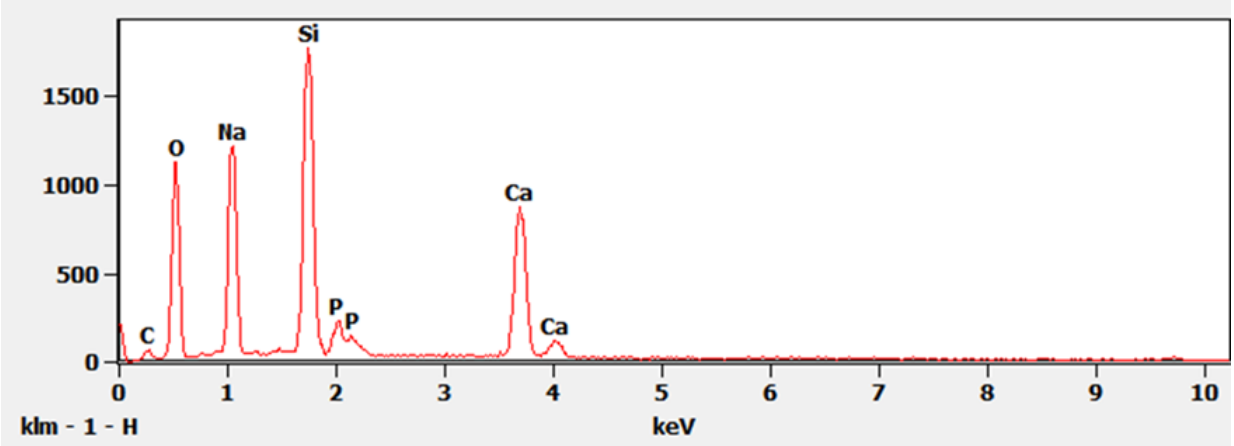

Figure 5.5. EDS spectra of sintered bioglass.
EDS showed the presence of Na, Si, P, and Ca in the sintered bioglass.

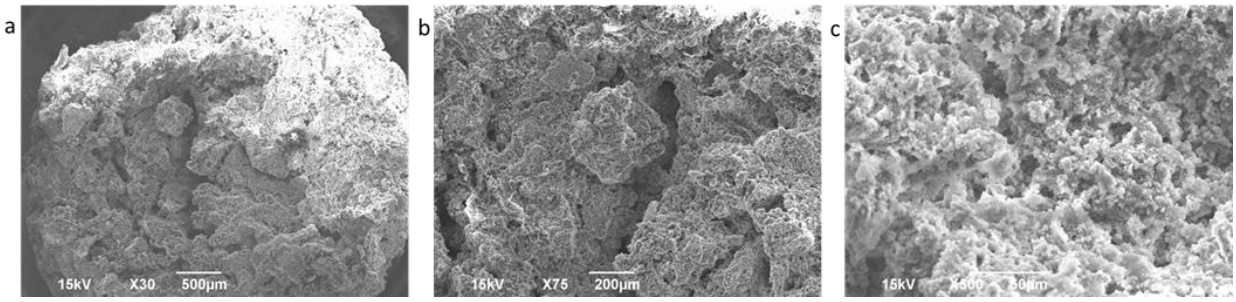

Figure 5.6. SEM image of ABVF-BG putty fabricated with BG as the bone graft substitute.
a) SEM of outer structure of ABVF-BG. b) and c) SEM of inner structure of ABVF-BG showing pores.

5.7.3. µ-CT of ABVF-BG

µ-CT was done on the ABVF-BG putty to assess the distribution of BG particles in the polymer matrix of ABVF-BG. µ-CT of the ABVF-BG showed homogenous distribution of BG particles embedded in the polymer matrix (Figure 5.7). The BG particles seems to be more densely packed (45.54% v/v vs 28.23% v/v) within the polymer matrix than the previous formulations with Pro Osteon (Figure 3.1 b).

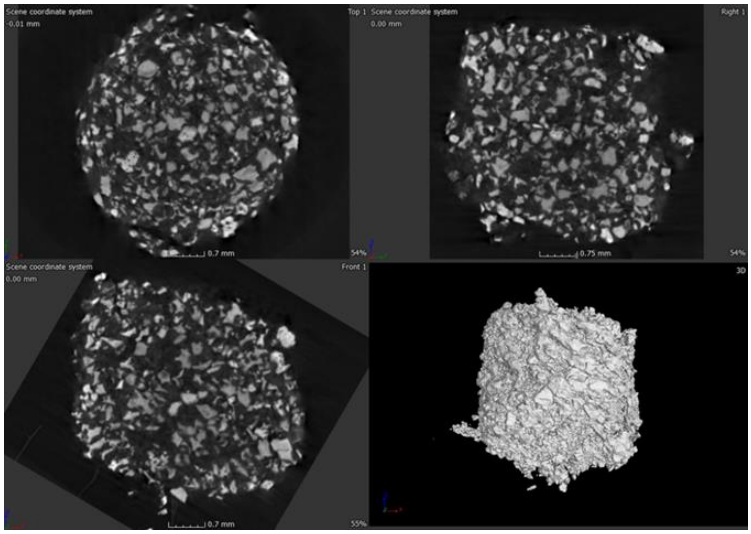

Figure 5.7. μ-CT image of ABVF-BG showing BG particles are homogenously distributed in the polymer matrix.

5.7.4. In Vitro Antimicrobial Activity Assay

Vancomycin released from ABVF-BG showed efficient antibacterial activity against S. aureus up to 6 weeks (Figure 5.8). At week 6, the standard deviation of the ZOI was large. But there was still some vancomycin left in the ABVF-BG after 6 weeks as residual antibacterial activity was seen from the extracted residue of the completely released ABVF-BG putty.

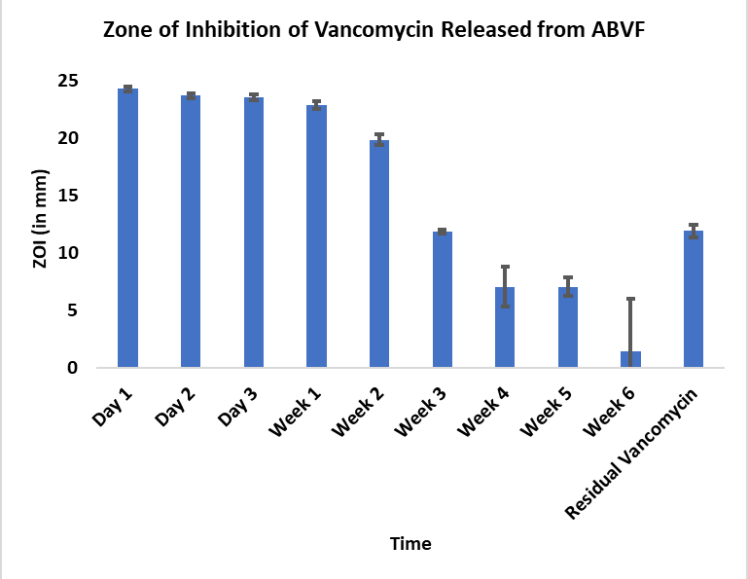

Figure 5.8. Zone of inhibition of released vancomycin from ABVF-BG against *S. aureus* (strain ATCC 49230).

5.7.5. In Vitro Cell Viability Assay

MG-63 osteoblasts cells were exposed to drug released media from ABVF-BG putty to assess the cytotoxicity of released vancomycin at different time points. Compared to control cells, which were not exposed to any vancomycin, no significant change in cell viability was observed in when cells were exposed to day 1 and week 3 drug released media (Figure 5.9). However, cell viability dipped to just over 80% at week one, a significant decrease ($p<0.05$) in viability compared to the control (Figure 5.9).

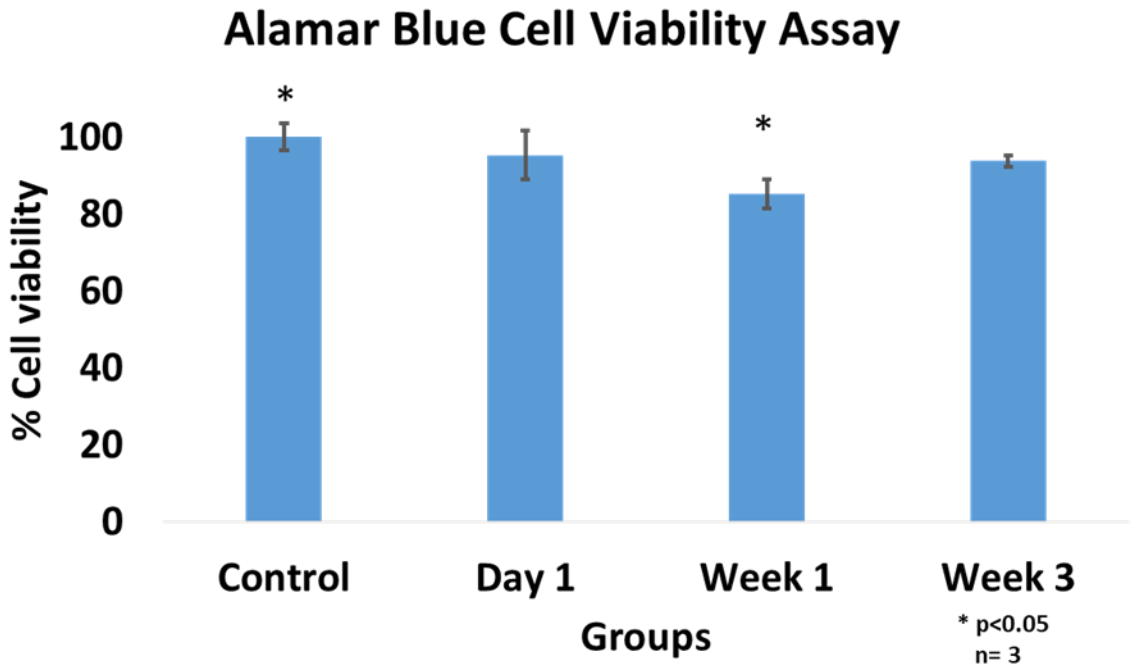

Figure 5.9. Cell viability of MG-63 cells when exposed to drug released media from bioglass based ABVF-BG.
No significant difference was seen in cell viability when cells were exposed to day 1 and week 3 drug release media, although a significant drop in cell viability was observed when cells were exposed to week 1 drug release sample.

5.7.6. In Vivo experiment

5.7.6.1. X-ray and μ-CT of Rat Bones

X-ray of the tibia in the infection control group (i.e., ABVF-BG putty with no antibiotic) showed classic signs of infection such as un-healed, osteolytic and deformed bone (Figure 5.10). Narrowing of marrow space is also visible. In contrast, treatment group rat bone showed no signs of infection and the bone seemed to have healed well (Figure 5.10). μ-CT images showed presence of infection in infection control rat tibia (Figure 5.11 a). The signs of osteomyelitis such as narrowing of marrow space, presence of puss filled fibrous capsule, sinus tract and deformed bone with ectopic bone growth are visible. Alternatively, healing bone without signs of infection was seen in treatment group rat bone μ-CT images. The hole drilled space was being filled by growing cancellous and cortical bone (Figure 5.11 b).

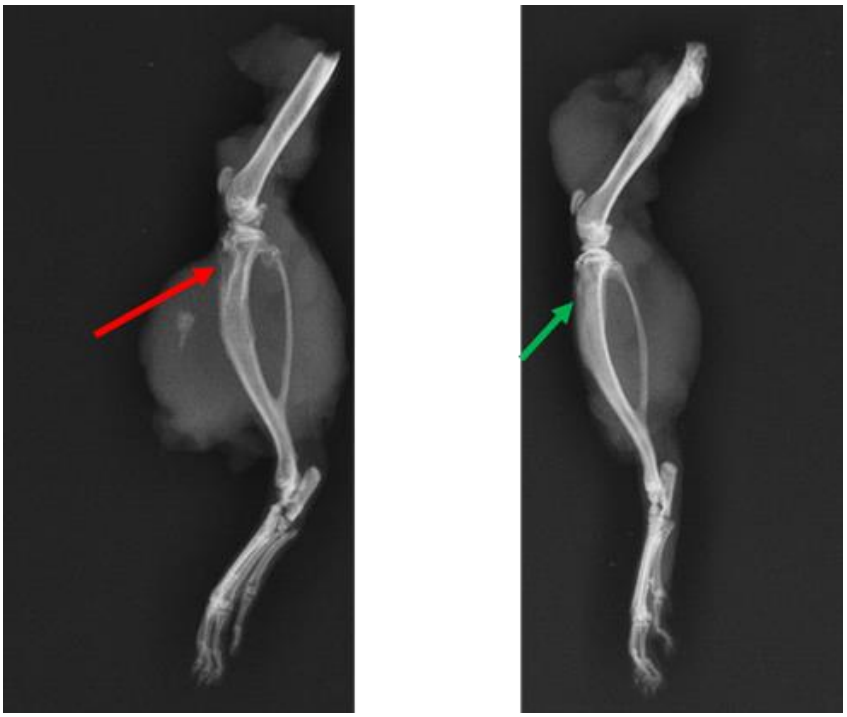

Figure 5.10. X-ray of rat tibia from different groups of osteomyelitis model.
Red arrow is showing osteomyelitic bone of control rat bone with infection. Green arrow is showing infection free, healed bone.

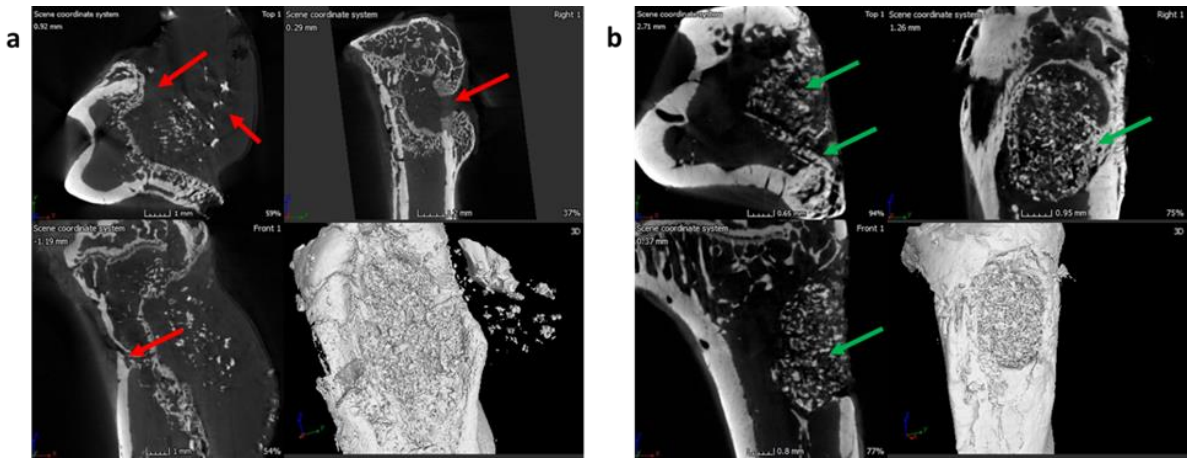

Figure 5.11. μ-CT radiographs of rat bones from different groups of osteomyelitis model. a) μ-CT image of the infection control group rat bone showed signs of infection: narrowing of marrow space, presence of puss filled fibrous capsule, sinus tract and deformed bone with ectopic bone growth (red arrows). b) The treatment group rat bone μ-CT image is showing signs of healing bone, formation of cortical and cancellous bone in the space where hole was drilled (green arrows).

5.7.7. Bacterial Colony Count

The bacterial colony count confirmed the infection visible in imaging (Figure 5.10 and 5.11 a) in infection control group rats. The control group rat bone showed high amount bacterial load ($4.63 \times 10^6 \pm 7.9 \times 10^5$ CFU/gram bone) (Figure 12). In contrast, treatment group rat tibia showed no bacterial growth in culture confirming absence of any infection (Figure 5.12). Here, 2 biological replicates and 4 technical replicates were used for bacterial colony count for each group.

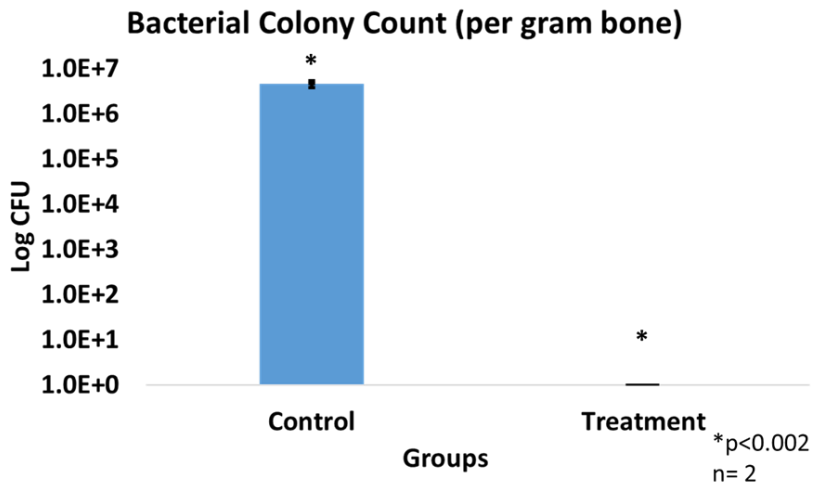

Figure 5.12. Bacterial colony count after culturing bacteria from rat bones of different groups. High amount of bacterial presence was seen in infection control group rat tibia. The treatment group rat showed no bacterial colony in culture.

5.7.8. Histology

To assess histological features of the bone at the surgical site, H&E staining was done. Tibia from the control rats showed unhealed bone, including a lack of new bone growth and the presence of fibrous tissue, a consequence of infection. Additionally, the presence of chronic infection was evident (red arrows, Figure 5.13a). On the contrary, bone from the treatment group showed ongoing bone healing, including new bone growth and osseointegration, likely resulting from the absence of infection (Figure 5.13b). It also showed limited mature collagen structure (green arrows, Figure 5.13b). These signs are consistent with the documented healing process of bone in the absence of infection.

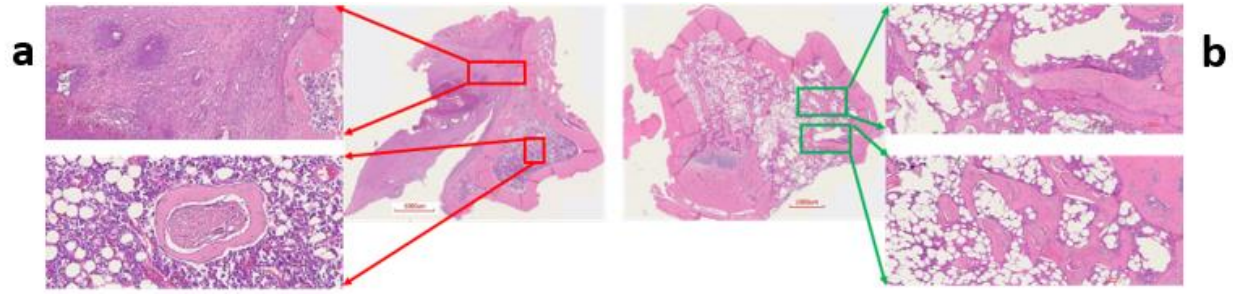

Figure 5.13. H&E staining of rat bone.
(a) Control rat bone. Note that there is growth with narrowing of the marrow space. Additionally, there are places of bone thickening and a large fibrous capsule with inflammatory cells. (b) Bone from the treatment group rat shows ongoing healing of the bone, including new bone formation in the defect. Osseointegratation of the host bone was seen, as the degradation of the ABVF-BG allowed new bone to in growth.

5.8. Discussion

Bioactive glass or BG has been a subject of interest in tissue engineering, specifically for orthopedic applications, because of its bone-bonding properties [177]. 45S5 amorphous BG powder, used in this study to synthesize BG scaffold, is particularly well known for its ability to bond bone. Its ability to bond bone can be attributed to the conversion of the BG material to a HA like layer. The conversion starts with the formation of a SiO_2-rich gel on the 45S5 glass surface by ion exchange reactions. Dissolution and diffusion of the ions from the BG through the SiO_2- rich gel layer, contributes to the reaction between Ca^{2+} and PO_4^{3-} ions from the surrounding liquid. This reaction ends in the growth of an HA like layer on the gel surface [178]. Although, BG may be good option as a bone void filler due to its bone healing properties, unlike other BVF materials, conventional casting and melt derived BG, as in our case, can be challenging to be used as an antibiotic carriers due to higher density and less porosity [179]. Sol-gel method derived BG, although, can be used to load antibiotics in their mesoporous structure, they show unpredictable antibiotic release, extremely low overall release (20-25%) of loaded drug and poor mechanical property [179]. Thus, BG composite, such as the ABVF-BG putty that we have developed, where BG particles are loaded in a biodegradable polymer matrix that

controls drug release, is a viable option for BG based antibiotic delivery for osteomyelitis treatment.

Perhaps as a consequence of its ability to bond bone, BG based bone void fillers, particularly when formulated as a putty, have previously been shown double the amount of bone formation after 6 weeks when compared to particulate BG in a sheep vertebral defect model [180]. Importantly, the putty matrix may have allowed more space for bone formation as the matrix degraded than tightly compacted particulate. Furthermore, a putty might prove preferable for both its handling characteristics as well as its immune interactions; migration of loose BG particulates have been shown to provoke inflammation [181].

To take advantage of the bone bonding and healing properties of BG in the current study, amorphous 45S5 BG powder was sintered to create a partially crystalline scaffold. Using the conditions described here (method 5.3.1.2) yielded the presence of $Na_2Ca_2Si_3O_9$ in the crystalline region after sintering (Figure 5.2 b) when compared to the amorphous 45S5 BG powder (Figure 5.2 a). The presence of $Na_2Ca_2Si_3O_9$, which was shown to be converted into an amorphous form in the presence of phosphate ions, is critical for the bioactivity of any BG based scaffold [174]. Previously, bioactivity of $Na_2Ca_2Si_3O_9$ crystals has been reported, showing that the combination of this non-phosphate bioactive crystal with phosphate ions from the BG particle leads to faster HA formation in vitro in SBF, similar to amorphous BG powder [182]. In a previous studies, the rate of HA crystal formation on crystalline BG particulate was slower when put into SBF, but the bioactivity was still preserved [183]. In current study, after subjecting the sintered BG particles to SBF, a peak corresponding to HA appeared in the XRD, and a reduced crystallinity of $Na_2Ca_2Si_3O_9$ was observed (Figure 5.2 c), which may indicate the crystalline $Na_2Ca_2Si_3O_9$

phase started to convert to a more amorphous form [174]. Nonetheless, bioactivity was preserved.

In addition to the traditional, albeit slightly slower, changes in the surface of the BG that lead to bone bonding and likely contribute to bone healing, the influence of porosity in this process cannot be neglected. In our current study, the sintered BG scaffold had a porous structure with varying pore sizes (Figure 5.3); this porosity was likely a result of the sacrificial polyurethane polymer template, although the variability of the pore sizes may reflect the BG structure somewhat collapsing in the absence of the polymer template during the sintering process. Additionally, the pore sizes of the template may be variable and not be well defined due to variation in the penetration of BG slurry into the polyurethane template. Regardless, a range of pore sizes is seen, which is important for vascularization and bone ingrowth. Different studies reported different pore sizes as optimal but there is no clear consensus. Pore size range of 150–710 μm bone tissue engineering [184], 5 – 600 μm for bone regeneration [185], 50 to 710 μm for bone regeneration and 5 μm for neovascularization [186] have been reported. Although there is much variation, it can be said that porous structure is necessary for bone tissue healing [187]. SEM image of the crushed BG scaffold showed particles was were used to formulate the ABVF-BG (Figure 5.4 a). A zoomed in view showed a densified structure of the particles with micropores, as noted in earlier studies [174]. Densification here is desired as this would provide a measure of structural integrity under compression. The EDS of the sintered BG confirmed the presence of the different elemental composition in the sintered BG (Figure 5.5) when compared to the amorphous BG powder used. Additionally, ABVF-BG putty prepared with sintered BG particles showed a porous macrostructure throughout the composition (Figure 5.6 b) as well as the presence of micropores throughout the structure (Figure 5.6 c). Macroporosity likely resulted

from the disbursement of sintered BG particles in a putty like polymer matrix. μ-CT of the ABVF-BG putty showed the homogenous distribution if the BG particles embedded in the polymer matrix (Figure 5.7). The packing density of the particles in the putty is a critical parameter that can be optimized to facilitate host bone cell infiltration and ingrowth. The BG-based ABVF-BG putty reported here has an appropriate spatial distribution of the BG particles in a degrading polymer matrix, which may be further optimized, offering a distinct advantage of our ABVF-BG putty over other BG particulate only fillers [180]. Ultimately, the presence of both a macro and micro pores as seen in the produced ABVF-BG putty would support bone tissue healing.

In addition to providing a significant advantage for bond bonding and regeneration, several types of particulate BG such as S53P4 and 45S5 have been shown to possess antibacterial properties in vitro due to increasing pH, osmotic pressure and calcium ion concentration [188] [189]. However, in another apparent disconnect between in vitro performance and in vivo efficacy, particulate BG fillers failed to exert any significant effect on infection prevention in a rabbit open tibial fracture model [190]. Mechanistically, the authors argued that the body's buffering capacity may have prevented an increase in pH sufficient to lead to bacterial killing. Nevertheless, the efficacy of BG in comparison to calcium sulfate antibiotic beads was assessed in a human trial of osteomyelitis. In that particular trial, the BG showed similar activity as calcium sulfate antibiotic beads; however, it must be noted that, both groups of patients received systemic antibiotic for 6-12 weeks as part of the trial, casting doubt on the efficacy of BG as an antimicrobial material [155].

Vancomycin still remains as the standard recommended antibiotic for treating osteomyelitis caused by *S. aureus* [148]. Moreover vancomycin is effective against methicillin-

resistant *Staphylococcus aureus* (MRSA) and the bacteria are slow to evolve resistance against vancomycin [173]. Although the BG in our putty was not shown to have innate antibacterial activity (data not shown), when incorporated into the reported ABVF-BG putty formulation, the drug released from showed antibacterial efficacy against *S. aureus* for up to 6 weeks (Figure 5.8), our targeted timeframe to treat osteomyelitis based on clinical data [150]. Residual antibacterial activity shown after 6 weeks release may be due to some vancomycin still trapped in the remaining polymer matrix. Although not a significant concern for this study, the complete release of drug the ABVF-BG putty should occur within the desired therapeutic window as to avoid inadvertently promoting the development of antibiotic resistant species, a consequence which has not been observed with any of our ABVF-BG putty formulations explored to date. Regardless, in the in vivo study no residual bacterial content could be cultured from the tibia of the treatment group, a significant reduction in bacterial content when compared to the control group, $p<0.002$. High bacterial content (4.63×10^6 CFU/ gram bone) was seen in the tibia harvested from the infection control group implanted with BG BVF putty with no antibiotic at (Figure 5.12). In addition, these rats had a puss filled capsule at the surgical site, which was separated from the bone and cultured, yielding incredibly high bacterial load, innumerable even after 10^8 fold dilution.

While the drug release milieu from the ABVF-BG putty effectively killed *S. aureus* both in vitro and in vivo, cytotoxicity is an important criterion to assess. In vitro cell viability assays showed no significant difference in osteoblast cell viability at day 1 and week 3 (although there was a significant dip in viability at week 1 (Figure 5.9). Nevertheless, cell viability remained about 85%, which is within the acceptable limit for medical devices and materials (viability above 70%) according to the International Organization for Standardization guidelines [191].

Interestingly, at day 1 when the drug concentration is anticipated to be the highest (Figure 5.8) and week 3, which corresponds to the predicted onset of degradation of the putty's polymer matrix, cell viability was not significantly reduced. Therefore, it is unclear why there was a decline in viability at week1.

Despite the conundrum surrounding our cytotoxicity assay, assays indicated the safety and efficacy of our ABVF-BG putty; hence, we proceeded to assess our ABVF-BG putty in vivo, with promising results. X-ray imaging showed healed or healing bone in the treatment group (Figure 5.10 b). In contrast, the infection control group showed the telltale signs of osteomyelitis: deformed bone, osteolysis, periosteal thickening and formation of sequestrum (Figure 5.10 a). μ-CT of the bones confirmed the finding. The treatment group bone showed no signs of osteomyelitis as the bone appeared to be healed with new bone formation and remodeling taking place (Figure 5.11 b). On the contrary, severe osteomyelitis was seen in the infection control group with decreased and deformed bone formation, narrowing marrow space and the formation of sinus tracts. Infection seemed to be spread to the posterior of the bone, and the presence of puss filled capsule was also seen (Figure 5.11 a).

A shortcoming of the current study was that the number of rats used per group was only 3. In future studies, the cohort size will be increased. It might also be of interest to see the effect of time in bone regeneration. That means to see how much bone regrowth happened at week 4, 6, 10 and 12. This remains as a future study of interest. But nevertheless, this study showed that bone regeneration was achieved at a satisfactory level and well as the infection is cured in the treatment group rats. All 3 control group rats remained infected at the end of study period with severe osteomyelitis demonstrated, while all the treatment group rats were cured and remained infection free.

5.9. Conclusions

The successful infection treatment and satisfactory bone healing in rats shows the promise of a BG based ABVF-BG putty to treat osteomyelitis. ABVF-BG provided effective release of vancomycin showing in vitro and in vivo efficacy against S. aureus. ABVF-BG was biodegradable and provided support for new bone growth. No adverse effects were seen on either overall rat health or on in vivo bone healing. The BG based ABVF-BG putty developed in this study can be a promising option for difficult to treat osteomyelitis in bone.

6. CONCLUSIONS AND FUTURE DIRECTIONS

Many attempts have been taken to develop novel methods to treat osteomyelitis over the years. Despite the efforts, the overall benefits for morbidity have been modest. Developing a local drug delivery vehicle with bone healing properties may address this challenging pathology. However, hitting the sweet spot to balance infection cure with implant degradation and bone regeneration can be difficult. Continuous strides need to be made to fight these infections so that antibiotic resistance, which is prevalent in recurrent osteomyelitis, can be prevented, thereby improving patients' lives.

In the scope of the current study, we have attempted to develop several different novel formulations in the search for alternative treatment options for osteomyelitis. In the second chapter, we used different custom-made polymers to design an antibiotic releasing bone void filler (ABVF) with putty-like material characteristics to provide bacterial killing for up to 6 weeks. Although certain custom polymers provided desirable in vitro kinetics, their synthetic yield was limited, potentially restricting future development and leading us to develop additional formulations around a commercial polymer blend. However, future experiments should consider the in vivo evaluation of the most promising custom polymers.

The next chapter describes the development of an easy to fabricate ABVF putty using commercially available and clinically used biodegradable polymers. The ease of the fabrication makes it viable for clinical use while the handling properties of a putty are in harmony with current clinical practice, being familiar to surgeons, who in many cases, mix and make bone void filler during or just prior to surgery. To achieve antibacterial activity for up to 6 weeks, the form of vancomycin was converted to a less soluble free-base form to slow down the drug release. This formulation achieved the desired drug release kinetics and provided an in vivo infection

cure and bone healing in a rodent model. A study in a larger sheep model should be done in the future to assess its utility in a model more akin to the biomechanics and biology of human bone.

Having established that ABVF containing vancomycin is effective against planktonic *S. aureus* in the bone in the 4th chapter, ABVF-C as a combination antibiotic delivery system was assessed to determine its effectiveness against *S. aureus* biofilm infections. Biofilm infections that involve orthopedic implants are extremely challenging to treat. Currently, implant removal and a multi-stage revision surgery is the standard clinical practice. Unfortunately, the antibiofilm antibiotic rifampicin cannot be incorporated into the most common cement based bone void filler, limiting the utility of bone cement for biofilm based infections, which are increasingly common. Importantly, rifampicin oral therapy is very often prescribed along with another antibiotic to treat these infections due to the development of resistance. Thus, our goal was to add a level of customization to the ABVF putty developed in chapter 3 to treat implant related biofilm infections by delivering a combination of rifampicin and vancomycin. We have successfully treated biofilm infections in a rat infection model using a mature biofilm grown on a k-wire. The rats remained infection free until the end of the study. This study specifically shows huge promise for the ABVF-C putty delivering antibiofilm combination antibiotics to treat biofilm infections. In future, larger cohorts of animals need to be included in a statistically powered in vivo study. A long-term survival study can also be carried out to see if there is any recurrence of infections if the implant is not removed from the bone.

In the final formulation, described in chapter 5, we wanted to include bioglass, which is known to possess bone-bonding properties and provides faster mineral apposition and bone healing. We have manufactured partially crystalline bioglass particles to formulate ABVF-BG putty containing vancomycin as the antibiotic. The ABVF-BG putty provided efficient in vitro

bacterial killing and inhibited infection in rats while providing good bone healing. This turned out to be a very promising formulation. In future, larger cohorts of animals need to be tested using this ABVF-BG. Additionally, it will be worthwhile to add rifampicin to the formulation to assess its ability to kill a biofilm.

In this dissertation, attempts were made to develop a customizable ABVF putty to treat osteomyelitis. The experiments and corresponding results show a very promising treatment alternative for recalcitrant osteomyelitis.

REFERENCES

1. Momodu, I.I.; Savaliya, V. Osteomyelitis. In *StatPearls*; StatPearls Publishing: Treasure Island (FL), 2019.
2. Kremers, H.M.; Nwojo, M.E.; Ransom, J.E.; Wood-Wentz, C.M.; Melton, L.J.; Huddleston, P.M. Trends in the Epidemiology of Osteomyelitis. *J. Bone Joint Surg. Am.* **2015**, *97*, 837–845.
3. Lima, A.L.L.; Oliveira, P.R.; Carvalho, V.C.; Cimerman, S.; Savio, E.; Diretrizes Panamericanas para el Tratamiento de las Osteomielitis e Infecciones de Tejidos Blandos Group Recommendations for the treatment of osteomyelitis. *Braz. J. Infect. Dis. Off. Publ. Braz. Soc. Infect. Dis.* **2014**, *18*, 526–534.
4. Campoccia, D.; Montanaro, L.; Arciola, C.R. The significance of infection related to orthopedic devices and issues of antibiotic resistance. *Biomaterials* **2006**, *27*, 2331–2339.
5. Kurtz, S.M.; Lau, E.; Schmier, J.; Ong, K.L.; Zhao, K.; Parvizi, J. Infection Burden for Hip and Knee Arthroplasty in the United States. *J. Arthroplasty* **2008**, *23*, 984–991.
6. Kurtz, S.; Ong, K.; Lau, E.; Mowat, F.; Halpern, M. Projections of Primary and Revision Hip and Knee Arthroplasty in the United States from 2005 to 2030. *J Bone Jt. Surg Am* **2007**, *89*, 780–785.
7. Tande, A.J.; Patel, R. Prosthetic Joint Infection. *Clin. Microbiol. Rev.* **2014**, *27*, 302–345.
8. Mortazavi, S.M.J.; Schwartzenberger, J.; Austin, M.S.; Purtill, J.J.; Parvizi, J. Revision Total Knee Arthroplasty Infection: Incidence and Predictors. *Clin. Orthop.* **2010**, *468*, 2052–2059.
9. Conterno, L.O.; da Silva Filho, C.R. Antibiotics for treating chronic osteomyelitis in adults. *Cochrane Database Syst Rev* **2009**, *3*.
10. Landersdorfer, C.B.; Bulitta, J.B.; Kinzig, M.; Holzgrabe, U.; Sörgel, F. Penetration of Antibacterials into Bone. *Clin. Pharmacokinet.* **2009**, *48*, 89–124.
11. Antonova, E.; Le, T.K.; Burge, R.; Mershon, J. Tibia shaft fractures: costly burden of nonunions. *BMC Musculoskelet. Disord.* **2013**, *14*, 42.
12. Diefenbeck, M.; Mückley, T.; Hofmann, G.O. Prophylaxis and treatment of implant-related infections by local application of antibiotics. *Injury* **2006**, *37*, S95–S104.
13. Schäberle, T.F.; Hack, I.M. Overcoming the current deadlock in antibiotic research. *Trends Microbiol.* **2014**, *22*, 165–167.
14. Antibiotic Resistance Threats in the United States, 2013 | Antibiotic/Antimicrobial Resistance | CDC Available online: https://www.cdc.gov/drugresistance/threat-report-2013/ (accessed on Feb 5, 2018).
15. Kraker, M.E.A. de; Stewardson, A.J.; Harbarth, S. Will 10 Million People Die a Year due to Antimicrobial Resistance by 2050? *PLOS Med.* **2016**, *13*, e1002184.
16. Europe, O.T.; Issue 1 MRSA, MRSE infection in joint replacement Available online: https://www.healio.com/orthopedics/business-of-orthopedics/news/print/orthopaedics-today-europe/%7Be8ac00f1-3716-4b13-9994-6409223494a9%7D/mrsa-mrse-infection-in-joint-replacement (accessed on Mar 24, 2018).
17. Brooks, A. Novel Local Bone Void Filling Antibiotic Carriers for the Treatment of Bone Infection. *Orthop. Res. Online J.* **2017**, *1*.
18. Brooks, B.D.; Brooks, A.E. Therapeutic strategies to combat antibiotic resistance. *Adv. Drug Deliv. Rev.* **2014**, *78*, 14–27.

19. Kalore, N.V.; Gioe, T.J.; Singh, J.A. Diagnosis and Management of Infected Total Knee Arthroplasty. *Open Orthop. J.* **2011**, *5*, 86–91.
20. Haidar, R.; Boghossian, A.D.; Atiyeh, B. Duration of post-surgical antibiotics in chronic osteomyelitis: empiric or evidence-based? *Int. J. Infect. Dis.* **2010**, *14*, e752–e758.
21. Gogia, J.S.; Meehan, J.P.; Di Cesare, P.E.; Jamali, A.A. Local Antibiotic Therapy in Osteomyelitis. *Semin. Plast. Surg.* **2009**, *23*, 100–107.
22. Tunney, M.M.; Patrick, S.; Gorman, S.P.; Nixon, J.R.; Anderson, N.; Davis, R.I.; Hanna, D.; Ramage, G. Improved detection of infection in hip replacements. *J. Bone Joint Surg. Br.* **1998**, *80-B*, 568–572.
23. Lian, X.; Mao, K.; Liu, X.; Wang, X.; Cui, F. In Vivo Osteogenesis of Vancomycin Loaded Nanohydroxyapatite/Collagen/Calcium Sulfate Composite for Treating Infectious Bone Defect Induced by Chronic Osteomyelitis Available online: https://www.hindawi.com/journals/jnm/2015/261492/ (accessed on Oct 24, 2017).
24. Morley, R.; Lopez, F.; Webb, F. Calcium sulphate as a drug delivery system in a deep diabetic foot infection. *The Foot* **2016**, *27*, 36–40.
25. The use of antibiotic impregnated absorbable calcium sulphate beads in management of infected joint replacement prostheses - ScienceDirect Available online: http://www.sciencedirect.com/science/article/pii/S2214963514000522?via%3Dihub (accessed on Oct 24, 2017).
26. Rauschmann, M.A.; Wichelhaus, T.A.; Stirnal, V.; Dingeldein, E.; Zichner, L.; Schnettler, R.; Alt, V. Nanocrystalline hydroxyapatite and calcium sulphate as biodegradable composite carrier material for local delivery of antibiotics in bone infections. *Biomaterials* **2005**, *26*, 2677–2684.
27. Ferguson, J.; Diefenbeck, M.; McNally, M. Ceramic Biocomposites as Biodegradable Antibiotic Carriers in the Treatment of Bone Infections. *J. Bone Jt. Infect.* **2017**, *2*, 38–51.
28. Bohner, M. Calcium orthophosphates in medicine: from ceramics to calcium phosphate cements. *Injury* **2000**, *31 Suppl 4*, 37–47.
29. Maier, G.S.; Roth, K.E.; Andereya, S.; Birnbaum, K.; Niedhart, C.; Lühmann, M.; Ohnsorge, J.; Maus, U. In Vitro Elution Characteristics of Gentamicin and Vancomycin from Synthetic Bone Graft Substitutes. *Open Orthop. J.* **2013**, *7*, 624–629.
30. Jones, Z.; Brooks, A.E.; Ferrell, Z.; Grainger, D.W.; Sinclair, K.D. A resorbable antibiotic eluting bone void filler for periprosthetic joint infection prevention. *J. Biomed. Mater. Res. B Appl. Biomater.* **2016**, *104*, 1632–1642.
31. Rahaman, M.N.; Day, D.E.; Bal, B.S.; Fu, Q.; Jung, S.B.; Bonewald, L.F.; Tomsia, A.P. Bioactive glass in tissue engineering. *Acta Biomater.* **2011**, *7*, 2355–2373.
32. Lindfors, N.; Geurts, J.; Drago, L.; Arts, J.J.; Juutilainen, V.; Hyvönen, P.; Suda, A.J.; Domenico, A.; Artiaco, S.; Alizadeh, C.; et al. Antibacterial Bioactive Glass, S53P4, for Chronic Bone Infections – A Multinational Study. In *A Modern Approach to Biofilm-Related Orthopaedic Implant Infections*; Advances in Experimental Medicine and Biology; Springer, Cham, 2016; pp. 81–92 ISBN 978-3-319-52273-9.
33. Xie, Z.; Liu, X.; Jia, W.; Zhang, C.; Huang, W.; Wang, J. Treatment of osteomyelitis and repair of bone defect by degradable bioactive borate glass releasing vancomycin. *J. Controlled Release* **2009**, *139*, 118–126.
34. Surgeons, A. Joint Revision Surgery - When Do I Need It? 2007 Available online: http://orthoinfo.aaos.org/topic.cfm?topic=A00510 (accessed on May 21, 2013).

35. Trampuz, A.; Widmer, A.F. Infections associated with orthopedic implants. *Curr. Opin. Infect. Dis.* **2006**, *19*, 349–356.
36. Campoccia, D.; Montanaro, L.; Speziale, P.; Arciola, C.R. Antibiotic-loaded biomaterials and the risks for the spread of antibiotic resistance following their prophylactic and therapeutic clinical use. *Biomaterials* **2010**, *31*, 6363–6377.
37. Ketonis, C.; Barr, S.; Adams, C.S.; Hickok, N.J.; Parvizi, J. Bacterial colonization of bone allografts: establishment and effects of antibiotics. *Clin. Orthop.* **2010**, *468*, 2113–2121.
38. Valle, A.G.D.; Bostrom, M.; Brause, B.; Harney, C.; Salvati, E.A. Effective bactericidal activity of tobramycin and vancomycin eluted from acrylic bone cement. *Acta Orthop.* **2001**, *72*, 237–240.
39. Fisman, D.N.; Reilly, D.T.; Karchmer, A.W.; Goldie, S.J. Clinical Effectiveness and Cost-Effectiveness of 2 Management Strategies for Infected Total Hip Arthroplasty in the Elderly. *Clin. Infect. Dis.* **2001**, *32*, 419–430.
40. Kurtz, S.M.; Lau, E.; Schmier, J.; Ong, K.L.; Zhao, K.; Parvizi, J. Infection burden for hip and knee arthroplasty in the United States. *J. Arthroplasty* **2008**, *23*, 984–991.
41. Brooks, B.D.; Brooks, A.E. Therapeutic strategies to combat antibiotic resistance. *Adv. Drug Deliv. Rev.* **2014**, *78*, 14–27.
42. Peel, T.N.; Buising, K.L.; Choong, P.F. Diagnosis and management of prosthetic joint infection. *Curr. Opin. Infect. Dis.* **2012**, *25*, 670–676.
43. Moran, E.; Masters, S.; Berendt, A.R.; McLardy-Smith, P.; Byren, I.; Atkins, B.L. Guiding empirical antibiotic therapy in orthopaedics: The microbiology of prosthetic joint infection managed by debridement, irrigation and prosthesis retention. *J. Infect.* **2007**, *55*, 1–7.
44. Bostrom, M.P.; Seigerman, D.A. The clinical use of allografts, demineralized bone matrices, synthetic bone graft substitutes and osteoinductive growth factors: a survey study. *HSS J.* **2005**, *1*, 9–18.
45. O'May, G.A.; Brady, R.A.; Prabhakara, R.; Leid, J.G.; Calhoun, J.H.; Shirtliff, M.E. Osteomyelitis. In *Biofilm Infections*; Bjarnsholt, T., Jensen, P.Ø., Moser, C., Høiby, N., Eds.; Springer New York, 2011; pp. 111–137 ISBN 978-1-4419-6083-2, 978-1-4419-6084-9.
46. Miclau, T.; Dahners, L.E.; Lindsey, R.W. In vitro pharmacokinetics of antibiotic release from locally implantable materials. *J. Orthop. Res. Off. Publ. Orthop. Res. Soc.* **1993**, *11*, 627–632.
47. Bozic, K.J.; Kurtz, S.M.; Lau, E.; Ong, K.; Chiu, V.; Vail, T.P.; Rubash, H.E.; Berry, D.J. The Epidemiology of Revision Total Knee Arthroplasty in the United States. *Clin. Orthop. Relat. Res.* **2009**, *468*, 45–51.
48. Harris, L.G.; Richards, R.G. Staphylococci and implant surfaces: a review. *Injury* **2006**, *37 Suppl 2*, S3-14.
49. Meneghini, R.M. Case Management: Revision Knee and Hip Replacement Surgery. *Adv. Prax. CME* **2015**, *15*.
50. Hetrick, E.M.; Schoenfisch, M.H. Reducing implant-related infections: active release strategies. *Chem. Soc. Rev.* **2006**, *35*, 780–789.
51. Kurtz, S.M.; Lau, E.; Watson, H.; Schmier, J.K.; Parvizi, J. Economic Burden of Periprosthetic Joint Infection in the United States. *J. Arthroplasty* **2012**, *27*, 61-65.e1.
52. Giannoudis, P.V.; Dinopoulos, H.; Tsiridis, E. Bone substitutes: an update. *Injury* **2005**, *36*, S20–S27.

53. Brooks, B.D.; Brooks, A.E.; Grainger, D.W. Antimicrobial Medical Devices in Preclinical Development and Clinical Use. In *Biomaterials Associated Infection*; Moriarty, T.F., Zaat, S.A.J., Busscher, H.J., Eds.; Springer New York, 2013; pp. 307–354 ISBN 978-1-4614-1030-0, 978-1-4614-1031-7.
54. Sevy, J.O.; Slawson, M.H.; Grainger, D.W.; Brooks, A.E. Assay method for polymer-controlled antibiotic release from allograft bone to target orthopaedic infections-biomed 2010. *Biomed. Sci. Instrum.* **2010**, *46*, 136.
55. Brooks, A.E.; Brooks, B.D.; Davidoff, S.N.; Hogrebe, P.C.; Fisher, M.A.; Grainger, D.W. Polymer-controlled release of tobramycin from bone graft void filler. *Drug Deliv. Transl. Res.* **2013**, *3*, 518–530.
56. Brooks, B.D.; Sinclair, K.D.; Davidoff, S.N.; Lawson, S.; Williams, A.G.; Coats, B.; Grainger, D.W.; Brooks, A.E. Molded polymer-coated composite bone void filler improves tobramycin controlled release kinetics. *J. Biomed. Mater. Res. B Appl. Biomater.* **2013**.
57. Brooks, B.D.; Sinclair, K.D.; Grainger, D.W.; Brooks, A.E. A resorbable antibiotic-eluting polymer composite bone void filler for perioperative infection prevention in a rabbit radial defect model. *PloS One* **2015**, *10*, e0118696.
58. Jones, Z.; Brooks, A.E.; Ferrell, Z.; Grainger, D.W.; Sinclair, K.D. A resorbable antibiotic eluting bone void filler for periprosthetic joint infection prevention. *J. Biomed. Mater. Res. B Appl. Biomater.* **2015**, n/a-n/a.
59. Makadia, H.K.; Siegel, S.J. Poly Lactic-co-Glycolic Acid (PLGA) as Biodegradable Controlled Drug Delivery Carrier. *Polymers* **2011**, *3*, 1377–1397.
60. Dhanaraju, M.D.; Sathyamoorthy, N.; Sundar, V.D.; Suresh, C. Preparation of poly (epsilon-caprolactone) microspheres containing etoposide by solvent evaporation method. *J. Pharm. Sci.* **2010**, *5*, 114–122.
61. Swanson, J.P.; Monteleone, L.R.; Haso, F.; Costanzo, P.J.; Liu, T.; Joy, A. A Library of Thermoresponsive, Coacervate-Forming Biodegradable Polyesters. *Macromolecules* **2015**, *48*, 3834–3842.
62. Gokhale, S.; Xu, Y.; Joy, A. A Library of Multifunctional Polyesters with "Peptide-Like" Pendant Functional Groups. *Biomacromolecules* **2013**, *14*, 2489–2493.
63. Curley, J.; Ortiz, D.; Brooks, B.D.; Brooks, A.E. Evaluation of Polycaprolactone Encapsulated Vancomycin for Controlled Drug Delivery from a Bone Void Filling Putty. *Biomed. Sci. Instrum.* **2016**.
64. Hasan, M.R.; Nodland, J.; Brooks, A.E. A MICROFLUIDIC PLATFORM FOR CONTINUOUS MONITORING OF DRUG RELEASE KINETICS. *Biomed. Sci. Instrum.* **2016**.
65. Budiasih, S.; Jiyauddin, K.; Logavinod, N.; Kaleemullah, M.; Jawad, A.; Samer, A.D.; Fadli, A.; Eddy, Y. Optimization of Polymer Concentration for Designing of Oral Matrix Controlled Release Dosage Form. *UK J. Pharm. Biosci.* **2014**, *2*, 54.
66. Maria Ann Woodruff, D.W.H. The return of a forgotten polymer-polycaprolactone in the 21st century. Prog Polym Sci. *Prog. Polym. Sci.* **2010**, *35*.
67. Andriano, K.P.; Chandrashekar, B.; McEnery, K.; Dunn, R.L.; Moyer, K.; Balliu, C.M.; Holland, K.M.; Garrett, S.; Huffer, W.E. Preliminary in vivo studies on the osteogenic potential of bone morphogenetic proteins delivered from an absorbable puttylike polymer matrix. *J. Biomed. Mater. Res.* **2000**, *53*, 36–43.

68. Anseth, K.S.; Wang, C.M.; Bowman, C.N. Reaction behaviour and kinetic constants for photopolymerizations of multi(meth)acrylate monomers. *Polymer* **1994**, *35*, 3243–3250.
69. Korsmeyer, R.W.; Gurny, R.; Doelker, E.; Buri, P.; Peppas, N.A. Mechanisms of solute release from porous hydrophilic polymers. *Int. J. Pharm.* **1983**, *15*, 25–35.
70. Siepmann, J.; Peppas, N.A. Modeling of drug release from delivery systems based on hydroxypropyl methylcellulose (HPMC). *Adv. Drug Deliv. Rev.* **2001**, *48*, 139–157.
71. Brazel, C.S.; Peppas, N.A. Modeling of drug release from Swellable polymers. *Eur. J. Pharm. Biopharm.* **2000**, *49*, 47–58.
72. Kosmidis, K.; Argyrakis, P.; Macheras, P. A Reappraisal of Drug Release Laws Using Monte Carlo Simulations: The Prevalence of the Weibull Function. *Pharm. Res.* **2003**, *20*, 988–995.
73. Siepmann, J.; Göpferich, A. Mathematical modeling of bioerodible, polymeric drug delivery systems. *Adv. Drug Deliv. Rev.* **2001**, *48*, 229–247.
74. Tang, Y.; Zhu, W.; Chen, K.; Jiang, H. New technologies in computer-aided drug design: Toward target identification and new chemical entity discovery. *Drug Discov. Today Technol.* **2006**, *3*, 307–313.
75. Jämsen, E.; Varonen, M.; Huhtala, H.; Lehto, M.U.K.; Lumio, J.; Konttinen, Y.T.; Moilanen, T. Incidence of Prosthetic Joint Infections After Primary Knee Arthroplasty. *J. Arthroplasty* **2010**, *25*, 87–92.
76. Sloan, M.; Sheth, N. Changing Demographics in Primary and Revision Total Joint Arthroplasty, 2000-2014.
77. AJRR_2016_Annual_Report_final.pdf.
78. Lamagni, T. Epidemiology and burden of prosthetic joint infections. *J. Antimicrob. Chemother.* **2014**, *69*, i5–i10.
79. CNN, S.S. More men, younger Americans having joint replacement surgery Available online: https://www.cnn.com/2018/03/06/health/hip-knee-replacement-surgeries-earlier-study/index.html (accessed on Mar 14, 2018).
80. Liu, X.-M.; Zhang, Y.; Chen, F.; Khutsishvili, I.; Fehringer, E.V.; Marky, L.A.; Bayles, K.W.; Wang, D. Prevention of Orthopedic Device-Associated Osteomyelitis Using Oxacillin-Containing Biomineral-Binding Liposomes. *Pharm. Res.* **2012**, *29*, 3169–3179.
81. ter Boo, G.-J.A.; Grijpma, D.W.; Moriarty, T.F.; Richards, R.G.; Eglin, D. Antimicrobial delivery systems for local infection prophylaxis in orthopedic- and trauma surgery. *Biomaterials* **2015**, *52*, 113–125.
82. Haidar, R.; Boghossian, A.D.; Atiyeh, B. Duration of post-surgical antibiotics in chronic osteomyelitis: empiric or evidence-based? *Int. J. Infect. Dis.* **2010**, *14*, e752–e758.
83. Biodegradable Mg-Cu alloy implants with antibacterial activity for the treatment of osteomyelitis: In vitro and in vivo evaluations. - PubMed - NCBI Available online: https://www.ncbi.nlm.nih.gov/pubmed/27573133 (accessed on Nov 24, 2018).
84. Miller, A.J.; Stimac, J.D.; Smith, L.S.; Feher, A.W.; Yakkanti, M.R.; Malkani, A.L. Results of Cemented vs Cementless Primary Total Knee Arthroplasty Using the Same Implant Design. *J. Arthroplasty* **2018**, *33*, 1089–1093.
85. Schachter, D. Bone void filler 2006.
86. Puga, A.M.; Rey-Rico, A.; Magariños, B.; Alvarez-Lorenzo, C.; Concheiro, A. Hot melt poly-ε-caprolactone/poloxamine implantable matrices for sustained delivery of ciprofloxacin. *Acta Biomater.* **2012**, *8*, 1507–1518.

87. Fraimow, H.S. Systemic Antimicrobial Therapy in Osteomyelitis. *Semin. Plast. Surg.* **2009**, *23*, 90–99.
88. Graziani, A.L.; Lawson, L.A.; Gibson, G.A.; Steinberg, M.A.; MacGregor, R.R. Vancomycin concentrations in infected and noninfected human bone. *Antimicrob. Agents Chemother.* **1988**, *32*, 1320–1322.
89. Patel, S.; Bernice, F. Vancomycin. In *StatPearls*; StatPearls Publishing: Treasure Island (FL), 2018.
90. Li, B.; Brown, K.V.; Wenke, J.C.; Guelcher, S.A. Sustained release of vancomycin from polyurethane scaffolds inhibits infection of bone wounds in a rat femoral segmental defect model. *J. Controlled Release* **2010**, *145*, 221–230.
91. Curley, J.; Hasan, M.R.; Larson, J.; Brooks, B.D.; Liu, Q.; Jain, T.; Joy, A.; Brooks, A.E. An Osteoconductive Antibiotic Bone Eluting Putty with a Custom Polymer Matrix. *Polymers* **2016**, *8*, 247.
92. Chomczynski, P.; Mackey, K. Short technical reports. Modification of the TRI reagent procedure for isolation of RNA from polysaccharide- and proteoglycan-rich sources. *BioTechniques* **1995**, *19*, 942–945.
93. TRIZOLRNAIsolation_092107_21453_284_10813_v1.pdf.
94. Stacer, R.G.; Husband, D.M.; Stacer, H.L. Viscoelastic Response and Adhesion Properties of Highly Filled Elastomers. *Rubber Chem. Technol.* **1987**, *60*, 227–244.
95. Mahmoudian, M.; Ganji, F. Vancomycin-loaded HPMC microparticles embedded within injectable thermosensitive chitosan hydrogels. *Prog. Biomater.* **2017**, *6*, 49–56.
96. Marinho, D.S.; Huf, G.; Ferreira, B.L.; Castro, H.; Rodrigues, C.R.; Sousa, V.P. de; Cabral, L.M. The study of vancomycin use and its adverse reactions associated to patients of a brazilian university hospital. *BMC Res. Notes* **2011**, *4*, 236.
97. Wahl, P.; Guidi, M.; Benninger, E.; Rönn, K.; Gautier, E.; Buclin, T.; Magnin, J.-L.; Livio, F. The levels of vancomycin in the blood and the wound after the local treatment of bone and soft-tissue infection with antibiotic-loaded calcium sulphate as carrier material. *Bone Jt. J.* **2017**, *99-B*, 1537–1544.
98. Bolton, W.K.; Benton, F.R.; Maclay, J.G.; Sturgill, B.C. Spontaneous Glomerular Sclerosis in Aging Sprague-Dawley Rats. **1976**, *85*, 26.
99. Dawley, S. Sprague Dawley Rat. 11.
100. Mader, J.T.; Calhoun, J. Bone, Joint, and Necrotizing Soft Tissue Infections. In *Medical Microbiology*; Baron, S., Ed.; University of Texas Medical Branch at Galveston: Galveston (TX), 1996 ISBN 978-0-9631172-1-2.
101. Carli, A.V.; Sethuraman, A.S.; Bhimani, S.J.; Ross, F.P.; Bostrom, M.P.G. Selected Heat-Sensitive Antibiotics Are Not Inactivated During Polymethylmethacrylate Curing and Can Be Used in Cement Spacers for Periprosthetic Joint Infection. *J. Arthroplasty* **2018**, *33*, 1930–1935.
102. Hafeman, A.E.; Zienkiewicz, K.J.; Carney, E.; Litzner, B.; Stratton, C.; Wenke, J.C.; Guelcher, S.A. Local Delivery of Tobramycin from Injectable Biodegradable Polyurethane Scaffolds. *J. Biomater. Sci. Polym. Ed.* **2010**, *21*, 95–112.
103. Hasan, R.; Brooks, A. Novel Local Bone Void Filling Antibiotic Carriers for the Treatment of Bone Infection. *1*, 3.
104. Chohfi, M.; Langlais, F.; Fourastier, J.; Minet, J.; Thomazeau, H.; Cormier, M. Pharmacokinetics, uses, and limitations of vancomycin-loaded bone cement. *Int. Orthop.* **1998**, *22*, 171–177.

105. Chohfi, M.; Langlais, F.; Fourastier, J.; Minet, J.; Thomazeau, H.; Cormier, M. Pharmacokinetics, uses, and limitations of vancomycin-loaded bone cement. *Int. Orthop.* **1998**, *22*, 171–177.
106. Le Ray, A.-M.; Gautier, H.; Laty, M.-K.; Daculsi, G.; Merle, C.; Jacqueline, C.; Hamel, A.; Caillon, J. In Vitro and In Vivo Bactericidal Activities of Vancomycin Dispersed in Porous Biodegradable Poly(ε-Caprolactone) Microparticles. *Antimicrob. Agents Chemother.* **2005**, *49*, 3025–3027.
107. Inzana, J.A.; Trombetta, R.P.; Schwarz, E.M.; Kates, S.L.; Awad, H.A. 3D printed bioceramics for dual antibiotic delivery to treat implant-associated bone infection. *Eur. Cell. Mater.* **2015**, *30*, 232–247.
108. Guelcher, S.A.; Brown, K.V.; Li, B.; Guda, T.; Lee, B.-H.; Wenke, J.C. Dual-purpose bone grafts improve healing and reduce infection. *J. Orthop. Trauma* **2011**, *25*, 477–482.
109. Chen, X.; Kidder, L.S.; Lew, W.D. Osteogenic protein-1 induced bone formation in an infected segmental defect in the rat femur. *J. Orthop. Res.* **2002**, *20*, 142–150.
110. Inzana, J.A.; Schwarz, E.M.; Kates, S.L.; Awad, H.A. Biomaterials approaches to treating implant-associated osteomyelitis. *Biomaterials* **2016**, *81*, 58–71.
111. Subbiahdoss, G.; Kuijer, R.; Grijpma, D.W.; van der Mei, H.C.; Busscher, H.J. Microbial biofilm growth vs. tissue integration: "The race for the surface" experimentally studied. *Acta Biomater.* **2009**, *5*, 1399–1404.
112. Benito, N.; Esteban, J.; Horcajada, J.P.; Ribera, A.; Soriano, A.; Sousa, R. Epidemiology of Prosthetic Joint Infection. In *Prosthetic Joint Infections*; Peel, T., Ed.; Springer International Publishing: Cham, 2018; pp. 5–53 ISBN 9783319652504.
113. Prieto, E.M.; Talley, A.D.; Gould, N.R.; Zienkiewicz, K.J.; Drapeau, S.J.; Kalpakci, K.N.; Guelcher, S.A. Effects of Particle Size and Porosity on In Vivo Remodeling of Settable Allograft Bone/Polymer Composites. *J. Biomed. Mater. Res. B Appl. Biomater.* **2015**, *103*, 1641–1651.
114. Shapoff, C.A.; Bowers, G.M.; Levy, B.; Mellonig, J.T.; Yukna, R.A. The effect of particle size on the osteogenic activity of composite grafts of allogeneic freeze-dried bone and autogenous marrow. *J. Periodontol.* **1980**, *51*, 625–630.
115. Coathup, M.J.; Cai, Q.; Campion, C.; Buckland, T.; Blunn, G.W. The effect of particle size on the osteointegration of injectable silicate-substituted calcium phosphate bone substitute materials. *J. Biomed. Mater. Res. B Appl. Biomater.* **2013**, *101B*, 902–910.
116. Fottner, A.; Nies, B.; Kitanovic, D.; Steinbrück, A.; Hausdorf, J.; Mayer-Wagner, S.; Pohl, U.; Jansson, V. In vivo evaluation of bioactive PMMA-based bone cement with unchanged mechanical properties in a load-bearing model on rabbits. *J. Biomater. Appl.* **2015**, *30*, 30–37.
117. Guo, F.; Du, C.; Yu, G.; Li, R. The Static and Dynamic Mechanical Properties of Magnetorheological Silly Putty Available online: https://www.hindawi.com/journals/amse/2016/7079698/ (accessed on Sep 19, 2018).
118. Solorio, L.; Babin, B.M.; Patel, R.B.; Mach, J.; Azar, N.; Exner, A.A. Noninvasive Characterization of In situ Forming Implants Using Diagnostic Ultrasound. *J. Control. Release Off. J. Control. Release Soc.* **2010**, *143*, 183–190.
119. Choong, P.F.M.; Dowsey, M.M.; Carr, D.; Daffy, J.; Stanley, P. Risk factors associated with acute hip prosthetic joint infections and outcome of treatment with a rifampinbased regimen. *Acta Orthop.* **2007**, *78*, 755–765.
120. *Biofilms in Infection Prevention and Control*; Elsevier, 2014; ISBN 978-0-12-397043-5.

121. Stoodley, P.; Nistico, L.; Johnson, S.; Lasko, L.-A.; Baratz, M.; Gahlot, V.; Ehrlich, G.D.; Kathju, S. Direct Demonstration of Viable Staphylococcus aureus Biofilms in an Infected Total Joint Arthroplasty. *J. Bone Joint Surg. Am.* **2008**, *90*, 1751–1758.
122. Ozturk, B.; Gunay, N.; Ertugrul, B.M.; Sakarya, S. Effects of vancomycin, daptomycin, and tigecycline on coagulase-negative staphylococcus biofilm and bacterial viability within biofilm: an in vitro biofilm model. *Can. J. Microbiol.* **2016**, *62*, 735–743.
123. Lima, A.L.L.; Oliveira, P.R.; Carvalho, V.C.; Cimerman, S.; Savio, E. Recommendations for the treatment of osteomyelitis. *Braz. J. Infect. Dis.* **2014**, *18*, 526–534.
124. Zimmerli, W.; Widmer, A.F.; Blatter, M.; Frei, R.; Ochsner, P.E.; Group, for the F.-B.I. (FBI) S. Role of Rifampin for Treatment of Orthopedic Implant–Related Staphylococcal Infections : A Randomized Controlled Trial. *JAMA* **1998**, *279*, 1537–1541.
125. Sridhar, A.; Sandeep, Y.; Krishnakishore, C.; Sriramnaveen, P.; Manjusha, Y.; Sivakumar, V. Fatal poisoning by isoniazid and rifampicin. *Indian J. Nephrol.* **2012**, *22*, 385–387.
126. McPherson, E.; Facs, M. Deactivation of Palacos R Bone Cement with the Addition of Rifampin Antibiotic Powder An In-Vivo Experience -Case Report. *Reconstr. Rev.* **2011**, *1*.
127. Trombetta, R.P.; Ninomiya, M.J.; El-Atawneh, I.M.; Knapp, E.K.; de Mesy Bentley, K.L.; Dunman, P.M.; Schwarz, E.M.; Kates, S.L.; Awad, H.A. Calcium Phosphate Spacers for the Local Delivery of Sitafloxacin and Rifampin to Treat Orthopedic Infections: Efficacy and Proof of Concept in a Mouse Model of Single-Stage Revision of Device-Associated Osteomyelitis. *Pharmaceutics* **2019**, *11*, 94.
128. Dorati, R.; DeTrizio, A.; Modena, T.; Conti, B.; Benazzo, F.; Gastaldi, G.; Genta, I. Biodegradable Scaffolds for Bone Regeneration Combined with Drug-Delivery Systems in Osteomyelitis Therapy. *Pharmaceuticals* **2017**, *10*, 96.
129. Nelson, C.L. The Current Status of Material Used for Depot Delivery of Drugs. *Clin. Orthop. Relat. Res. 1976-2007* **2004**, *427*, 72–78.
130. Tennent, D.J.; Shiels, S.M.; Sanchez, C.J.; Niece, K.L.; Akers, K.S.; Stinner, D.J.; Wenke, J.C. Time-Dependent Effectiveness of Locally Applied Vancomycin Powder in a Contaminated Traumatic Orthopaedic Wound Model. *J. Orthop. Trauma* **2016**, *30*, 531–537.
131. Cardile, A.P.; Sanchez, C.J.; Samberg, M.E.; Romano, D.R.; Hardy, S.K.; Wenke, J.C.; Murray, C.K.; Akers, K.S. Human plasma enhances the expression of Staphylococcal microbial surface components recognizing adhesive matrix molecules promoting biofilm formation and increases antimicrobial tolerance In Vitro. *BMC Res. Notes* **2014**, *7*, 457.
132. Shiels, S.M.; Tennent, D.J.; Akers, K.S.; Wenke, J.C. Determining potential of PMMA as a depot for rifampin to treat recalcitrant orthopaedic infections. *Injury* **2017**, *48*, 2095–2100.
133. Owens, B.D.; Wenke, J.C. Early wound irrigation improves the ability to remove bacteria. *J. Bone Joint Surg. Am.* **2007**, *89*, 1723–1726.
134. Shiels, S.M.; Tennent, D.J.; Lofgren, A.L.; Wenke, J.C. Topical rifampin powder for orthopaedic trauma part II: Topical rifampin allows for spontaneous bone healing in sterile and contaminated wounds. *J. Orthop. Res.* **2018**, *36*, 3142–3150.
135. Shiels, S.M.; Tennent, D.J.; Wenke, J.C. Topical rifampin powder for orthopedic trauma part I: Rifampin powder reduces recalcitrant infection in a delayed treatment musculoskeletal trauma model. *J. Orthop. Res.* **2018**, *36*, 3136–3141.
136. Patel, R. Biofilms and Antimicrobial Resistance. *Clin. Orthop. Relat. Res.* **2005**, *437*, 41.

137. Gagnon, R.F.; Richards, G.K.; Kostiner, G.B. Time-kill efficacy of antibiotics in combination with rifampin against Staphylococcus epidermidis biofilms. *Adv. Perit. Dial. Conf. Perit. Dial.* **1994**, *10*, 189–192.
138. Sanchez, C.J.; Mende, K.; Beckius, M.L.; Akers, K.S.; Romano, D.R.; Wenke, J.C.; Murray, C.K. Biofilm formation by clinical isolates and the implications in chronic infections. *BMC Infect. Dis.* **2013**, *13*, 47.
139. Pascual, A.; Ramirez de Arellano, E.; Perea, E.J. Activity of glycopeptides in combination with amikacin or rifampin against Staphylococcus epidermidis biofilms on plastic catheters. *Eur. J. Clin. Microbiol. Infect. Dis. Off. Publ. Eur. Soc. Clin. Microbiol.* **1994**, *13*, 515–517.
140. Peck, K.R.; Kim, S.W.; Jung, S.-I.; Kim, Y.-S.; Oh, W.S.; Lee, J.Y.; Jin, J.H.; Kim, S.; Song, J.-H.; Kobayashi, H. Antimicrobials as potential adjunctive agents in the treatment of biofilm infection with Staphylococcus epidermidis. *Chemotherapy* **2003**, *49*, 189–193.
141. Rathbone, C.R.; Cross, J.D.; Brown, K.V.; Murray, C.K.; Wenke, J.C. Effect of various concentrations of antibiotics on osteogenic cell viability and activity. *J. Orthop. Res. Off. Publ. Orthop. Res. Soc.* **2011**, *29*, 1070–1074.
142. Sanchez, C.J.; Ward, C.L.; Romano, D.R.; Hurtgen, B.J.; Hardy, S.K.; Woodbury, R.L.; Trevino, A.V.; Rathbone, C.R.; Wenke, J.C. Staphylococcus aureus biofilms decrease osteoblast viability, inhibits osteogenic differentiation, and increases bone resorption in vitro. *BMC Musculoskelet. Disord.* **2013**, *14*, 187.
143. Wood, C.A.; Kohlhepp, S.J.; Kohnen, P.W.; Houghton, D.C.; Gilbert, D.N. Vancomycin enhancement of experimental tobramycin nephrotoxicity. *Antimicrob. Agents Chemother.* **1986**, *30*, 20–24.
144. Prosthetic-Joint Infections | NEJM Available online: https://www.nejm.org/doi/full/10.1056/NEJMra040181?url_ver=Z39.88-2003&rfr_id=ori%3Arid%3Acrossref.org&rfr_dat=cr_pub%3Dpubmed (accessed on Jul 28, 2019).
145. Kluin, O.S.; Busscher, H.J.; Neut, D.; Mei, H.C. van der Poly(trimethylene carbonate) as a carrier for rifampicin and vancomycin to target therapy-recalcitrant staphylococcal biofilms. *J. Orthop. Res.* **2016**, *34*, 1828–1837.
146. ter Boo, G.-J.A.; Grijpma, D.W.; Moriarty, T.F.; Richards, R.G.; Eglin, D. Antimicrobial delivery systems for local infection prophylaxis in orthopedic- and trauma surgery. *Biomaterials* **2015**, *52*, 113–125.
147. Romanò, C.L.; Logoluso, N.; Meani, E.; Romanò, D.; Vecchi, E.D.; Vassena, C.; Drago, L. A comparative study of the use of bioactive glass S53P4 and antibiotic-loaded calcium-based bone substitutes in the treatment of chronic osteomyelitis: a retrospective comparative study. *Bone Jt. J* **2014**, *96-B*, 845–850.
148. Lew, D.P.; Waldvogel, F.A. Osteomyelitis. *Lancet Lond. Engl.* **2004**, *364*, 369–379.
149. Haas, D.W.; McAndrew, M.P. Bacterial osteomyelitis in adults: Evolving considerations in diagnosis and treatment. *Am. J. Med.* **1996**, *101*, 550–561.
150. Anagnostakos, K.; Hitzler, P.; Pape, D.; Kohn, D.; Kelm, J. Persistence of bacterial growth on antibiotic-loaded beads: Is it actually a problem? *Acta Orthop.* **2008**, *79*, 302–307.
151. Zalavras, C.G.; Patzakis, M.J.; Holtom, P. Local Antibiotic Therapy in the Treatment of Open Fractures and Osteomyelitis. *Clin. Orthop. Relat. Res. 1976-2007* **2004**, *427*, 86–93.

152. Schlickewei, C.W.; Yarar, S.; Rueger, J.M. Eluting antibiotic bone graft substitutes for the treatment of osteomyelitis in long bones. A review: evidence for their use? Available online: https://www.dovepress.com/eluting-antibiotic-bone-graft-substitutes-for-the-treatment-of-osteomy-peer-reviewed-fulltext-article-ORR (accessed on Sep 20, 2019).
153. Dion, A.; Langman, M.; Hall, G.; Filiaggi, M. Vancomycin release behaviour from amorphous calcium polyphosphate matrices intended for osteomyelitis treatment. *Biomaterials* **2005**, *26*, 7276–7285.
154. Lindfors, N.C.; Hyvönen, P.; Nyyssönen, M.; Kirjavainen, M.; Kankare, J.; Gullichsen, E.; Salo, J. Bioactive glass S53P4 as bone graft substitute in treatment of osteomyelitis. *Bone* **2010**, *47*, 212–218.
155. Ferrando, A.; Part, J.; Baeza, J. Treatment of Cavitary Bone Defects in Chronic Osteomyelitis: Bioactive glass S53P4 vs. Calcium Sulphate Antibiotic Beads. *J. Bone Jt. Infect.* **2017**, *2*, 194–201.
156. Miguez-Pacheco, V.; Hench, L.L.; Boccaccini, A.R. Bioactive glasses beyond bone and teeth: Emerging applications in contact with soft tissues. *Acta Biomater.* **2015**, *13*, 1–15.
157. Dissolution patterns of biocompatible glasses in 2-amino-2-hydroxymethyl-propane-1,3-diol (Tris) buffer - ScienceDirect Available online: https://www.sciencedirect.com/science/article/pii/S174270611200428X?via%3Dihub (accessed on Feb 28, 2018).
158. Jones, J.R. Review of bioactive glass: From Hench to hybrids. *Acta Biomater.* **2013**, *9*, 4457–4486.
159. Adams, L.A.; Essien, E.R.; Adesalu, A.T.; Julius, M.L. Bioactive glass 45S5 from diatom biosilica. *J. Sci. Adv. Mater. Devices* **2017**, *2*, 476–482.
160. Peltola, M.; Aitasalo, K.; Suonpää, J.; Varpula, M.; Yli-Urpo, A. Bioactive glass S53P4 in frontal sinus obliteration: A long-term clinical experience. *Head Neck* **2006**, *28*, 834–841.
161. Oonishi, H.; Hench, L.L.; Wilson, J.; Sugihara, F.; Tsuji, E.; Matsuura, M.; Kin, S.; Yamamoto, T.; Mizokawa, S. Quantitative comparison of bone growth behavior in granules of Bioglass, A-W glass-ceramic, and hydroxyapatite. *J. Biomed. Mater. Res.* **2000**, *51*, 37–46.
162. Schepers, E.J.; Ducheyne, P. Bioactive glass particles of narrow size range for the treatment of oral bone defects: a 1-24 month experiment with several materials and particle sizes and size ranges. *J. Oral Rehabil.* **1997**, *24*, 171–181.
163. Xynos, I.D.; Edgar, A.J.; Buttery, L.D.K.; Hench, L.L.; Polak, J.M. Gene-expression profiling of human osteoblasts following treatment with the ionic products of Bioglass® 45S5 dissolution. *J. Biomed. Mater. Res.* **2001**, *55*, 151–157.
164. Ionic Products of Bioactive Glass Dissolution Increase Proliferation of Human Osteoblasts and Induce Insulin-like Growth Factor II mRNA Expression and Protein Synthesis - ScienceDirect Available online: https://www.sciencedirect.com/science/article/pii/S0006291X00935034 (accessed on Mar 1, 2018).
165. Hench, L.L. Genetic design of bioactive glass. *J. Eur. Ceram. Soc.* **2009**, *29*, 1257–1265.
166. Carlisle, E.M. Silicon: A requirement in bone formation independent of vitamin D<Subscript>1</Subscript>. *Calcif. Tissue Int.* **1981**, *33*, 27–34.
167. Damen, J.J.M.; Cate, J.M.T. Silica-induced Precipitation of Calcium Phosphate in the Presence of Inhibitors of Hydroxyapatite Formation. *J. Dent. Res.* **1992**, *71*, 453–457.

168. Hoppe, A.; Güldal, N.S.; Boccaccini, A.R. A review of the biological response to ionic dissolution products from bioactive glasses and glass-ceramics. *Biomaterials* **2011**, *32*, 2757–2774.
169. Maeno, S.; Niki, Y.; Matsumoto, H.; Morioka, H.; Yatabe, T.; Funayama, A.; Toyama, Y.; Taguchi, T.; Tanaka, J. The effect of calcium ion concentration on osteoblast viability, proliferation and differentiation in monolayer and 3D culture. *Biomaterials* **2005**, *26*, 4847–4855.
170. Marie, P.J. The calcium-sensing receptor in bone cells: A potential therapeutic target in osteoporosis. *Bone* **2010**, *46*, 571–576.
171. Julien, M.; Khoshniat, S.; Lacreusette, A.; Gatius, M.; Bozec, A.; Wagner, E.F.; Wittrant, Y.; Masson, M.; Weiss, P.; Beck, L.; et al. Phosphate-Dependent Regulation of MGP in Osteoblasts: Role of ERK1/2 and Fra-1. *J. Bone Miner. Res.* **2009**, *24*, 1856–1868.
172. Stoor, P.; Frantzen, J. Influence of bioactive glass S53P4 granules and putty on osteomyelitis associated bacteria in vitro. *Biomed. Glas.* **2017**, *3*, 79–85.
173. Walraven, C.J.; North, M.S.; Marr-Lyon, L.; Deming, P.; Sakoulas, G.; Mercier, R.-C. Site of infection rather than vancomycin MIC predicts vancomycin treatment failure in methicillin-resistant Staphylococcus aureus bacteraemia. *J. Antimicrob. Chemother.* **2011**, *66*, 2386–2392.
174. Chen, Q.Z.; Thompson, I.D.; Boccaccini, A.R. 45S5 Bioglass®-derived glass–ceramic scaffolds for bone tissue engineering. *Biomaterials* **2006**, *27*, 2414–2425.
175. Haugen, H.; Will, J.; Köhler, A.; Hopfner, U.; Aigner, J.; Wintermantel, E. Ceramic TiO2-foams: characterisation of a potential scaffold. *J. Eur. Ceram. Soc.* **2004**, *24*, 661–668.
176. Kokubo, T.; Hata, K.; Nakamura, T.; Yamamuro, T. Apatite Formation on Ceramics, Metals and Polymers Induced by a CaO SiO2 Based Glass in a Simulated Body Fluid. In *Bioceramics*; Bonfield, W., Hastings, G.W., Tanner, K.E., Eds.; Butterworth-Heinemann, 1991; pp. 113–120 ISBN 978-0-7506-0269-3.
177. Bonding mechanisms at the interface of ceramic prosthetic materials - Hench - 1971 - Journal of Biomedical Materials Research - Wiley Online Library Available online: https://onlinelibrary.wiley.com/doi/abs/10.1002/jbm.820050611 (accessed on Sep 20, 2019).
178. Huang, W.; Day, D.E.; Kittiratanapiboon, K.; Rahaman, M.N. Kinetics and mechanisms of the conversion of silicate (45S5), borate, and borosilicate glasses to hydroxyapatite in dilute phosphate solutions. *J. Mater. Sci. Mater. Med.* **2006**, *17*, 583–596.
179. Rahaman, M.N.; Bal, B.S.; Huang, W. Review: Emerging developments in the use of bioactive glasses for treating infected prosthetic joints. *Mater. Sci. Eng. C* **2014**, *41*, 224–231.
180. Wang, Z.; Lu, B.; Chen, L.; Chang, J. Evaluation of an osteostimulative putty in the sheep spine. *J. Mater. Sci. Mater. Med.* **2011**, *22*, 185–191.
181. Kobayashi, H.; Turner, A.S.; Seim, H.B.; Kawamoto, T.; Bauer, T.W. Evaluation of a silica-containing bone graft substitute in a vertebral defect model. *J. Biomed. Mater. Res. A* **2010**, *92*, 596–603.
182. Peitl, O.; Dutra Zanotto, E.; Hench, L.L. Highly bioactive P2O5–Na2O–CaO–SiO2 glass-ceramics. *J. Non-Cryst. Solids* **2001**, *292*, 115–126.
183. Filho, O.P.; Torre, G.P.L.; Hench, L.L. Effect of crystallization on apatite-layer formation of bioactive glass 45S5. *J. Biomed. Mater. Res.* **1996**, *30*, 509–514.

184. Agrawal, C.M.; Ray, R.B. Biodegradable polymeric scaffolds for musculoskeletal tissue engineering. *J. Biomed. Mater. Res.* **2001**, *55*, 141–150.
185. Karande, T.S.; Ong, J.L.; Agrawal, C.M. Diffusion in Musculoskeletal Tissue Engineering Scaffolds: Design Issues Related to Porosity, Permeability, Architecture, and Nutrient Mixing. *Ann. Biomed. Eng.* **2004**, *32*, 1728–1743.
186. Kramschuster, A.; Turng, L.-S. 17 - Fabrication of Tissue Engineering Scaffolds. In *Handbook of Biopolymers and Biodegradable Plastics*; Ebnesajjad, S., Ed.; Plastics Design Library; William Andrew Publishing: Boston, 2013; pp. 427–446 ISBN 978-1-4557-2834-3.
187. Feng, B.; Jinkang, Z.; Zhen, W.; Jianxi, L.; Jiang, C.; Jian, L.; Guolin, M.; Xin, D. The effect of pore size on tissue ingrowth and neovascularization in porous bioceramics of controlled architecture in vivo. *Biomed. Mater.* **2011**, *6*, 015007.
188. Stoor, P.; Söderling, E.; Salonen, J.I. Antibacterial effects of a bioactive glass paste on oral microorganisms. *Acta Odontol. Scand.* **1998**, *56*, 161–165.
189. Allan, I.; Newman, H.; Wilson, M. Antibacterial activity of particulate bioglass against supra- and subgingival bacteria. *Biomaterials* **2001**, *22*, 1683–1687.
190. Xie, Z.-P.; Zhang, C.-Q.; Yi, C.-Q.; Qiu, J.-J.; Wang, J.-Q.; Zhou, J. Failure of particulate bioglass to prevent experimental staphylococcal infection of open tibial fractures. *J. Antimicrob. Chemother.* **2008**, *62*, 1162–1163.
191. ISO 10993-5:2009(en), Biological evaluation of medical devices — Part 5: Tests for in vitro cytotoxicity Available online: https://www.iso.org/obp/ui/#iso:std:iso:10993:-5:ed-3:v1:en (accessed on Sep 21, 2019).

APPENDIX A

Table A.1. Vancomycin release kinetics from each ABVF formulation tested fitted into different drug release kinetics model.

Formulation	**Zero-order (R^2)**	**First-order (R^2)**	**Korsmeyer-peppas (R^2)**	**Higuchi (R^2)**	**Hixon-Crowell (R^2)**
1-A	0.14	0.45	0.92	0.29	0.26
1-B	0.34	0.66	0.74	0.54	0.54
1-C	0.14	0.41	0.94	0.29	0.26
1-D	0.16	0.51	0.98	0.32	0.33
1-E	0.14	0.45	0.93	0.29	0.26
1-F	0.14	0.45	0.96	0.29	0.26
2	0.26	0.52	0.51	0.46	0.41
3-A	0.14	0.45	0.90	0.29	0.27
3-B	0.15	0.39	0.93	0.30	0.26
3-C	0.14	0.40	0.97	0.29	0.24
3-D	0.14	0.42	0.96	0.29	0.25
3-E	0.14	0.47	0.63	0.29	0.27
3-F	0.13	0.46	0.94	0.28	0.24
4-A	0.49	0.78	0.76	0.69	0.69
4-B	0.27	0.71	0.83	0.43	0.53
4-C	0.63	0.83	0.71	0.81	0.76
4-D	0.17	0.57	0.82	0.33	0.37
5-A	0.89	0.84	0.77	0.80	0.86
5-B	0.92	0.94	0.93	0.96	0.98
6-A	0.81	0.98	0.95	0.92	0.92
6-B	0.32	0.74	0.84	0.53	0.59
6-C	0.67	0.99	0.96	0.87	0.91
7-A	0.15	0.47	0.63	0.29	0.27
7-B	0.13	0.46	0.94	0.28	0.24

The amount of vancomycin was plotted against time on the *x*-axis. Individual replicates of each formulation, indicated by the letter, were then fitted to each of the common pharmacokinetic models to identify the best fit according to R^2.

APPENDIX B

B.1. HPLC Validation of Vancomycin Free-base

HPLC was carried out using the following method. Briefly, mobile phase contained 0.1% TFA in water and 0.1% TFA in acetonitrile. The flow rate was set at 1 mL/min. Vancomycin salt stock solution and different fractions during the vancomycin free-base preparation (VancFB2) was analyzed to see if there are by-products. The wavelength was 280 nm and Waters Corporation Alliance e2695 with PDA detector HPLC system (Milford, MA, USA) was used with a C18 column (XTERRA RP 18 5mm 4.6x250 mm column). HPLC validation of V-fb showed that no additional by product was created during the V-fb production. The peaks appeared at the same spot for V-fb as it did for V-HCl (Figure B2.1).

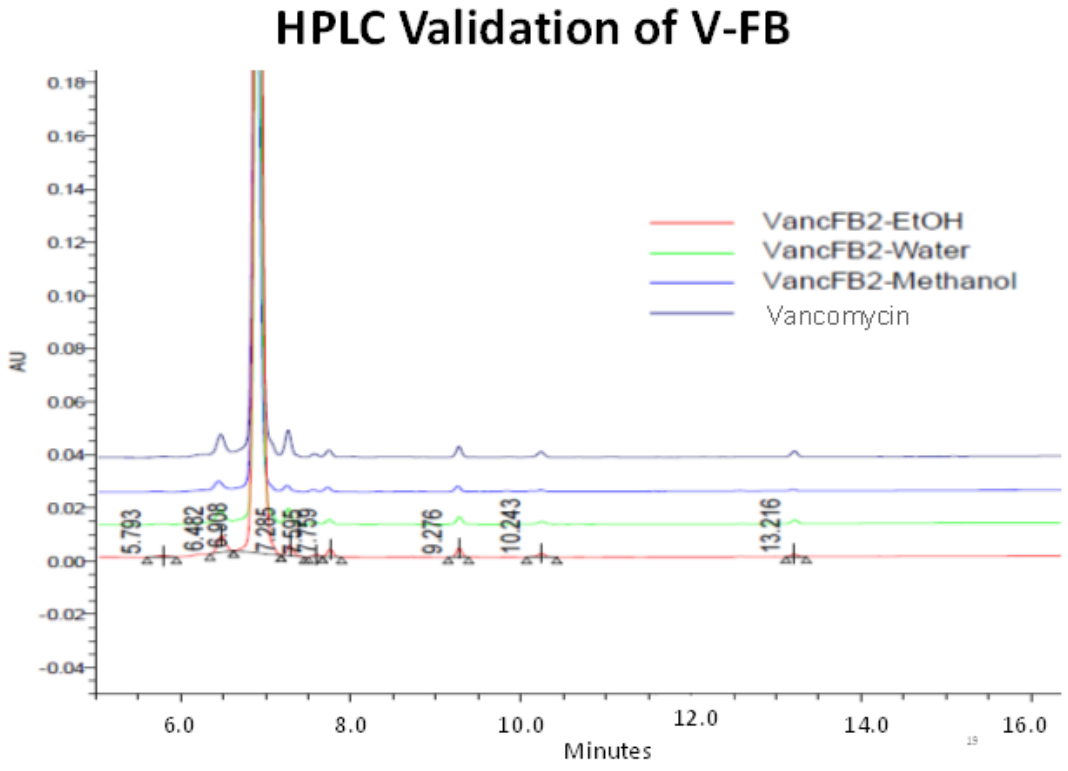

Figure B.1. HPLC validation of V-fb.
The peaks appeared at the same time for both V-HCl and V-fb confirming the production of V-fb.

B.2. In Vitro Bioactivity of V-fb

To compare the in vitro bioactivity of prepared V-fb and V-HCl, a Kirby-bauer ZOI (zone of inhibition) assay was done using different concentrations of the drugs against *Staphylococcus aureus* (ATCC 49230) as described in the manuscript. Bioactivity of V-fb and V-HCl against *S. aureus* measured via ZOI assay was similar. No significant difference was seen between the ZOI with no bacterial growth at a particular concentration (n=3 for each concentration) (Figure B2.2).

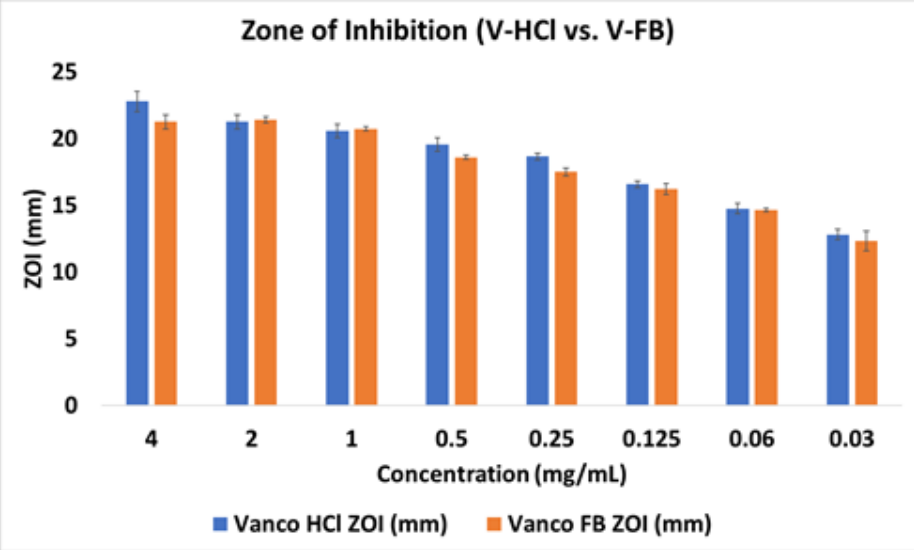

Figure B.2. The bioactivity comparison of V-HCl and V-FB via a Kirby Bauer zone of inhibition study against *S. aureus* strain 49230 at 1.0 x 10^7 CFU/mL concentration.

B.3. DSC Analysis of Polymers and Drug

DSC analysis was done by heat ramp at 10 C/ min using a TA instrument DSC Q2000 (TA Instruments, New Castle, DE, USA). In Figure B2.3, melting of PCL and PEG is seen. PCL shows melting at 68.15C and PEG melts at 65.97C. PLGA is amorphous, so no melting peak was seen. In the polymer mixture with NMP and PBS, the curve was broader, probably due to the presence of PBS and solvent NMP. Notably, PCL and PLGA are miscible in the NMP solvent. In the presence of PBS, there is a small broad peak seen at around 38 C, although melting seems to

happen at 30.52 C. The shape of the curve changes when vancomycin was added (Figure B2.4). Again, the peaks are broad, probably due to the several entities present in the mixture. The melting happened at a lower temperature than the individual polymers. Further characterization of the polymer mixture may be needed. Nevertheless, the mixture showed putty like consistency.

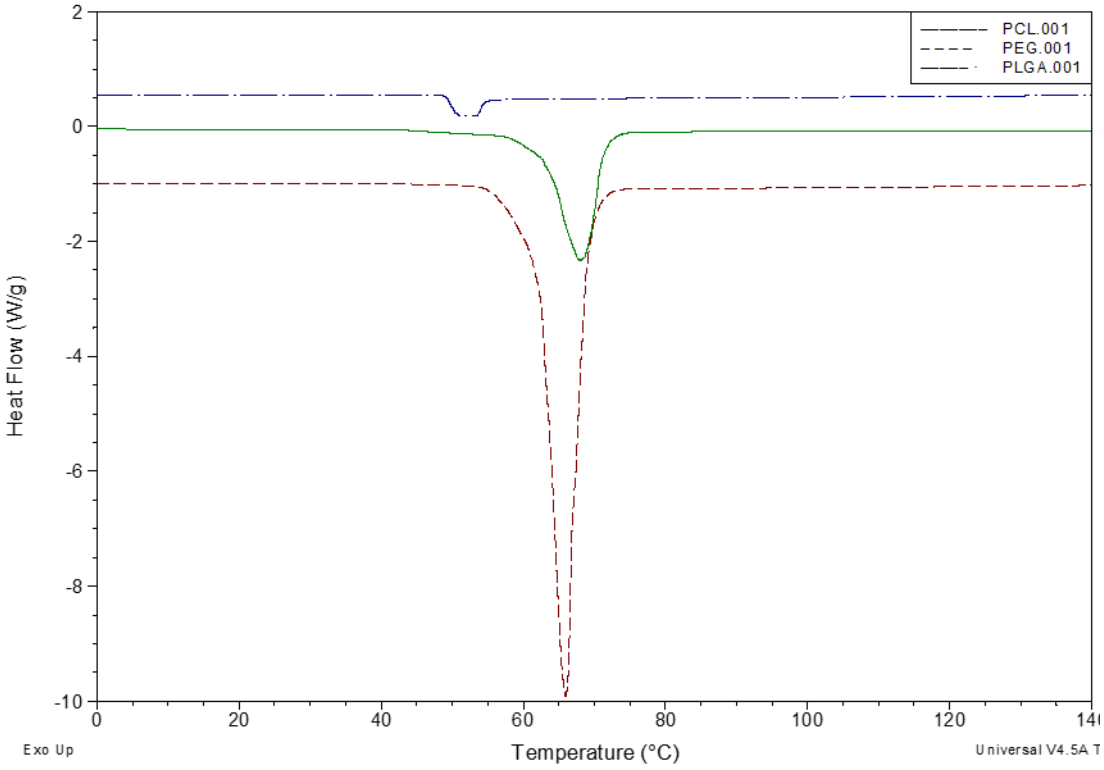

Figure B.3. DSC curve of PLGA, PEG, PCL.

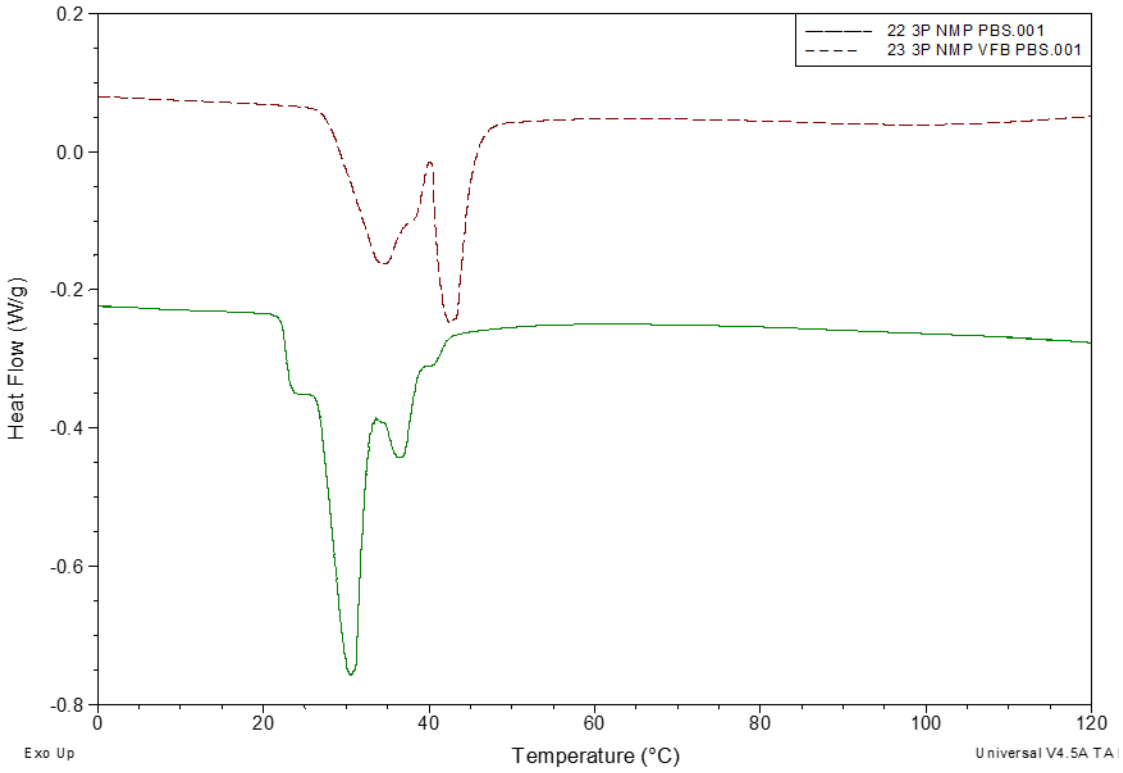

Figure B.4. DSC curve of polymers, NMP, PBS and vancomycin mixture (maroon), and mixture without vancomycin (green).
They appear different with wide melting range and seems to have two melting points (maroon) and the thermal behavior also changed as vancomycin was introduced. The melting points are lower than each of the individual polymers.

B.4. Making of Bone Crusher

From a local hardware store three components (Figure B 2.4): the bottom part (A) screws on to the barrel (B). The piston (C) then can be used to pulverize the bone using a hammer. (D) is the finished crusher. The crusher was autoclaved before being used for pulverizing the snap-frozen bone.

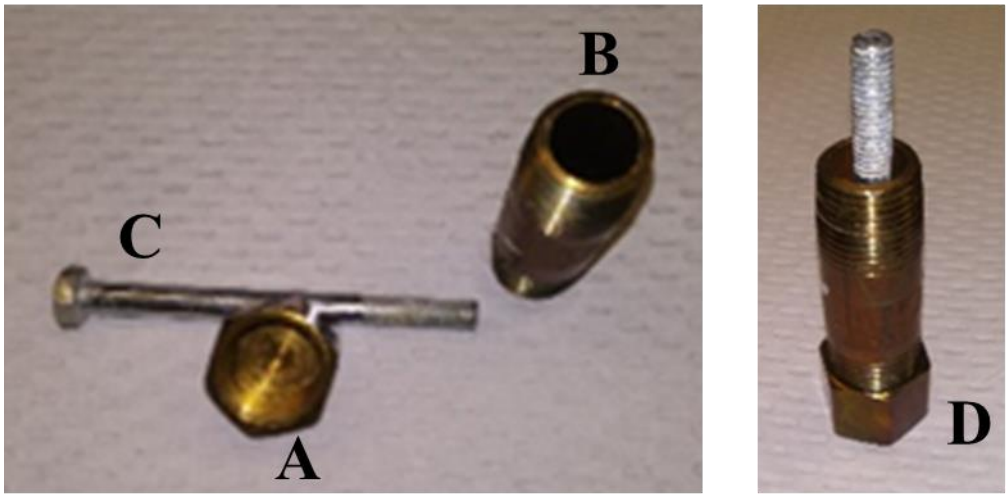

Figure B.5. Construction of custom-made bone crusher.
The bone crusher was made using three components. The bottom part (A) screws on to the barrel (B). The piston (C) then can be used to pulverize the bone using a hammer. (D) is the finished crusher.

Table B.1. Vancomycin release kinetics from ABVF fitted into different kinetics equation.

	Zero-order	**First-order**	**Korsmeyer-Peppas**	**Higuchi**	**Hixon-Crowell**
R^2	0.7181	0.9478	0.9964	0.8939	0.907

Korsemeyer-Peppas equation seems to have the best fitted model with high R^2 value.

APPENDIX C

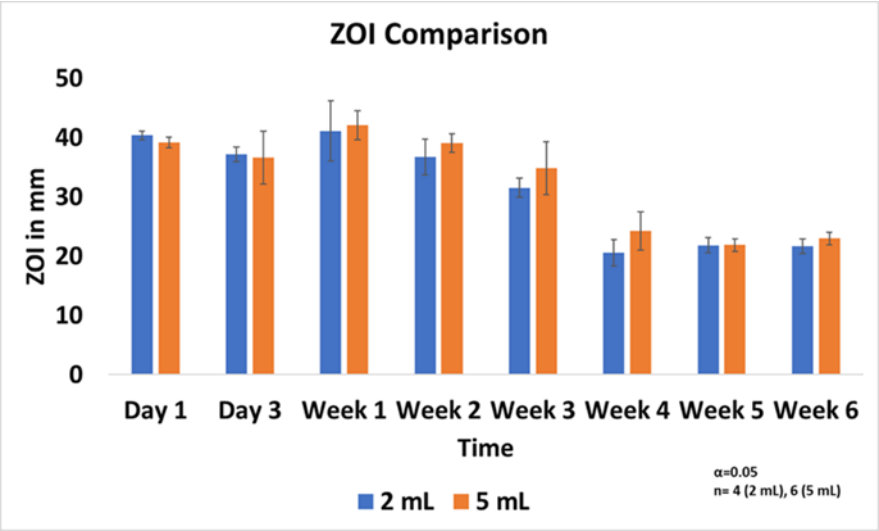

Figure C.1. Zone of Inhibition comparison of drugs release from ABVF in different volume of release media.
The one of inhibition study done with released drug in 2 mL and 5 mL release media showed similar antibacterial activity.

Figure C.2. X-ray of rat bone from cohort one rat.
Cohort 1 rats received blank BVF, BVF putty without antibiotic, and showed signs of osteomyelitis.